Duquesne University

Duquesne Scholarship Collection

Electronic Theses and Dissertations

Winter 12-18-2020

Functionalized Materials from Atom Transfer Radical Processes

Sean Fischer

Follow this and additional works at: https://dsc.duq.edu/etd

 Part of the Analytical Chemistry Commons, and the Polymer Chemistry Commons

Recommended Citation

FUNCTIONALIZED MATERIALS FROM ATOM TRANSFER RADICAL PROCESSES

A Dissertation

Submitted to the Bayer School of Natural and Environmental Sciences

Duquesne University

In partial fulfillment of the requirements for

the degree of Doctor of Philosophy

By

Sean M. Fischer

December 2020

FUNCTIONALIZED MATERIALS FROM ATOM TRANSFER RADICAL

PROCESSES

By

Sean M. Fischer

Approved September 3rd, 2020

<table>
<tr><td>―――――――――――――――――――
Stephanie J. Wetzel
Professor of Chemistry
(Committee Chair)</td><td>―――――――――――――――――――
Ellen S. Gawalt
Chair, Department of Chemistry and
Biochemistry
Professor of Chemistry
(Committee Member)</td></tr>
<tr><td>―――――――――――――――――――
Bruce Beaver
Professor of Chemistry
(Committee Member)</td><td>―――――――――――――――――――
Wilson S. Meng
Professor of Pharmaceutics
(Outside Reader)</td></tr>
<tr><td>―――――――――――――――――――
Philip Reeder
Dean, Bayer School of Natural and
Environmental Sciences</td><td></td></tr>
</table>

ABSTRACT

FUNCTIONALIZED MATERIALS FROM ATOM TRANSFER RADICAL PROCESSES

By

Sean M. Fischer

December 2020

Dissertation supervised by Stephanie J. Wetzel

This work is focused on the synthesis, characterization, and application of functionalized materials prepared from atom transfer radical processes. Atom transfer radical processes encompass both atom transfer radical addition (ATRA) and polymerization (ATRP) reactions, both of which are catalyzed by ppm amounts of copper complexes. The synthetic efforts of ATRA include increasing adduct selectivity through optimization of reaction conditions to generate small molecules in high to moderate yields. ATRA provides retention of the halogen moiety, which is an attractive functional group that can be further modified with other transformations. Specifically, the copper-catalyzed azide-alkyne [3+2] cycloaddition (CuAAC) allows for the realization of various applications due to the robust nature and host of "click-able" targets. This, in conjunction with the stout nature of ATRA, enables these materials to have use in all aspects of biomedical applications.

ATRP reactions were primarily utilized to prepare homo- and block copolymers using a photoinduced methodology. The photoATRP reaction enables polymerization of various acrylate-based monomers in a one-pot, multi-step fashion, generating block copolymers without the need for polymer isolation prior to additional block additions. Specifically, the photoATRP reaction was utilized to generate amphiphilic block copolymers containing a hydrophilic/hydrophobic section. When subjected to specific environments (solvent/temp/concentration/etc.), these amphiphiles have the ability to form micelles, of which can be utilized for small molecule encapsulation. These polymers would find use in all areas of biomedicine, such as bioimaging or drug delivery. It was envisioned that the polymerization could be employed to a host of multifunctional/star-shaped initiators, which may enable the formation of unimolecular micelles, a characteristic which is highly sought over.

Additionally, ATRP was utilized to prepare polymeric materials to characterize by means of MS/MS. Very similar to proteomics, subjecting these polymeric materials to collisional induced dissociation (CID) experiments enables proficient end-group and block identification based on measured fragments.

This work provides significant contributions to several fields: small molecule synthesis using ATRA in conjunction with CuAAC, block copolymer formation via ATRP, as well as the application of functionalized materials from the aforementioned methods. Moreover, these materials acted as an excellent scaffold to conduct MS/MS experiments to contribute to the growing field commonly referred to as "polymeromics."

DEDICATION

This dissertation is dedicated to my family and friends who have supported my goal of achieving a higher education.

ACKNOWLEDGEMENT

particular, who I worked with on a multitude of Forensic-related projects, something I may not have had the opportunity to experience otherwise. I am very proud that she is pursuing a doctorate in Forensic Chemistry.

I would also like to thank the instrument shop: Dan Bodnar, Lance Crosby, and Chris Lawless. I would also like to extend thanks to the Department of Chemistry and Biochemistry, as well as the Dean's office. Dr. Philip Reeder and Dr. Phillip Palmer were an integral part of my transition into Dr. Wetzel's lab, as they provided professional and financial guidance.

For my personal acknowledgements, I would first like to thank my fiancé Rachel. She has been there for me the entire time, through the good and bad times. She was always supportive of me and pushed me when I needed a nudge. I truly do not think I could have achieved this goal of mine without her by my side. I always thought how difficult graduate school was, but then I think of how much harder it may be to actually support someone going through it. I would like to thank my Mom, Dad, and stepfather Dave for the support through the whole process. To my best friend Harry, my little bro, thank you for pushing me. We may not have always seen eye-to-eye, but I don't think I'll ever have the chance to meet such a wholesome person who never fails to make me chuckle.

TABLE OF CONTENTS

LIST OF FIGURES

LIST OF TABLES

LIST OF ABBREVIATIONS

ATRA	atom transfer radical addition
ATRP	atom transfer radical polymerization
AGET	activators generated by electron transfer
ARGET	activators re-generated by electron transfer
ICAR	initiators for continuous activator generation
AIBN	azobisisobutyronitrile
V-70	2,2'-azobis(4-methoxy-2,4-dimethylvaleronitrile)
PhotoATRA	photoinduced atom transfer radical addition
PhotoATRP	photoinduced atom transfer radical polymerization
3^0	tertiary
2^0	secondary
1^0	primary
GPC	gel permeation chromatography
M_n	number average molecular weight
M_w	weight average molecular weight
M_z	Z-average molecular weight
$M\eta$	viscosity average molecular weight
Đ	polydispersity index
NMR	nuclear magnetic resonance spectroscopy
MHz	megahertz
^1H	hydrogen

^{13}C	carbon
MS	mass spectrometry
HRMS	high-resolution mass spectrometry
MS/MS	tandem mass spectrometry
CID	collision-induced dissociation
MALDI	matrix-assisted laser desorption ionization
Q-TOF	quadrupole time-of-flight
CuAAC	copper-catalyzed azide-alkyne [3+2] cycloaddition
EBiB	ethyl-2-bromoisobutyrate
PBiB	propargyl bromoisobutyrate
BBiBE	1,2-bis(bromoisobutyryloxy)ethane
TBiBE	1,1,1-tris(2-bromoisobutyryloxymethyl)ethane
PTBiB	pentaerythritol tetrakis(2-bromoisobutyrate)
DPBiB	dipentaerythritol hexakis(2-bromoisobutyrate)
EGDA	ethylene glycol diacrylate
$SnCl_2$	tin chloride
HCl	hydrochloric acid
NaN_3	sodium azide
NaAsc	sodium ascorbate
EtOAC	ethyl acetate
$CDCl_3$	deuterated chloroform
M	molarity
Hν	radiation

UV	ultraviolet
LED	light-emitting diode
MA	methyl acrylate
EA	ethyl acrylate
BA	butyl acrylate
EGMEA	ethylene glycol methyl ether acrylate
LA	lauryl acrylate
dEGEEA	di(ethylene glycol)ethyl ether acrylate
Me$_6$TREN	tris[2-(dimethylamino)ethyl]amine
TPMA	tris(2-pyridylmethyl)amine
MeOH	methanol
DMSO	dimethylsulfoxide
DCM	dichloromethane
THF	tetrahydrofuran
CuSO$_4$*5H$_2$O	copper sulfate pentahydrate

1. INTRODUCTION

1.1 *History of atom transfer radical processes*

The ability to add halogenated compounds to alkenes or alkynes via radical means is one of the fundamental reactions in organic chemistry.[1-2] Copper-catalyzed atom transfer radical addition (ATRA) and polymerization (ATRP) reactions are often used to facilitate this organic transformation[3-7] due to the precise and facile C-C bond formation. These reactions originate from the Kharasch addition,[8-9] which stemmed from the discovery of "the peroxide effect" in 1937. It was found that anti-Markovnikov addition of HBr to unsymmetrical alkenes was favored in the presence of peroxide initiators. Subsequent experiments showed that peroxides act as free-radical initiators through the generation of bromine radicals by a homolytic cleavage of an HBr bond. The generated radical can propagate across the double bond of an alkene onto the least substituted carbon atom, producing a secondary radical. The more-stable secondary radical can then abstract a hydrogen, forming an anti-Markovnikov product (Scheme 1).
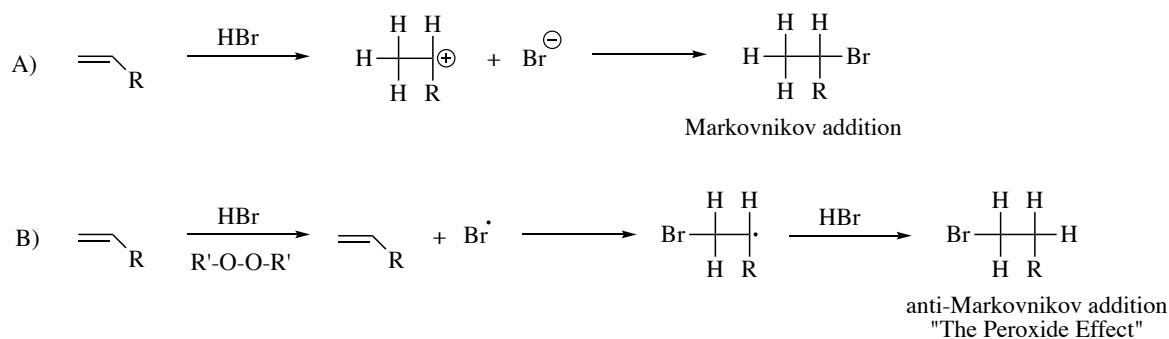
Scheme 1. Addition of HBr to unsymmetrical alkenes in the absence (A) and presence (B) of free radical peroxide initiators.

The addition of polyhalogenated substrates to alkenes in the presence of free radical initiators or light was also extensively studied by Kharasch,[9] which is akin to modern-day ATRA (Scheme 2). These reactions generated high monoadduct yields for simple α-olefins but were

greatly reduced for alkenes which readily polymerize via free radical means (styrene, methyl (meth)acrylate, and acrylonitrile). The decreased monoadduct yields were attributed to radical-radical coupling and disproportionation reactions.

Initiation:

AIBN $\xrightarrow{D}$ [CN radical] + N_2

[CN radical] + Br_3C-Br $\xrightarrow{k_i}$ [NC/Br species] + $CBr_3^{\cdot}$

Propagation:

CBr_3 + [alkene]R $\xrightarrow{k_{add}}$ Br_3C[radical]R $\xrightarrow{k_p}$ Br_3C[polymer]R

Br_3C[radical]R + Br_3C-Br $\xrightarrow{k_{tr}}$ Br_3C[Br species]R + CBr_3

monoadduct
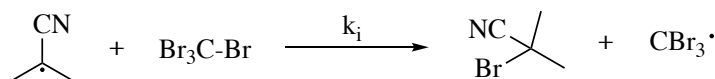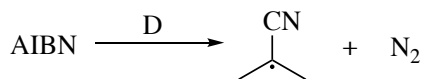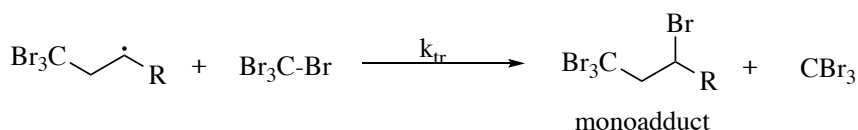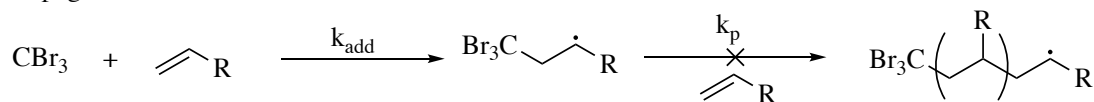
Termination:

radical-radical coupling

CBr_3 + CBr_3 $\xrightarrow{k_t}$ $Br_3C{-}CBr_3$

[CN radical] + [CN radical] $\xrightarrow{k_t}$ [CN coupled product]

Br_3C[radical]R + Br_3C[radical]R $\xrightarrow{k_t}$ Br_3C[coupled]CBr_3

etc.
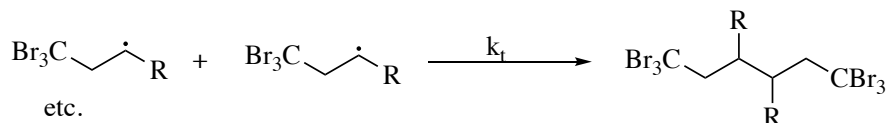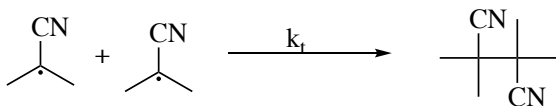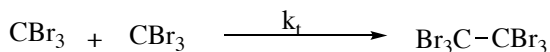
Scheme 2. Kharasch addition of CCl_4 to alkenes in the presence of free radical initiator AIBN.

Seminal research conducted by Minisci et al. in 1956 revealed that providing a better halogen transfer agent can significantly increase product selectivity.[10] It was discovered accidentally, when a free-radical polymerization was attempted in a steel autoclave. The resulting product had over 50% monoadduct yield and was eventually determined to be the result

of the steel autoclave corroding, producing iron chloride. This succession of breakthroughs led to the birth of transition metal-catalyzed ATRA and ATRP. Since the discovery, a variety of transition metals have been found to catalyze these reactions. Copper has been the most extensively studied metal in atom transfer radical processes,[11] most likely due to the cost-effective nature. Other transition metals such as iron,[12] ruthenium,[13] and nickel[14] were also found to be efficient regarding product selectivity. However, the focus of this work utilizes copper.

1.2 *Mechanistic aspects of ATRA/ATRP*

The catalytic cycle, shown in Figure 3, begins with the homolytic cleavage of an alkyl halide bond by the transition metal activator species ($[Cu^I L_m X]$) to generate an alkyl radical and corresponding deactivator species ($[Cu^{II} L_m X][X]$). The organic radical can then add across the double bond of an alkene in an anti-Markovnikov fashion, forming a more-stable secondary radical. The deactivator species can have a halogen abstracted by the secondary radical, forming a monoadduct and regenerating the activator species (ATRA). Alternatively, this methodology can be extended to ATRP if the conditions are modified such that more than one monomer addition occurs. This can be accomplished if the radical species, before and after monomer addition, possess similar reactivity, resulting in a chain-growth polymerization in which several monomers can be added during the activation step.[15] This methodology enables the production of polymers with predetermined molecular weights, controlled chemical compositions, and well-defined functionalities.[15-26]
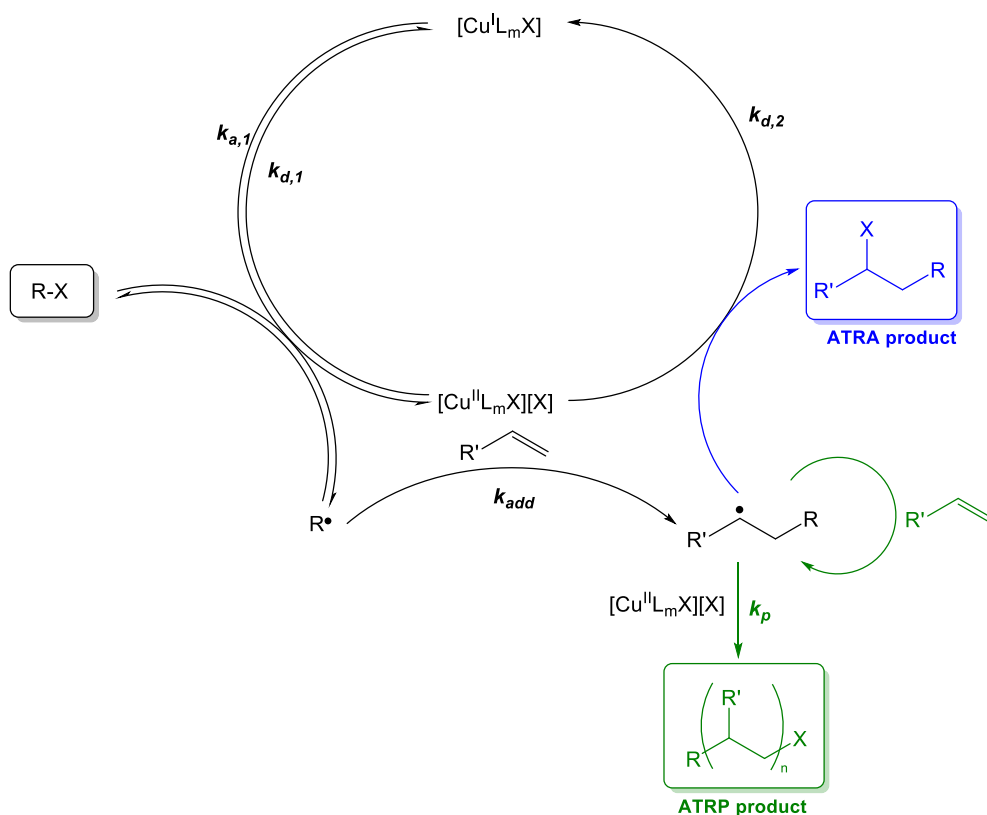
Scheme 3. Proposed mechanism for copper-catalyzed ATRA/ATRP.

1.3 *Greening of the catalytic process*

Initially, ATRA was not utilized to its full potential in small molecule and natural product synthesis, mainly due to the large amount of transition metal complex needed to achieve high selectivity (10-30 mol% relative to alkene). This presented problems regarding product separation and catalyst regeneration, making the process environmentally unfriendly and costly.[3] Originally, the solution to this problem was addressed through the mechanistically-similar ATRP, in which a reducing agent was employed to continuously regenerate the activator species.[27] [28]

There are a variety of methods which can be utilized for catalyst activation. In Activators Generated by Electron Transfer (AGET), reducing agents are added in a stoichiometric amount to generate the activator species from the air-stable Cu^{II} catalyst (deactivator).[29] AGET ATR

processes use reducing agents which are unable to initiate new polymer chains such as copper[0], tin[II] ethylhexanoate, triethylamine, and ascorbic acid.[21]

When performing ATR processes, unavoidable radical-radical termination reactions will occur, where the activator species (Cu[I]) is constantly being converted to the deactivator (Cu[II]). This leads to the accumulation of deactivator (Cu[II]) in solution, which slows the monomer addition rate, hindering conversion. To combat this problem, Activators ReGenerated by Electron Transfer (ARGET) ATR process can be used. ARGET is mechanistically similar to AGET, however a large excess of reducing agent is used rather than a stoichiometric amount.[21, 30-31] The deactivator which was accumulating in solution is continuously converted to the activator species, enabling a rapid conversion with a low concentration of catalyst.

Perhaps the most conventional method of regenerating the catalyst is by use of free radical initiators. When performing Initiators for Continuous Activator Regeneration (ICAR) ATRP, free radicals are continuously generated using conventional radical initiators such as AIBN or V-70 and is typically initiated by heat. These free radical generators are used to slowly reduce the deactivator species (Cu[II]) which accumulate in solution.[3, 28] This provides a similar system to an ARGET ATR processes, both of which are industrially-relevant due to the low copper concentrations required.

1.3.1 *Photoinduced atom transfer radical processes*

The use of photo catalysts have emerged as a promising methodology to perform ATR processes under mild and ecologically benign conditions.[32-49] The simple preparation and minimal use of additives is an attractive quality that further promotes the greening of these organic transformations. Small contributions from interactions between the alkyl halide and ligand, ligand and monomer, and photochemical cleavage of alkyl halides are present in these

reactions, which are similar to an ICAR-based system. However, the major pathway to radical (re)generation is the photochemical reduction of Cu^{II} complex by free amine moieties.[35, 41-42]

$$X-Cu^{II}L_n \xrightarrow{\text{hv}} Cu^{I}L_n + X^{\bullet}$$

$$R-X \xrightarrow{\text{hv}} R^{\bullet} + X^{\bullet}$$

$$L + M \xrightarrow{\text{hv}} L^{+\bullet} + M^{-\bullet}$$

$$R-X + L \xrightarrow{\text{hv}} R^{\bullet} + L^{+\bullet} + X^{-}$$

$$X-Cu^{II}L_n + L \xrightarrow{\text{hv}} Cu^{I}L_n + L^{+\bullet} + X^{-}$$
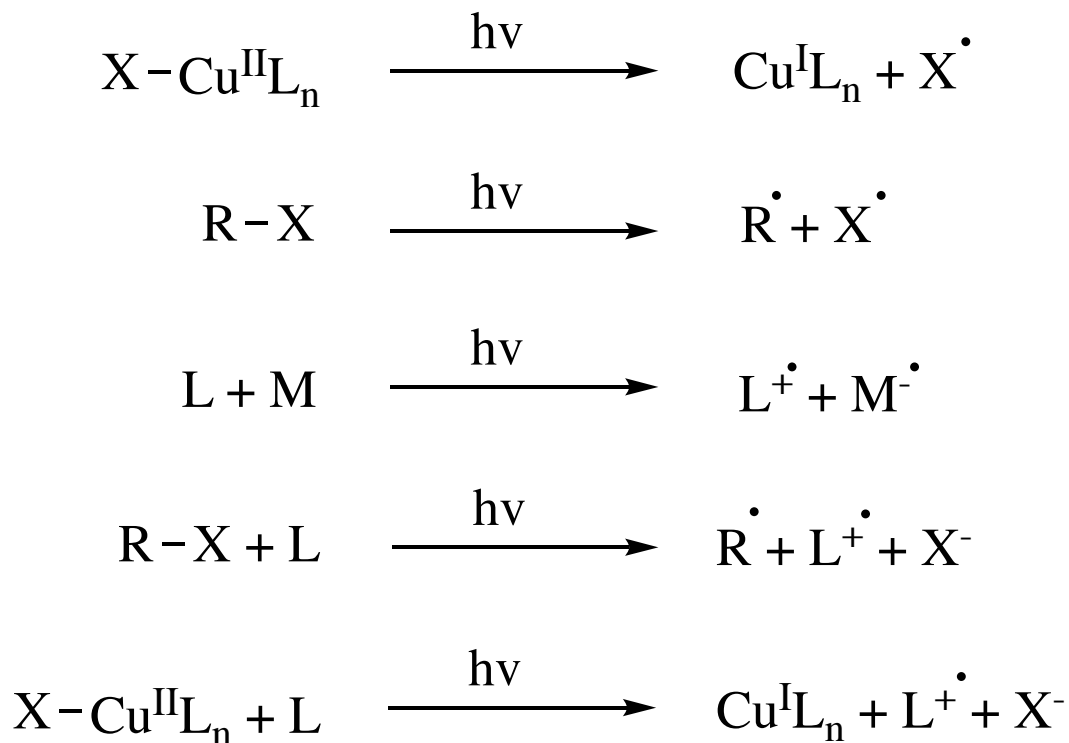
Scheme 4. Proposed activator regeneration pathway in photoinduced ATRP.[42]

1.3.2 *Towards monohalogenated initiators*

The pioneering efforts to ATR processes have focused on using highly active polyhalogenated initiators, due to low catalyst loadings, minimal additives, and short reaction times. However, focus has recently transitioned to using less active tri, bi, and monohalogenated substrates. Although they may be less active, they are particularly attractive for ATRA and ATRP reactions. The halide functionality in the resulting products can be easily reduced, eliminated, displaced, or converted to a Grignard reagent. Additionally, it can serve as a further radical precursor for more monomer additions.[50] Changing the initiating source for ATRP processes can have a variety of effects on the reaction course. For example, changing the degree of initiating substitution can have a drastic effect on the activator rate (k_a) where $3^0 > 2^0 > 1^0$. The

halogen functionality present can also affect the activator rate constant, where I > Br > Cl. Additionally, the radical stabilization group can influence the activator rate.[51-53]

1.3.3 *Application of atom transfer radical products*

Atom transfer radical addition is primarily utilized for small molecule synthesis; therefore, it is an excellent candidate for biomolecule formation. The retention of the halogen moiety is a particularly attractive quality which allows for alternative organic transformations.[54-55] One reaction of interest falls under the "click chemistry" umbrella: the azide-alkyne [3+2] cycloaddition (CuAAC).[56-63] The simple and robust technique allows for the realization of triazole-bearing compounds which have been found as excellent bioimaging targets.

Polymers prepared by ATRP have an even greater impact in the realm of material science, as they have been found in all aspects of surface chemistry, opto-electronics, carbon-capture, and used as drug delivery systems.[64] The use of ATRP-synthesized polymeric materials to delivery therapeutic molecules has been extensively studied over the past few decades.[65-72] One appealing quality to this controlled-radical polymerization technique lies within the ability to form complex, yet pre-determined, macromolecular architectures through a host of methodologies, such as the "core-first" or "arm-first" synthetic route.[67, 73-74]

1.4 *Characterization of synthetic materials*

1.4.1 *Gel Permeation Chromatography (GPC)*

The properties of polymers can often be correlated to the average molecular weight, such as mechanical properties, processability, and solution characteristics. Polymerization techniques provide a distribution of chain lengths and understanding the distribution effects are crucial for the predictive design of polymer systems. Therefore, it is imperative to determine the average molecular weight and overall distribution of the polymer sample. Some common examples

include end-group analysis, fractionation, and ultracentrifugation. However, the most common method for polymer molecular weight realization is Gel Permeation Chromatography (GPC). GPC is a type of liquid chromatography, which differs from reversed-phase or normal-phase with separation occurring from the hydrodynamic volume in solution rather than molecular interactions with mobile/stationary phase. GPC is typically conducted in relatively dilute solutions to ensure the polymer chains are independent and do not become coiled with one another.[75-77]

GPC columns are packed with porous particles, which have varying size distributions and porosities, which dictate the separating ability of the column. Pairing these columns with a viscometer, light scattering, or refractive index detector enables a straight-forward determination of molecular weights $(\overline{Mn}, \overline{Mw}, \overline{Mz}, \overline{M\eta})$. The heterogeneity of the polymer samples is then obtained through the equation:

$$\text{Đ} = \frac{\overline{Mw}}{\overline{Mn}}$$

1.4.2 *Nuclear Magnetic Resonance (NMR)*

Beginning in the 1960's, continuous wave NMR spectroscopy had proven itself to be a powerful tool for determining the chemical microstructure of synthetic materials.[78] Since then, modern NMR spectrometers have shifted towards a pulsed Fourier transform type, which enables the identification of end-groups, branches, and defects.[76] These characterization procedures can be employed using dilute, semi-dilute, concentrated, or even solid polymer samples. Additionally, the evaluation of average copolymer composition or polymer tacticity can be determined using NMR spectroscopy.[75, 77]

1.4.3 *Mass Spectrometry (MS) and Tandem Mass Spectrometry (MS/MS)*

Polymer science and engineering applications have substantially increased since the introduction of soft-ionization methods such as matrix-assisted laser-desorption ionization (MALDI) and electrospray ionization (ESI).[79-81] These ionization sources enable coupling with a mass analyzer, which reveals a great number of advantages, especially one that provides high-resolution spectra such as a quadrupole-time-of-flight (Q-TOF) instrument.[82-83] This macromolecular characterization allows access to molecular weight distributions, expressed in their dispersity ($Đ$), and mass-to-charge ratios.[84] However, mass spectrometry alone is unable to provides detailed structural information.[85-86] Collision-induced dissociation (CID) can be performed to elucidate copolymer sequences or architectures, differentiate isobaric or isomeric species, or characterize end-groups.[87-90] This is crucial for the predictive design and fabrication of polymeric materials.[33, 91]

1.5 *Challenges, outlook, and future perspective of atom transfer radical processes*

Throughout the past decade, a variety of new functionalized materials have been introduced to the world by atom transfer radical processes. Regarding ATRP, companies have already started production of ATRP-based polymers in fields of pigments, cosmetics, adhesives, and chromatographic packings. It is envisioned that future ATRP-based polymers will be used for drug delivery, coatings for cardiovascular stents, degradable plastics, and optoelectronics. ATRP has several advantages over other controlled radical methods; however, there are still some limitations which will be addressed with future research. Although at ppm levels, the use of transition-metal catalysts is not appealing, especially regarding biomedical applications. Removal and recycling of the transition-metal catalyst is suggested to make the polymerization technique as eco-friendly as possible. Synthetically, it is anticipated that the monomer scope will

be extended to more functionally relevant analogues. Additionally, investigating new polymer compositions and architectures valuable for determining better structure-function relationships.

The motivation of the three following chapters of this work is to elucidate new synthetic materials which can be created using atom transfer radical processes. This will be accomplished through photoinduced ATRA reactions using monohalogenated initiators (Chapter 2), photoinduced ATRP for amphiphilic block copolymers for small molecule encapsulation (Chapter 3), and sequential analysis of polymers produced from ATRP reactions (Chapter 4).

1.6 *References*

1.	Curran, D. P., The Design and Application of Free Radical Chain Reactions in Organic Synthesis. Part 1. *Synthesis* **1988,** (06), 417-439.

2.	Curran, D. P., The Design and Application of Free Radical Chain Reactions in Organic Synthesis. Part 2. *Synthesis* **1988,** (07), 489-513.

3.	Pintauer, T., ATOM TRANSFER RADICAL ADDITION (ATRA) CATALYZED BY PPM AMOUNTS OF COPPER COMPLEXES. *Polymer Preprints* **2008,** *49* (2), 12-13.

4.	Pintauer, T., "Greening" of Copper Catalyzed Atom Transfer Radical Addition (ATRA) and Cyclization (ATRC) Reactions. *ACS symposium series* **2009,** *1023* (Controlled/Living Radical Poly), 63-84.

5.	Bussey, K. A.; Cavalier, A. R.; Mraz, M. E.; Oshin, K. D.; Sarjeant, A.; Pintauer, T., Synthesis, characterization, X-ray crystallography analysis, and catalytic activity of bis(2-pyridylmethyl)amine copper complexes containing coupled pendent olefinic arms in atom transfer radical addition (ATRA) reactions. *Polyhedron* **2016,** *114*, 256-267.

6.	Reiser, O., Shining Light on Copper: Unique Opportunities for Visible-Light-Catalyzed Atom Transfer Radical Addition Reactions and Related Processes. *Acc Chem Res* **2016,** *49* (9), 1990-6.

7.	Pintauer, T.; Matyjaszewski, K., Structural aspects of copper catalyzed atom transfer radical polymerization. *Coordination Chemistry Reviews* **2005,** *249* (11–12), 1155-1184.

8.	Kharasch, M. S. E., H.; Mayo, F. R. , THE PEROXIDE EFFECT IN THE ADDITION OF REAGENTS TO UNSATURATED COMPOUNDS. XV. THE ADDITION OF HYDROGEN BROMIDE TO 1- AND 2-BROMO AND CHLORO-PROPENES. *Journal of Organic Chemistry* **1937,** *2*, 288-302.

9.   Kharasch, M. S.; Jensen, E. V.; Urry, W. H., Addition of Carbon Tetrachloride and Chloroform to Olefins. *Science* **1945,** *102* (2640), 128-128.

10.   Minisci, F., Free-Radical Additions of Olefins in the Presence of Redox Systems. *Accounts of Chemical Research* **1975,** *8*, 165-171.

11.   Pintauer, T., Catalyst Regeneration in Transition-Metal-Mediated Atom-Transfer Radical Addition (ATRA) and Cyclization (ATRC) Reactions. *European Journal of Inorganic Chemistry* **2010,** *2010* (17), 2449-2460.

12.   Eckenhoff, W. T.; Biernesser, A. B.; Pintauer, T., Structural characterization and investigation of iron(III) complexes with nitrogen and phosphorus based ligands in atom transfer radical addition (ATRA). *Inorganica Chimica Acta* **2012,** *382*, 84-95.

13.   Lee, J.; Grandner, J. M.; Engle, K. M.; Houk, K. N.; Grubbs, R. H., In Situ Catalyst Modification in Atom Transfer Radical Reactions with Ruthenium Benzylidene Complexes. *Journal of the American Chemical Society* **2016,** *138* (22), 7171-7177.

14.   Stol, M.; Snelders, D. J. M.; Godbole, M. D.; Havenith, R. W. A.; Haddleton, D.; Clarkson, G.; Lutz, M.; Spek, A. L.; van Klink, G. P. M.; van Koten, G., 2,6-Bis(oxazolinyl)phenylnickel(II) Bromide and 2,6-Bis(ketimine)phenylnickel(II) Bromide: Synthesis, Structural Features, and Redox Properties. *Organometallics* **2007,** *26* (16), 3985-3994.

15.   Matyjaszewski, K., From Atom Transfer Radical Addition to Atom Transfer Radical Polymerization. *Current Organic Chemistry* **2002,** *6*, 67-82.

16.   Braunecker, W. A.; Matyjaszewski, K., Controlled/living radical polymerization: Features, developments, and perspectives. *Progress in Polymer Science* **2007,** *32* (1), 93-146.

17.   Braunecker, W. A.; Pintauer, T.; Tsarevsky, N. V.; Kickelbick, G.; Krzysztof, M., Towards understanding monomer coordination in atom transfer radical polymerization: synthesis

of [CuI(PMDETA)(π-M)][BPh4] (M = methyl acrylate, styrene, 1-octene, and methyl methacrylate) and structural studies by FT-IR and 1H NMR spectroscopy and X-ray crystallography. *Journal of Organometallic Chemistry* **2005,** *690* (4), 916-924.

18.   Braunecker, W. A.; Tsarevsky, N. V.; Gennaro, A.; Matyjaszewski, K., Thermodynamic Components of the Atom Transfer Radical Polymerization Equilibrium: Quantifying Solvent Effects. *Macromolecules* **2009,** *42* (17), 6348-6360.

19.   Braunecker, W. A.; Tsarevsky, N. V.; Pintauer, T.; Gil, R. R.; Matyjaszewski, K., Quantifying Vinyl Monomer Coordination to CuI in Solution and the Effect of Coordination on Monomer Reactivity in Radical Copolymerization. *Macromolecules* **2005,** *38* (10), 4081-4088.

20.   Matyjaszewski, K., Architecturally Complex Polymers with Controlled Heterogeneity. *Science* **2011,** *333* (6046), 1104-1105.

21.   Matyjaszewski, K., Atom Transfer Radical Polymerization (ATRP): Current Status and Future Perspectives. *Macromolecules* **2012,** *45* (10), 4015-4039.

22.   Matyjaszewski, K.; Jakubowski, W.; Min, K.; Tang, W.; Huang, J.; Braunecker, W. A.; Tsarevsky, N. V., Diminishing catalyst concentration in atom transfer radical polymerization with reducing agents. *Proceedings of the National Academy of Sciences* **2006,** *103* (42), 15309.

23.   Matyjaszewski, K.; Miller, P. J.; Pyun, J.; Kickelbick, G.; Diamanti, S., Synthesis and Characterization of Star Polymers with Varying Arm Number, Length, and Composition from Organic and Hybrid Inorganic/Organic Multifunctional Initiators. *Macromolecules* **1999,** *32* (20), 6526-6535.

24.   Matyjaszewski, K.; Paik, H.-j.; Shipp, D. A.; Isobe, Y.; Okamoto, Y., Free-Radical Intermediates in Atom Transfer Radical Addition and Polymerization: Study of Racemization, Halogen Exchange, and Trapping Reactions. *Macromolecules* **2001,** *34* (10), 3127-3129.

25.   Matyjaszewski, K.; Tsarevsky, N. V., Nanostructured functional materials prepared by atom transfer radical polymerization. *Nat Chem* **2009,** *1* (4), 276-288.

26.   Matyjaszewski, K.; Xia, J., Atom Transfer Radical Polymerization. *Chemical Reviews* **2001,** *101* (9), 2921-2990.

27.   Bussey, K. A.; Connell, J. R.; McGlone, A. R.; Mraz, M. E.; Oshin, K. D.; Pintauer, T.; Oliver, A. G., Crystal structure of {(but-3-en-1-yl)bis-[(pyridin-2-yl)meth-yl]amine-κ(3) N,N′,N″}di-chlorido-copper(II) diethyl ether hemisolvate. *Acta Crystallographica Section E: Crystallographic Communications* **2015,** *71* (Pt 3), 309-311.

28.   Pintauer, T.; Matyjaszewski, K., Atom transfer radical addition and polymerization reactions catalyzed by ppm amounts of copper complexes. *Chemical Society Reviews* **2008,** *37* (6), 1087-1097.

29.   Li, W.; Matyjaszewski, K., Star Polymers via Cross-Linking Amphiphilic Macroinitiators by AGET ATRP in Aqueous Media. *Journal of the American Chemical Society* **2009,** *131* (30), 10378-10379.

30.   Ding, H.; Park, S.; Zhong, M.; Pan, X.; Pietrasik, J.; Bettinger, C. J.; Matyjaszewski, K., Facile Arm-First Synthesis of Star Block Copolymers via ARGET ATRP with ppm Amounts of Catalyst. *Macromolecules* **2016**.

31.   Kwak, Y.; Magenau, A. J. D.; Matyjaszewski, K., ARGET ATRP of Methyl Acrylate with Inexpensive Ligands and ppm Concentrations of Catalyst. *Macromolecules* **2011,** *44* (4), 811-819.

32.   Anastasaki, A.; Nikolaou, V.; McCaul, N. W.; Simula, A.; Godfrey, J.; Waldron, C.; Wilson, P.; Kempe, K.; Haddleton, D. M., Photoinduced Synthesis of α,ω-Telechelic Sequence-Controlled Multiblock Copolymers. *Macromolecules* **2015,** *48* (5), 1404-1411.

33. Anastasaki, A.; Nikolaou, V.; Pappas, G. S.; Zhang, Q.; Wan, C.; Wilson, P.; Davis, T. P.; Whittaker, M. R.; Haddleton, D. M., Photoinduced sequence-control via one pot living radical polymerization of acrylates. *Chemical Science* **2014,** *5* (9), 3536-3542.

34. Anastasaki, A.; Nikolaou, V.; Zhang, Q.; Burns, J.; Samanta, S. R.; Waldron, C.; Haddleton, A. J.; McHale, R.; Fox, D.; Percec, V.; Wilson, P.; Haddleton, D. M., Copper(II)/Tertiary Amine Synergy in Photoinduced Living Radical Polymerization: Accelerated Synthesis of ω-Functional and α,ω-Heterofunctional Poly(acrylates). *Journal of the American Chemical Society* **2014,** *136* (3), 1141-1149.

35. Frick, E.; Anastasaki, A.; Haddleton, D. M.; Barner-Kowollik, C., Enlightening the Mechanism of Copper Mediated PhotoRDRP via High-Resolution Mass Spectrometry. *Journal of the American Chemical Society* **2015,** *137* (21), 6889-6896.

36. Garlets, Z. J.; Nguyen, J. D.; Stephenson, C. R. J., The Development of Visible-Light Photoredox Catalysis in Flow. *Israel Journal of Chemistry* **2014,** *54* (4), 351-360.

37. Paria, S. R., Oliver, Copper in Photocatalysis. *ChemCatChem* **2014,** *6*, 2477-2483.

38. Wallentin, C.-J.; Nguyen, J. D.; Finkbeiner, P.; Stephenson, C. R. J., Visible Light-Mediated Atom Transfer Radical Addition via Oxidative and Reductive Quenching of Photocatalysts. *Journal of the American Chemical Society* **2012,** *134* (21), 8875-8884.

39. Yang, Q.; Dumur, F.; Morlet-Savary, F.; Poly, J.; Lalevée, J., Photocatalyzed Cu-Based ATRP Involving an Oxidative Quenching Mechanism under Visible Light. *Macromolecules* **2015,** *48* (7), 1972-1980.

40. Yang, Q.; Lalevée, J.; Poly, J., Development of a Robust Photocatalyzed ATRP Mechanism Exhibiting Good Tolerance to Oxygen and Inhibitors. *Macromolecules* **2016**.

41.   Pan, X.; Tasdelen, M. A.; Laun, J.; Junkers, T.; Yagci, Y.; Matyjaszewski, K., Photomediated controlled radical polymerization. *Progress in Polymer Science* **2016,** *62*, 73-125.

42.   Ribelli, T. G.; Konkolewicz, D.; Bernhard, S.; Matyjaszewski, K., How are Radicals (Re)Generated in Photochemical ATRP? *Journal of the American Chemical Society* **2014,** *136* (38), 13303-13312.

43.   Zhou, Y.-N.; Guo, J.-K.; Li, J.-J.; Luo, Z.-H., Photoinduced Iron(III)-Mediated Atom Transfer Radical Polymerization with In Situ Generated Initiator: Mechanism and Kinetics Studies. *Industrial & Engineering Chemistry Research* **2016,** *55* (39), 10235-10242.

44.   Pan, X.; Malhotra, N.; Simakova, A.; Wang, Z.; Konkolewicz, D.; Matyjaszewski, K., Photoinduced Atom Transfer Radical Polymerization with ppm-Level Cu Catalyst by Visible Light in Aqueous Media. *Journal of the American Chemical Society* **2015,** *137* (49), 15430-15433.

45.   Balili, M. N. C.; Pintauer, T., Photoinitiated ambient temperature copper-catalyzed atom transfer radical addition (ATRA) and cyclization (ATRC) reactions in the presence of free-radical diazo initiator (AIBN). *Dalton Transactions* **2011,** *40* (12), 3060-3066.

46.   Cohen, N. A.; Tillman, E. S.; Thakur, S.; Smith, J. R.; Eckenhoff, W. T.; Pintauer, T., Effect of the Ligand in Atom Transfer Radical Polymerization Reactions Initiated by Photodimers of 9-Bromoanthracene. *Macromolecular Chemistry and Physics* **2009,** *210* (3-4), 263-268.

47.   Cetin, M. M.; Hodson, R. T.; Hart, C. R.; Cordes, D. B.; Findlater, M.; Casadonte Jr, D. J.; Cozzolino, A. F.; Mayer, M. F., Characterization and photocatalytic behavior of 2,9-di(aryl)-1,10-phenanthroline copper(i) complexes. *Dalton Transactions* **2017,** *46* (20), 6553-6569.

48.   Doran, S.; Yilmaz, G.; Yagci, Y., Tandem Photoinduced Cationic Polymerization and CuAAC for Macromolecular Synthesis. *Macromolecules* **2015,** *48* (20), 7446-7452.

49.   Hossain, A.; Bhattacharyya, A.; Reiser, O., Copper's rapid ascent in visible-light photoredox catalysis. *Science* **2019,** *364* (6439), eaav9713.

50.   Pintauer, T., Towards the development of highly active copper catalysts for atom transfer radical addition (ATRA) and polymerization (ATRP). *Chemical Papers* **2016,** *70* (1), 22-42.

51.   Eckenhoff, W. T.; Biernesser, A. B.; Pintauer, T., Kinetic and Mechanistic Aspects of Atom Transfer Radical Addition (ATRA) Catalyzed by Copper Complexes with Tris(2-pyridylmethyl)amine. *Inorganic Chemistry* **2012,** *51* (21), 11917-11929.

52.   Eckenhoff, W. T.; Pintauer, T., Atom transfer radical addition (ATRA) catalyzed by copper complexes with tris[2-(dimethylamino)ethyl]amine (Me6TREN) ligand in the presence of free-radical diazo initiator AIBN. *Dalton Transactions* **2011,** *40* (18), 4909-4917.

53.   Eckenhoff, W. T. P., Tomislav, Copper Catalyzed Atom Transfer Radical Addition (ATRA) and Cyclization (ATRC) Reactions in the Presence of Reducing Agents. *Catalysis Reviews* **2010,** *52*, 1-59.

54.   Tornøe, C. W.; Christensen, C.; Meldal, M., Peptidotriazoles on Solid Phase: [1,2,3]-Triazoles by Regiospecific Copper(I)-Catalyzed 1,3-Dipolar Cycloadditions of Terminal Alkynes to Azides. *The Journal of Organic Chemistry* **2002,** *67* (9), 3057-3064.

55.   Wang, Q.; Chan, T. R.; Hilgraf, R.; Fokin, V. V.; Sharpless, K. B.; Finn, M. G., Bioconjugation by Copper(I)-Catalyzed Azide-Alkyne [3 + 2] Cycloaddition. *Journal of the American Chemical Society* **2003,** *125* (11), 3192-3193.

56.   Ricardo, C.; Pintauer, T., Copper catalyzed atom transfer radical cascade reactions in the presence of free-radical diazo initiators as reducing agents. *Chemical Communications* **2009,** (21), 3029-3031.

57.   Ricardo, C. L.; Pintauer, T., One-Pot Sequential Azide–Alkyne [3+2] Cycloaddition and Atom Transfer Radical Addition (ATRA): Expanding the Scope of In Situ Copper(I) Regeneration in the Presence of Environmentally Benign Reducing Agent. *European Journal of Inorganic Chemistry* **2011,** *2011* (8), 1292-1301.

58.   Ricardo, C. L.; Pintauer, T., Synthesis of Functionalized Polytriazoles via One-Pot Sequential Copper-Catalyzed Azide-Alkyne [3+2] Cycloaddition and Atom Transfer Radical Addition (ATRA). *Israel Journal of Chemistry* **2012,** *52* (3/4), 320-327.

59.   Ricardo, C. L. P., Tomislav, Highly Efficient Organicand Macromolecular Synthesis Using Sequential CopperCatalyzed Azide-Alkyne [3+2] Cycloaddition and ATRA/ATRP. *ACS symposium series* **2012,** *1100* (Progress in Controlled Radical), 73-98.

60.   Evans, V.; Duncanson, P.; Motevalli, M.; Watkinson, M., An investigation into the synthesis of azido-functionalised coumarins for application in 1,3-dipolar "click" cycloaddition reactions. *Dyes and Pigments* **2016,** *135*, 36-40.

61.   Fokin, V. V.; Matyjaszewski, K., CuAAC: The Quintessential Click Reaction. In *Organic Chemistry – Breakthroughs and Perspectives*, Wiley-VCH Verlag GmbH & Co. KGaA: 2012; pp 247-277.

62.   Kolb, H. C.; Finn, M. G.; Sharpless, K. B., Click Chemistry: Diverse Chemical Function from a Few Good Reactions. *Angewandte Chemie International Edition* **2001,** *40* (11), 2004-2021.

63.   Kolb, H. C.; Sharpless, K. B., The growing impact of click chemistry on drug discovery. *Drug Discovery Today* **2003,** *8* (24), 1128-1137.

64.   Matyjaszewski, K.; Tsarevsky, N. V., Macromolecular Engineering by Atom Transfer Radical Polymerization. *Journal of the American Chemical Society* **2014,** *136* (18), 6513-6533.

65.   Adams, M. L.; Lavasanifar, A.; Kwon, G. S., Amphiphilic block copolymers for drug delivery. *Journal of Pharmaceutical Sciences* **2003,** *92* (7), 1343-1355.

66.   Aryal, S.; Prabaharan, M.; Pilla, S.; Gong, S., Biodegradable and biocompatible multi-arm star amphiphilic block copolymer as a carrier for hydrophobic drug delivery. *Int J Biol Macromol* **2009,** *44* (4), 346-352.

67.   Khanna, K.; Varshney, S.; Kakkar, A., Miktoarm star polymers: advances in synthesis, self-assembly, and applications. *Polymer Chemistry* **2010,** *1* (8), 1171-1185.

68.   Kurniasih, I. N.; Keilitz, J.; Haag, R., Dendritic nanocarriers based on hyperbranched polymers. *Chemical Society Reviews* **2015,** *44* (12), 4145-4164.

69.   Langer, R., Drug delivery and targeting. *Nature* **1998,** *392* (6679), 5.

70.   Li, Y.; Guo, H.; Zheng, J.; Gan, J.; Zhang, Y.; Guan, X.; Wu, K.; Lu, M., Synthesis and encapsulation of an amphiphilic thermoresponsive star polymer with [small beta]-cyclodextrin and hyperbranched poly(oligo(ethylene glycol)methacrylate) as building blocks. *RSC Advances* **2014,** *4* (97), 54268-54281.

71.   Prausnitz, M. R.; Langer, R., Transdermal drug delivery. *Nature Biotechnology* **2008,** *26* (11), 1261-1268.

72.   Richard, R. E.; Schwarz, M.; Ranade, S.; Chen, A. K.; Matyjaszewski, K.; Sumerlin, B., Acrylate-based copolymers preapred by ATRP as matrices for drug delivery. *ACS Symposium Series* **2006,** *1* (1), 234-251.

73.   Blencowe, A.; Tan, J. F.; Goh, T. K.; Qiao, G. G., Core cross-linked star polymers via controlled radical polymerisation. *Polymer* **2009,** *50* (1), 5-32.

74.   Gao, H.; Matyjaszewski, K., Synthesis of Miktoarm Star Polymers via ATRP Using the "In−Out" Method: Determination of Initiation Efficiency of Star Macroinitiators. *Macromolecules* **2006,** *39* (21), 7216-7223.

75.   Yang, R., *Analytical Methods for Polymer Characterization*. 1 ed.; CRC Press Taylor and Francis Group: 2018; Vol. 1.

76.   Charles E. Carraher, J., *Introduction to Polymer Chemistry*. 3 ed.; CRC Press Taylor and Francis Group: 2013; Vol. 1, p 1-530.

77.   Young, R. J.; Lovell, P. A., *Introduction to Polymers*. 3 ed.; CRC Press Taylor and Francis Group: 2011.

78.   Ivin, K. J., Characterization of copolymers by NMR spectroscopy. *Pure and Applied Chemistry* **1983,** *55* (10), 1529-1540.

79.   Wesdemiotis, C., Multidimensional Mass Spectrometry of Synthetic Polymers and Advanced Materials. *Angewandte Chemie International Edition* **2017,** *56* (6), 1452-1464.

80.   Wesdemiotis, C.; Solak, N.; Polce, M. J.; Dabney, D. E.; Chaicharoen, K.; Katzenmeyer, B. C., Fragmentation pathways of polymer ions. *Mass Spectrometry Reviews* **2011,** *30* (4), 523-559.

81.   Altuntaş, E.; Krieg, A.; Baumgaertel, A.; Crecelius, A. C.; Schubert, U. S., ESI, APCI, and MALDI tandem mass spectrometry of poly(methyl acrylate)s: A comparison study for the structural characterization of polymers synthesized via CRP techniques and the software application to analyze MS/MS data. *Journal of Polymer Science Part A: Polymer Chemistry* **2013,** *51* (7), 1595-1605.

82.   Altuntaş, E.; Schubert, U. S., "Polymeromics": Mass spectrometry based strategies in polymer science toward complete sequencing approaches: A review. *Analytica Chimica Acta* **2014,** *808*, 56-69.

83.   Amalian, J.-A.; Trinh, T. T.; Lutz, J.-F.; Charles, L., MS/MS Digital Readout: Analysis of Binary Information Encoded in the Monomer Sequences of Poly(triazole amide)s. *Analytical Chemistry* **2016,** *88* (7), 3715-3722.

84.   Chaicharoen, K.; Polce, M. J.; Singh, A.; Pugh, C.; Wesdemiotis, C., Characterization of linear and branched polyacrylates by tandem mass spectrometry. *Analytical and Bioanalytical Chemistry* **2008,** *392* (4), 595-607.

85.   Crotty, S.; Gerişlioğlu, S.; Endres, K. J.; Wesdemiotis, C.; Schubert, U. S., Polymer architectures via mass spectrometry and hyphenated techniques: A review. *Analytica Chimica Acta* **2016,** *932*, 1-21.

86.   Altuntaş, E.; Kempe, K.; Crecelius-Vitz, A.; Richard, H.; Schubert, U., *ESI-MS & MS/MS Analysis of Poly (2-oxazoline) s with Different Side Groups*. 2010.

87.   Yol, A. M.; Dabney, D. E.; Wang, S.-F.; Laurent, B. A.; Foster, M. D.; Quirk, R. P.; Grayson, S. M.; Wesdemiotis, C., Differentiation of Linear and Cyclic Polymer Architectures by MALDI Tandem Mass Spectrometry (MALDI-MS2). *Journal of The American Society for Mass Spectrometry* **2013,** *24* (1), 74-82.

88.   Yol, A. M.; Janoski, J.; Quirk, R. P.; Wesdemiotis, C., Sequence Analysis of Styrenic Copolymers by Tandem Mass Spectrometry. *Analytical Chemistry* **2014,** *86* (19), 9576-9582.

89.   Yol, A. M.; Wesdemiotis, C., Multidimensional mass spectrometry methods for the structural characterization of cyclic polymers. *Reactive and Functional Polymers* **2014,** *80*, 95-108.

90.   Bates, F. S.; Hillmyer, M. A.; Lodge, T. P.; Bates, C. M.; Delaney, K. T.; Fredrickson, G. H., Multiblock Polymers: Panacea or Pandora's Box? *Science* **2012,** *336* (6080), 434-440.

91.   Porel, M.; Alabi, C. A., Sequence-Defined Polymers via Orthogonal Allyl Acrylamide Building Blocks. *Journal of the American Chemical Society* **2014,** *136* (38), 13162-13165.

2. DESIGN AND SYNTHESIS OF SMALL FUNCTIONALIZED MOLECULES USING ATOM TRANSFER RADICAL ADDITION

2.1 *Motivation*

The objective of this project was to develop a methodology to synthesize ATRA products in high yields utilizing common monomers and a variety of multifunctional initiators. The initiator architecture varied between linear, telechelic, and star-shaped, providing an excellent scaffold to perform additional organic transformations. Specifically, the copper-catalyzed azide-alkyne cycloaddition (CuAAC) was used to "click" functionalized coumarin dye onto the small molecules, which fluoresce upon formation of the triazole linkage. These small molecules would be excellent candidates for bioimaging applications, as the fluorescent properties only become visible upon reaction completion due to the quenching effect the azide moiety provides on the coumarin dye. Method optimization began using the telechelic initiator to determine ideal reaction conditions. It is envisioned that once optimized; the methodology will be extended to other multifunctional, star-shaped initiators.

2.2 *Research Objectives*

Specific Aim 1: Synthesis and characterization of multifunctional initiators/alkenes (**1-8**) and monohalogenated initiators (**9-10**) for copper-catalyzed ATRA/ATRP (Figure 2.1).

Specific Aim 2: Screening the synthetic capability of photoinduced, copper-catalyzed ATRA of multifunctional initiators to various alkenes and monohalogenated initiators to multifunctional alkenes.

Specific Aim 3: Isolate desired adducts and characterize using ^{1}H NMR spectroscopy and mass spectrometry. Perform CuAAC to generate functionalized polytriazoles and further characterize.

BBiBE (1) TBiBE (2) PTBiB (3) DPBiB (4)

EGDA (5) TETA (6) PETA (7) DPHA (8)

PBiB (9) BMPAP (10) EBiB (11)
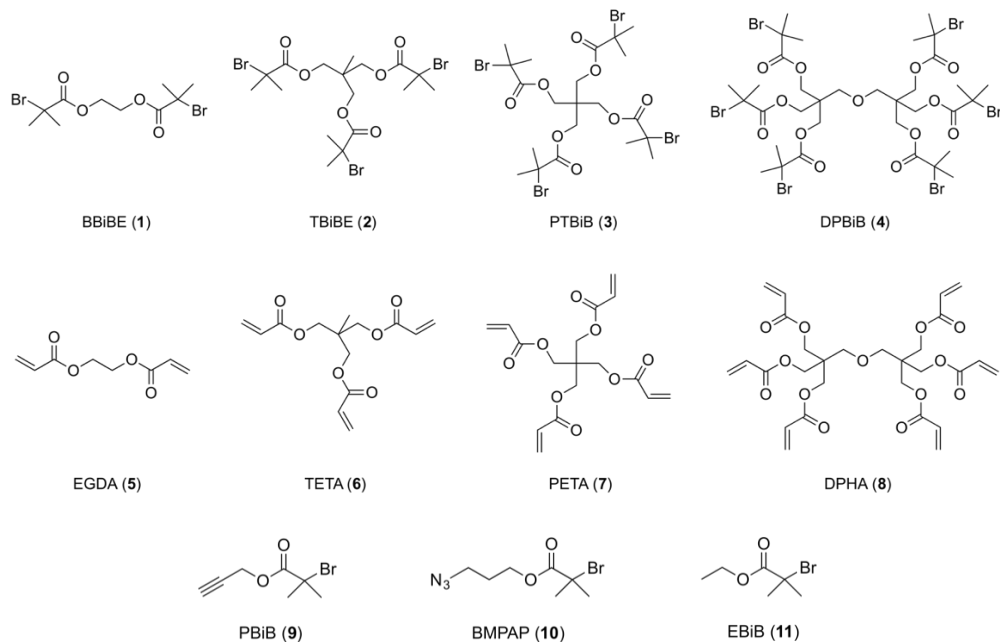
Figure 2.1 Proposed multifunctional initiators (**1-4**), multifunctional alkenes (**5-8**), and monohalogenated initiators (**9-11**) utilized in atom transfer radical processes.

2.3 *Introduction to PhotoATRA and CuAAC*

The ability to add halogenated compounds to alkenes or alkynes via radical means is one of the fundamental reactions in organic chemistry.[1-2] Copper-catalyzed atom transfer radical addition (ATRA) is often used to facilitate this transformation due to the precise and facile carbon-carbon bond formation.[3-8] Traditionally, ATRA is conducted in the presence of reducing agents to generate the copper (I) species in situ. More recently, the emergence of photoinduced ATRA reactions have eliminated the need for additional reagents to reduce the copper (II) species, making the process more synthetically attractive.[8-20] Coupling this efficient process with a host of multifunctional initiators allows for the synthesis of well-defined architectures, which act as an excellent scaffold for adding interesting functionalities.

Another example of a synthetically attractive carbon-carbon bond-forming reaction falls under the "click" chemistry umbrella. In 2001, the revival of an old style of organic synthesis

was defined in response to the demands of modern chemistry. The term was coined "click chemistry," and designated reactions which are modular, broad in scope, generate high yields, and produce nonhazardous byproducts that can be removed without chromatography. The process characteristics include simple reaction conditions, readily available starting material, and benign or no solvents.[21-22] Of those reactions which meet the stringent criteria, the copper-catalyzed azide-alkyne [3+2] cycloaddition (CuAAC) was the first to achieve "click status." Popularized by the seminal work of the Sharpless[21] and Meldal[23] laboratories, this reaction is accompanied with a myriad of attractive qualities. To date, CuAAC has demonstrated efficacy through reliability, robustness, and desirable properties of the triazole moiety.[24-28] Various applications of this chemistry have been found in aspects of bioconjugation,[29] materials science,[30] transition metal chelation,[26] pharmaceutical drug screenings,[31] and also radiolabeling.[32]

2.4 *Results and Discussion*

2.4.1 *S.A. #1: Preparation of initiators, alkenes, and coumarin dye*

The preparation of multifunctional initiators (**1-4**), multifunctional alkenes (**5-8**), and monohalogenated initiators (**9-10**) were adopted from methods previously reported in the literature.[33-39] Initiator **11** was purchased commercially due to the inexpensive nature in comparison with the other proposed brominated species. All initiator reactions proceeded via esterification of primary alcohols using stoichiometric amounts of α-bromoisobutyryl bromide and triethylamine as a proton sink. The synthesis of initiators **1**, **2**, **9**, and **10** progressed efficiently based on ^{1}H NMR spectra of crude reaction mixtures; however, they were purified via flash chromatography to ensure a pure product. After initiator **10** was prepared and purified, a simple substitution reaction using sodium azide was utilized to displace the halogen functionality

for an azide moiety. Multifunctional alkenes were prepared in a similar fashion, but the esterification was carried out using a stoichiometric amount of acryloyl chloride with triethylamine as a proton sink. The synthesis of alkenes **5** and **6** proceeded smoothly but were also purified with normal phase flash chromatography. All ^{1}H NMR spectra of purified initiators and alkenes can be viewed in the Appendix.

The coumarin dye proposed for this work was prepared in a multi-step process adopted from the literature,[40] first beginning with the preparation of 3-nitro-7-diethylaminocoumarin. This was accomplished by treating 4-(dimethylamino)salicylaldehyde with a stoichiometric amount of ethylnitroacetate under reflux in n-butanol. From there, an amination of the nitro group could be accomplished using SnCl$_2$ and HCl. Substitution of the amino group with an azide moiety was conducted using NaN$_3$, and the bright yellow powder was afforded after column chromatography as 3-azido-7-diethylaminocoumarin. The preparation of the azide-bearing coumarin dye can be viewed in Scheme 2.1. ^{1}H NMR spectra of the precursors and purified final product can be viewed in the Appendix.
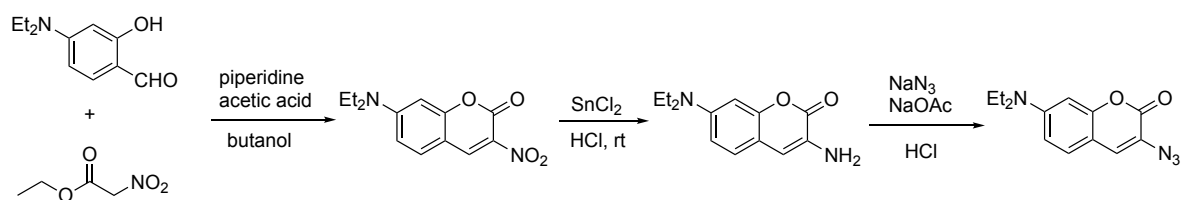
Scheme 2.1 Preparation of 3-azido-7-diethylaminocoumarin

2.4.2 *S.A. #2: Screening the synthetic capability of photoATRA*

To elucidate ideal reaction conditions, a baseline was obtained using literature photoATRP conditions[11] with a stoichiometric amount of monomer to hinder oligomerization. Within 3 hours, nearly 94% monomer conversion was achieved with an underwhelming 34% diadduct yield (Figure 2.2). This trend suggests the system is highly active regarding monomer

conversion; however, the product selectivity is poor. This can be attributed to radical termination reactions and/or oligomerization via repeat monomer addition.
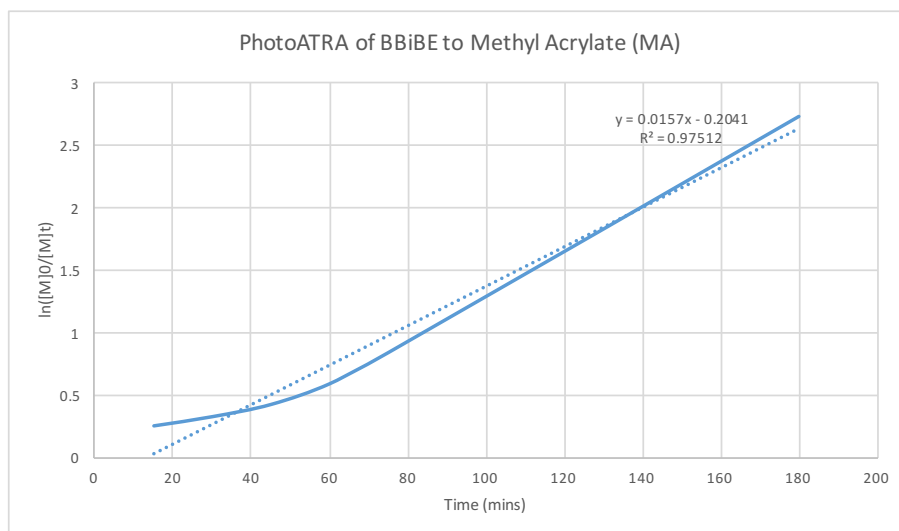
Figure 2.2 Copper-catalyzed photoATRA of bifunctional initiator BBiBE (**1**) to methyl acrylate (MA). Conditions: $[BBiBE]_0:[MA]_0:[CuBr_2]_0:[Me_6TREN]_0$ = 1:2:0.02:0.12 at ambient temperature in DMSO. $[Alkene]_0$ = 50% (v/v). Wavelength of light used = 365 nm. Conversions/yields were calculated from ^1H NMR spectra using p-dimethoxybenzene as an internal reference (relative errors are ±10%).

Evaluating the solvent system was the first parameter to optimize, as it can heavily influence the equilibrium constant for atom transfer processes, $K_{ATRA/ATRP}$. Dimethylsulfoxide (DMSO) was originally chosen as the solvent due to the high $K_{ATRA/ATRP}$ value, which ultimately governs the rate of polymerization. Due to the poor diadduct yield, methanol was chosen as an alternative. This is attributed to the lower value for the equilibrium constant associated with methanol and also it is a commonly used solvent for traditional ATRA reactions.

The monomer conversion and diadduct yields of BBiBE to various acrylates can be viewed in Table 2.1. The data indicates a marginal difference between the two solvent systems, both providing rapid monomer conversion with catalyst loadings as low as 0.02 mol%, relative to

initiator. Methanol had provided a slightly higher product selectivity across the acrylates which were screened. In the case of BBiBE (**1**) to ethyl acrylate (EA) (Entries 5-8), methanol afforded up to 7% higher yield than the comparative DMSO reaction. However, the yields obtained have been less than desirable, with the highest reaching 39% (Entry 1, DMSO; Entry 2, MeOH). Methanol was chosen as a solvent for further studies, as it provided slightly higher yields during the study. It is also a much more desirable solvent to work with as it can be easily removed under vacuum, whereas DMSO requires multiple water washes to be eliminated.

Table 2.1 Copper-catalyzed photoATRA of BBiBE (**1**) to various alkenes in dimethylsulfoxide (DMSO) and methanol (MeOH).
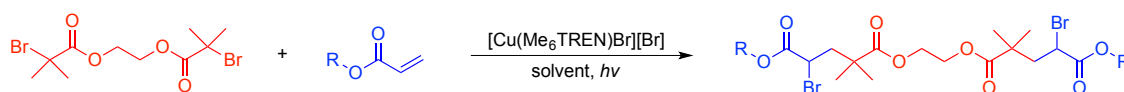
Entry[a]	Alkene	[Initiator]$_0$:[Cu^{II}]$_0$	% Conv. (DMSO)	% Yield (DMSO)	% Conv. (MeOH)	% Yield (MeOH)
1	MA	250:1	93	39	97	34
2		500:1	98	34	95	39
3		1000:1	81	34	86	38
4		5000:1	62	30	63	36
5	EA	250:1	99	30	99	33
6		500:1	95	29	97	34
7		1000:1	83	30	77	37
8		5000:1	45	24	60	33
9	EGMEA	250:1	100	25	99	27
10		500:1	97	30	99	27
11		1000:1	70	29	99	26
12		5000:1	55	29	81	31
13	PA	250:1	73	31	90	32
14		500:1	64	31	90	30
15		1000:1	47	29	82	31
16		5000:1	57	31	63	31

[a]All reactions were performed with [Cu(Me$_6$TREN)Br][Br] in DMSO or MeOH for 24 hours at ambient temperature. [Alkene]$_0$ = 2.68 M. Wavelength of light used = 365 nm. Conversions/yields were calculated from ^{1}H NMR spectra using *p*-dimethoxybenzene as an internal reference (relative errors are ±10%).

To increase the selectivity of the desired diadduct, the alkene concentration was altered in a comparative study between BBiBE (**1**) and EA. The preliminary data indicates that the yields are not substantially impacted when varying the alkene concentration between 1.34 M and 4.02 M. As expected, the monomer conversion exceeded 99% with the higher alkene concentrations (Entries 5, 9, and 10); however, the product selectivity was slightly impacted. The highest yield for the reaction of BBiBE (**1**) to EA was 39% (Entries 1 and 2), with conversions of 85% and 80%, respectively. An alkene concentration of 1.34 M was utilized with future reactions, as lower alkene concentrations tend to retard polymerization.

Table 2.2 Varying alkene concentrations in copper-catalyzed photoATRA of BBiBE (**1**) to EA.
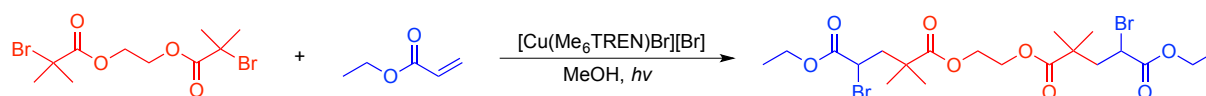
Entry[a]	[Alkene]$_0$	[Initiator]$_0$:[Cu^{II}]$_0$	% Conversion	% Yield
1	1.34 M	250:1	85	39
2		500:1	80	39
3		1000:1	44	34
4		5000:1	35	29
5	2.68 M	250:1	99	33
6		500:1	97	34
7		1000:1	77	37
8		5000:1	60	33
9	4.02 M	250:1	99	29
10		500:1	99	29
11		1000:1	93	33
12		5000:1	51	32

[a] All reactions were performed with [Cu(Me$_6$TREN)Br][Br] in MeOH for 24 hours at ambient temperature. Wavelength of light used = 365 nm. Conversions/yields were calculated from ^{1}H NMR spectra using *p*-dimethoxybenzene as an internal reference (relative errors are ±10%).

To further increase product selectivity, a new catalyst and higher loading was utilized. Preliminary results signify the product selectivity is not substantially impacted when changing the catalyst to [Cu^{II}(TPMA)Br][Br]. Increasing the catalyst loading did increase the overall rate

of the reaction, reaching 75-86% conversion in just 8 hours (Table 2.3). However, the selectivity

was minimally affected, as the highest diadduct yield observed was 44% using a catalyst loading

of 2 mol%, relative to initiator (Entry 3). Moving forward, the TPMA catalyst complex was

utilized as it is synthesized in a simpler fashion than Me_6TREN, which requires an arduous

distillation for purification.

Table 2.3 Varying RX concentrations, relative to alkene, in copper-catalyzed photoATRA of

BBiBE (**1**) to MA.
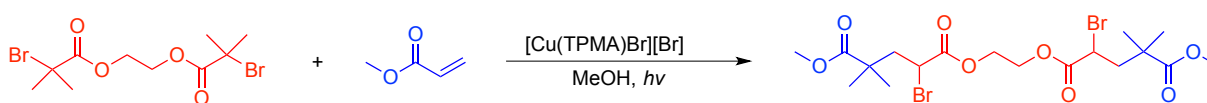
Entry[a]	[Initiator]$_0$:[Cu^{II}]$_0$	% Conversion	% Yield
1	10:1	86	39
2	25:1	78	41
3	50:1	73	44
4	100:1	75	41

[a] Reaction was performed with [Cu(TPMA)Br][Br] in MeOH for 8 hours at ambient
temperature. [Alkene]$_0$ = 1.34 M. Wavelength of light used = 365 nm. Conversions/yields
were calculated from ^{1}H NMR spectra using *p*-dimethoxybenzene as an internal reference
(relative errors are ±10%).

In a quest for increased product selectivity, an extensive literature search was performed

on recent photoinduced radical reactions with varying temperature. Haddleton et al. hypothesized

that lower reaction temperatures would hinder unwanted termination events and/or side

reactions. Indeed, the use of a cooling plate for the homopolymerization of MA allotted a

narrower dispersity (Đ = 1.20 vs. 1.40 for typical UV experiment).[19] A similar system was

utilized to probe whether temperature had implications on product selectivity in photoATRA

reactions. The system consisted of ice-cooled water which flowed through tubing continuously,

located inside of the UV reactor. The temperature inside of the UV reactor was measured to be

55 °C for a typical UV experiment, whereas the water-cooled UV box reached only 30 °C.

Encouragingly, an overall slight increase in selectivity was observed for the photoATRA of

BBiBE (**1**) to MA under similar conditions. Using a 1000:1 catalyst loading provided 86%

conversion and 45% yield (Entry 3), which is a 1% increase from the previous diadduct yield

using 20x less catalyst.

Table 2.4 PhotoATRA of BBiBE (**1**) to MA using decreased temperatures.
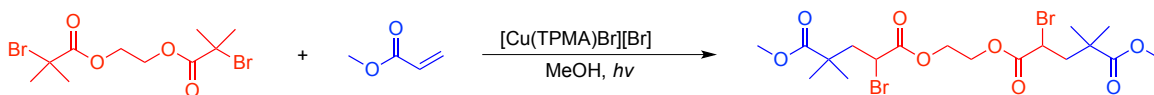
Entry[a]	$[\text{Initiator}]_0:[\text{Cu}^{II}]_0$	% Conversion	% Yield
1	250:1	87	44
2	500:1	82	43
3	1000:1	86	45
4	5000:1	86	35

[a] Reaction was performed with [Cu(TPMA)Br][Br] in MeOH for 24 hours at decreased temperature (~30 °C). [Alkene]$_0$ = 1.34 M. Wavelength of light used = 365 nm. Conversions/yields were calculated from ^{1}H NMR spectra using p-dimethoxybenzene as an internal reference (relative errors are ±10%).

Still unsatisfied by the overall selectivity of the reaction, we probed increasing the alkyl halide

concentration in solution, relative to alkene. This should promote single monomer additions to

each reactive site on the bifunctional initiator, increasing the selectivity of the desired product.

This is owed to the higher stability of the tertiary radical on the unreacted alkyl halide, rather

than re-activating a secondary radical, which is less stable. The experiment consisted of 3

different reactions of varying alkyl halide concentrations: [Initiator]$_0$:[Alkene]$_0$ = 1.5:2, 2:2, and

4:2, where the typical water-cooled UV experiment contained a stoichiometric amount of

monomer ([Initiator]$_0$:[Alkene]$_0$ = 1:2). As expected, quantitative conversion was observed for

higher catalyst loadings using an increased alkyl halide concentration (Figure 2.3A).

Promisingly, the reactions exhibited an increase in selectivity (Figure 2.3B). The highest yield

observed was 54%, using the [Initiator]$_0$:[Alkene]$_0$ = 1.5:2 (blue). Through optimizing

photoATRA reaction conditions, the yield of BBiBE (**1**) to MA was significantly increased from 34% to 54%. It is envisioned that a comparable yield will be obtained once this methodology is extended to other multifunctional initiators.
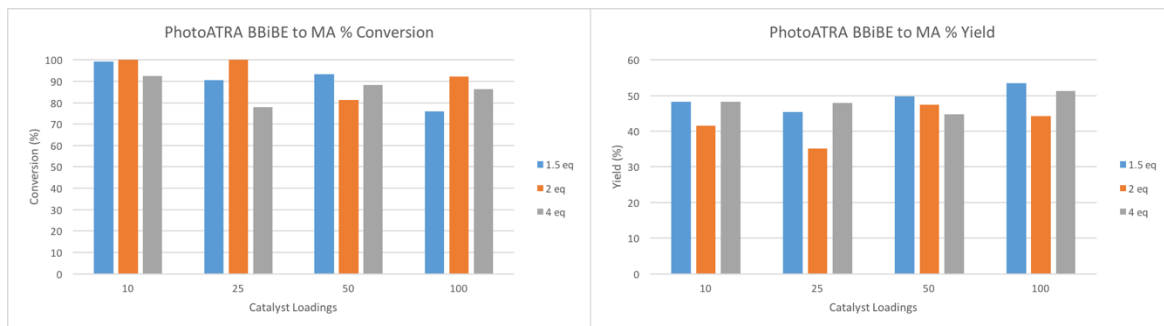
Figure 2.3 Conversion (left) and yield (right) from photoATRA of BBiBE (**1**) to MA using excess alkyl halide. Reaction was performed with [Cu(TPMA)Br][Br] in MeOH for 20 hours at decreased temperature (~30 °C). [Alkene]$_0$ = 1.34 M. Wavelength of light used = 365 nm. Conversions/yields were calculated from ^{1}H NMR spectra using *p*-dimethoxybenzene as an internal reference (relative errors are ±10%).

      Looking towards achieving higher diadduct selectivity, a new reaction strategy was implemented in which monohalogenated initiators were added to a multifunctional alkene. This will generate species with a nearly-identical molecular architecture to the previous method. It is envisioned that this solution will not only provide a higher yield but will eliminate the problem of constitutional isomeric separation. The first reaction performed consisted of the azide-terminated BMPAP (**10**) and EGDA (**5**). Promising results were obtained conducting the photoATRA reaction with non-optimized conditions (Table 2.5). All catalyst loadings provided quantitative conversion of starting material in just 6 hours. The highest yield observed was 47%, using one mol% of catalyst, relative to initiator (Entry 1). Using as low as 0.1 mol% of catalyst provided a yield of 40% (Entry 4).

Table 2.5 PhotoATRA of BMPAP (**10**) to EGDA (**5**) using non-optimized conditions.
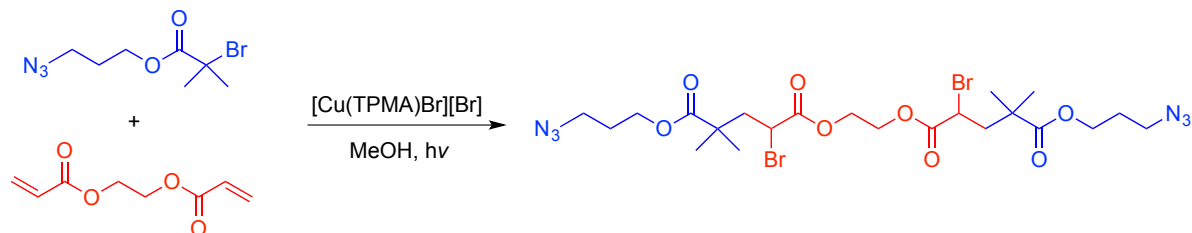
Entry[a]	[Initiator]$_0$:[Cu^{II}]$_0$	% Conversion	% Yield
1	100:1	99	47
2	250:1	99	43
3	500:1	99	41
4	1000:1	99	40

[a] Reaction was performed with [Cu(TPMA)Br][Br] in MeOH for 24 hours at ambient temperature. [Alkene]$_0$ = 1.34 M. Wavelength of light used = 365 nm. Conversions/yields were calculated from ^{1}H NMR spectra using *p*-dimethoxybenzene as an internal reference (relative errors are ±10%).

Evaluating the light source was an additional parameter to optimize, as it most influenced the increase in yields in the previous photoATRA reactions using BBiBE (**1**). Three different light sources were used in a comparative study to evaluate which radiation provided good conversion with an acceptable selectivity: The traditional UV light source, a water-cooled UV light source, and a light-emitting diode (LED) lamp with color adjustments. Astounding results were observed for the study (Table 2.6). The UV lamp reaction did exhibit a high conversion of 95% in just 4 hours; however, the selectivity was diminished with a 47% yield (Entry 1). An increased reaction time of 12 hours was utilized for the water-cooled UV reaction, providing a conversion of 89%. The selectivity was positively impacted, and a 12% increase in yield was observed (Entry 2). Using the blue LED light required a longer reaction time (20 hours), but still afforded a 93% conversion and a gratifying yield of 70% (Entry 3). The LED light source will be used in future reactions, but with white light instead. A more comprehensive coverage of the visible spectrum will provide faster conversions with comparable selectivity.

Table 2.6 PhotoATRA of BMPAP (**10**) to EGDA (**5**) using various light sources.
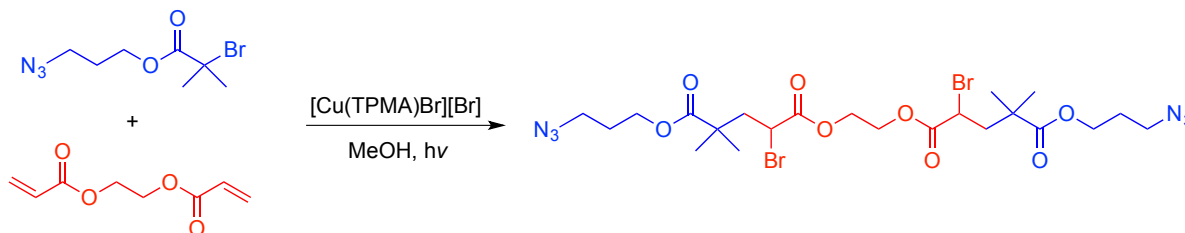
Entry[a]	Light Source	Time (hr)	% Conversion	% Yield
1	UV	4	94	47
2	Water-cooled UV	12	89	56
3	Blue LED	20	93	70

[a] Reaction was performed with 2 mol% [Cu(TPMA)Br][Br] relative to initiator in MeOH. [Alkene]$_0$ = 0.75 M. Blue LED light source used. Conversions/yields were calculated from ^{1}H NMR spectra using *p*-dimethoxybenzene as an internal reference (relative errors are ±10%).

Enthused by results, the alkyne-terminated PBiB (**9**) replaced BMPAP (**10**) to ensure the LED light system was working for a variety of initiator substrates. A baseline was first obtained using the non-optimized conditions for the photoATRA of PBiB (**9**) to EGDA (**5**). Initial observations indicate the reaction behaves very similarly as the previous non-optimized reaction employing BMPAP (**10**). The 250:1 and 500:1 loading both provided 87% conversion with a 49% and 47% yield, respectively. Using 0.1 mole% provided a slightly lower conversion of 81% while still generating a modest yield of 48% (Entry 3).

Table 2.7 PhotoATRA of PBiB (**9**) to EGDA (**5**) using non-optimized conditions.
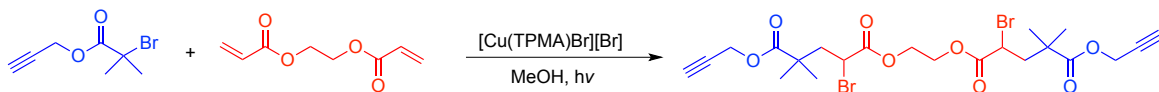
Entry[a]	$[\text{Initiator}]_0:[\text{Cu}^{II}]_0$	% Conversion	% Yield
1	250:1	87	49
2	500:1	87	47
3	1000:1	81	48
4	5000:1	83	39

[a] Reaction was performed with [Cu(TPMA)Br][Br] in MeOH for 24 hours. $[\text{Alkene}]_0 = 2.0$ M. Wavelength of light used = 365 nm. Conversions/yields were calculated from ^{1}H NMR spectra using *p*-dimethoxybenzene as an internal reference (relative errors are ±10%).

Employing previously-optimized conditions from BMPAP (**10**) to EGDA (**5**) had a substantial impact on the selectivity of the photoATRA reactions (Table 2.8). Utilizing the white LED light source instead of the UV lamp allowed the reaction mixture to stay near room temperature, which hindered oligomerization. Providing excess alkyl halide initiator, relative to alkene, influenced the atom transfer radical process to favor single additions, rather than polymerizations. More dilute conditions should provide less polymerization, as the previous reactions exhibited a noticeable increase in viscosity. A final optimization experiment was performed to test the effect of altering the alkene concentration in solution. Four different concentrations were gauged: 0.75 M, 1.00 M, 1.25 M, and 1.34 M, and compared against the previous reaction ($[\text{alkene}]_0$=2.0 M). As expected, the reactions containing higher alkene concentrations exhibit a near-quantitative or quantitative conversion (Entries 1 and 2). However, it was noted that the 1.00 M reaction vessel displayed excellent selectivity, generating a 73% yield (Entry 3). Also, the mixture was not as viscous, enabling a more efficient product handling and NMR sample preparation.

Table 2.8 PhotoATRA of PBiB (**9**) to EGDA (**5**) altering alkene concentration.
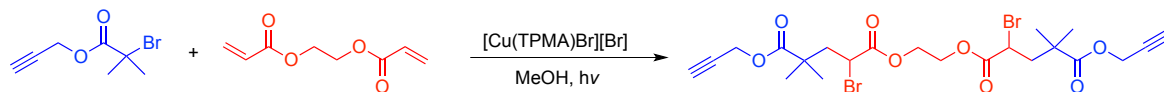
Entry[a]	[Alkene]$_0$ (M)	% Conversion	% Yield
1	1.34	99	64
2	1.25	97	67
3	1.00	93	73
4	0.75	84	63

[a] Reaction was performed with [Cu(TPMA)Br][Br] in MeOH for 24 hours. [Alkene]$_0$ was varied. White LED light source used. Conversions/yields were calculated from ^{1}H NMR spectra using *p*-dimethoxybenzene as an internal reference (relative errors are ±10%).

Through optimizing the reaction conditions, the photoATRA of BMPAP (**10**) to EGDA (**5**) afforded a significant increase in yield from 47% to 70% while still providing adequate conversion in a reasonable reaction time. Moreover, the reaction of PBiB (**9**) to EGDA (**5**) displayed quantitative conversions while drastically increasing yields from 49% to 73%. Based on data generated from preliminary results, the optimized photoinduced ATRA reactions show excellent potential in small molecule synthesis. Moving forward, this methodology will be extended to other multifunctional acrylate species in efforts to expand the synthetic capability through the synthesis of small, star-shaped molecules.

2.4.3 S.A. #3: CuAAC reactions using isolated photoATRA products

PhotoATRA reactions using BBiBE (**1**) were implemented to isolate larger quantities of desired diadducts to perform future transformations. Diadducts were separated from one another using flash column chromatography with an EtOAc/hexanes eluent. Compounds that did not retain azide or alkyne groups had the halogen functionality substituted for an azido moiety via S$_N$2 with sodium azide in DMF. Preliminary data, shown in Table 2.9, indicate a relatively facile conversion with the employed diadducts. The conversion of BBiBE-MA afforded a 63% yield

(Entry 1), whereas the ethyl- and ethylene glycol methyl ether acrylate substrates afforded a 75% and 56% yield, respectively (Entries 2 and 3).

Table 2.9 Conversion of halogen functionality to azide from BBiBE (**1**) diadduct.
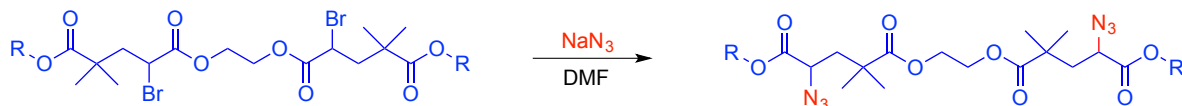
Entry[a]	R =	Yield[b]
1	Methyl	63
2	Ethyl	75
3	Methyl Ethylene Glycol	56

[a]All azide conversions were carried out under the following conditions: [Halogen]$_0$:[NaN$_3$]$_0$ = 1:1.5. [Adduct]$_0$ = 0.1 M. Reaction was conducted in DMF at room temperature for 24 hours. [b]Yields were calculated from mass of the final product.

Triadducts generated from the photoATRA of TBiBE (**2**) to various acrylates also had been separated in an analogous fashion. It was noted that, although HRMS confirmed the presence of triadducts only, ^{1}H NMR analysis reveals multiple additions occurring on the same side of initiator. This generates constitutional isomers that are unable to be separated from one another using flash column chromatography, making the ^{1}H NMR spectra appear unclean. The halogen functionalities were similarly substituted for azide moieties. Overall, the yields were slightly higher for the trifunctional adduct with regards to the bifunctional counterpart (Table 2.10). The conversion of TBiBE-MA afforded an acceptable yield of 76% (Entry 1); whereas the TBiBE-EA generated an excellent yield of 84% (Entry 2). ^{1}H NMR spectra of the isolated adducts and corresponding azides can be viewed in the Appendix.
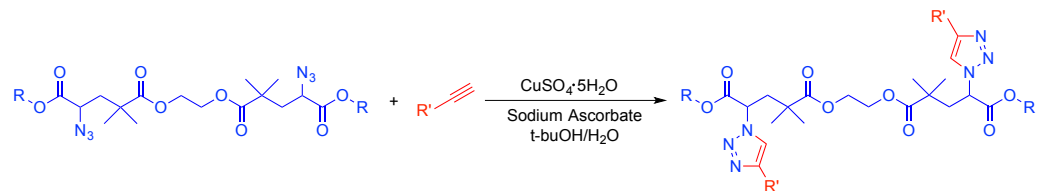
Table 2.10 Conversion of halogen functionality to azide from TBiBE (**2**) triadduct.
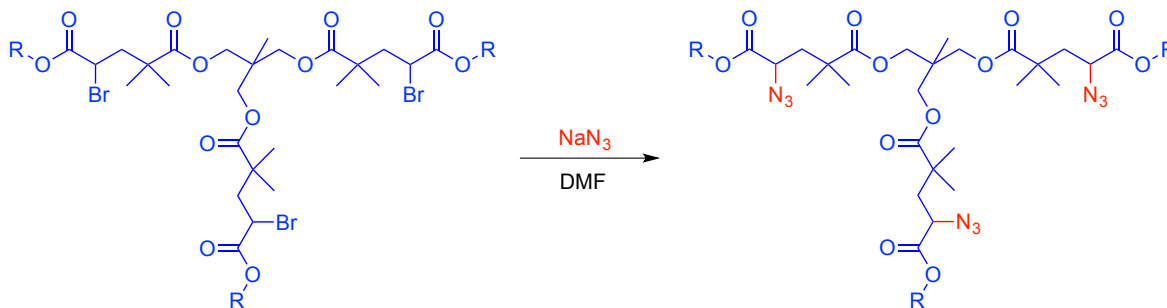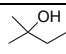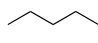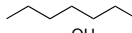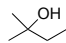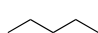
Entry[a]	R =	Yield[b]
1	Methyl	76
2	Ethyl	84
3	Methyl Ethylene Glycol	66

[a]All azide conversions were carried out under the following conditions: $[Halogen]_0 : [NaN_3]_0 = 1:1.5$. Reaction was conducted in DMF at room temperature for 24 hours. [b]Yields were calculated from mass of the final product.

Once azide moieties were incorporated, CuAAC was performed to generate corresponding, triazole-functionalized molecules. Click reactions are conducted in a *t*-buOH/H$_2$O media using sodium ascorbate as a reducing agent. Upon formation, the insoluble triazole-bearing compound precipitated out of solution in the form of an oil, which was extracted using diethyl ether. Yields ranged from poor to excellent for the CuAAC reactions conducted using the separated diadducts (Table 2.11). For the reaction of 3-methyl-1-pentyn-3-ol with diadduct BBiBE-MA, an excellent yield of 93% was observed (Entry 1); however, using an identical substrate with 1-hexyne and 1-octyne, yields of 46% and 45% were obtained, respectively (Entries 2 and 3). An increased yield of 70% was generated using BBiBE-EA and 1-hexyne (Entry 5).

Table 2.11 CuAAC of BBiBE (**1**) diadduct with various alkynes.

Entry[a]	R =	R' =	Yield[b]
1	CH$_3$	(OH structure)	93
2		(chain structure)	46
3		(chain structure)	45
4	CH$_2$CH$_3$	(OH structure)	58
5		(chain structure)	70

[a]Click conditions: [Azide]$_0$:[Alkyne]$_0$:[CuSO$_4$•5H$_2$O]$_0$:[NaAsc]$_0$ = 1:2:0.05:0.3 in
t-butanol/H$_2$O (1:1) medium at 60 °C for 12 hours. [Alkyne]$_0$ = 0.2 M in solution.
[b]Isolated yield calculated from mass of final product.

Overall, higher conversions were obtained when the trifunctional adducts were employed
with analogous alkynes (Table 2.12). Reactions between 3-methyl-1-pentyn-3-ol with isolated
TBiBE-MA, TBiBE-EA, and TBiBE-EGMEA engendered isolated yields of 80%, 74%, and
59%, respectively (Entries 1, 2, and 3). The reaction of 1-hexyne and TBiBE-EGMEA produced
a yield of 69% (Entry 4), which is comparative to the reaction of BBiBE-EA with 1-hexyne.
Literature reports[44] indicate many triazole-bearing compounds are insoluble within this medium,
meaning they will precipitate as a solid product upon formation. A possible alternative to
increase low yields would be adjusting the solvent system, to favor product precipitation. This
would allow for the preferred filtration method, as compared to extraction.

Table 2.12 CuAAC of TBiBE (**2**) triadduct with various alkynes.
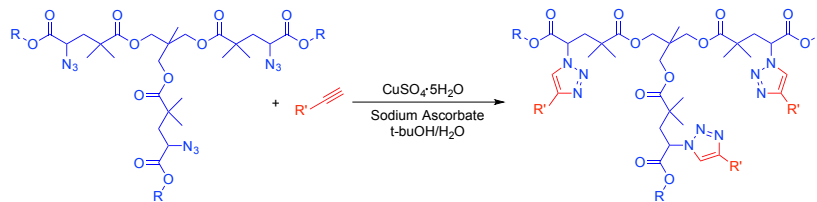
Entry[a]	R =	R' =	Yield[b]
1	CH_3	OH	80
2	CH_2CH_3	OH	74
3	$CH_2CH_2OCH_3$	OH	59
4	$CH_2CH_2OCH_3$		69

[a]Click conditions: $[Azide]_0$:$[Alkyne]_0$:$[CuSO_4 \bullet 5H_2O]_0$:$[NaAsc]_0$ = 1:2:0.05:0.3 in *t*-butanol/H_2O (1:1) medium at 60 °C for 12 hours. $[Alkyne]_0$ = 0.2 M in solution.
[b]Isolated yield calculated from mass of final product.

Desired adducts from photoATRA reactions of monohalogenated initiators to multifunctional alkenes were also isolated in an analogous fashion. It is valuable to point out that employing this synthetic route eliminates the formation of constitutional isomers in the mixture. This provides clean ^{1}H NMR spectra for BMPAP-EGDA and PBiB-EGDA, which can be viewed in the Appendix (Figure A2.13 and A2.14, respectively). Furthermore, there was the desired retention of the halogen moiety, as there is an azide/alkyne already present. PBiB-EGDA was further transformed using CuAAC with 3-azido-7-diethylamino coumarin, to generate a traizole-functionalized molecule (Figure A2.15). The original conditions for the previous CuAAC reactions were employed, but there were solubility issues regarding the coumarin dye. After exploring alternative reaction media, DMSO was found to solubilize starting materials and was chosen as the solvent. Unfortunately, there was only enough starting material to complete one CuAAC. After 24 hours reacting in a dark drawer, the product was precipitated out of solution, only to find partial starting material conversion. The desired product was isolated with chromatography to illustrate a successful click reaction through fluorescence. The reactants

themselves have no fluorescent properties; however, upon formation of the 1,4-triazole linkage, the product fluoresces intensely (Figure 2.4).
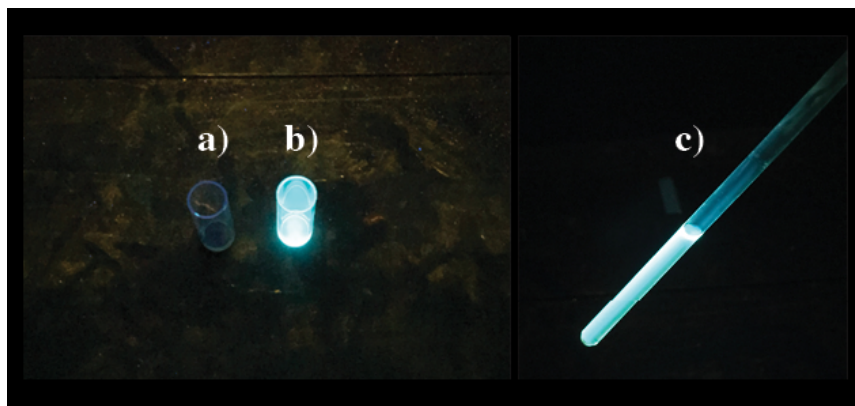
Figure 2.4 Crude reaction mixture before (a) and after (b) CuAAC, diluted with DCM. Isolated product (c) diluted with CDCl$_3$. All images photographed under 365 nm light source (UV).

2.5 *Conclusion*

The objective of this research was to synthesize small functionalized molecules using a photoinduced atom transfer radical polymerization in conjunction with a copper-catalyzed azide-alkyne cycloaddition. Through optimization, this unique methodology generated atom transfer products with a satisfying yield, which were upwards of 70% product selectivity. Prior to optimizations, the photoATRA process was affording yields around 30%, which is quite poor. These atom transfer products contained an alkyne or azide end group, making them suitable for conducting CuAAC with a functionalized Coumarin dye. This transformation afforded near-quantitative yields due to the robust nature of the CuAAC reaction. The reaction mixture prior to CuAAC exhibited no fluorescent activity; however, upon formation of the triazole linkage, the solution exhibited sharp fluorescence. It is envisioned that this methodology will be extended to other multifunctional alkenes using monohalogenated initiators for the production of fluorescent star-shaped molecules, which may have use in bioimaging or labelling.

2.6 *References*

1.   Curran, D. P., The Design and Application of Free Radical Chain Reactions in Organic Synthesis. Part 1. *Synthesis* **1988,** (06), 417-439.

2.   Curran, D. P., The Design and Application of Free Radical Chain Reactions in Organic Synthesis. Part 2. *Synthesis* **1988,** (07), 489-513.

3.   Pintauer, T., ATOM TRANSFER RADICAL ADDITION (ATRA) CATALYZED BY PPM AMOUNTS OF COPPER COMPLEXES. *Polymer Preprints* **2008,** *49* (2), 12-13.

4.   Pintauer, T., "Greening" of Copper Catalyzed Atom Transfer Radical Addition (ATRA) and Cyclization (ATRC) Reactions. *ACS symposium series* **2009,** *1023* (Controlled/Living Radical Poly), 63-84.

5.   Pintauer, T.; Matyjaszewski, K., Structural aspects of copper catalyzed atom transfer radical polymerization. *Coordination Chemistry Reviews* **2005,** *249* (11–12), 1155-1184.

6.   Bussey, K. A.; Cavalier, A. R.; Mraz, M. E.; Oshin, K. D.; Sarjeant, A.; Pintauer, T., Synthesis, characterization, X-ray crystallography analysis, and catalytic activity of bis(2-pyridylmethyl)amine copper complexes containing coupled pendent olefinic arms in atom transfer radical addition (ATRA) reactions. *Polyhedron* **2016,** *114*, 256-267.

7.   Bussey, K. A.; Connell, J. R.; McGlone, A. R.; Mraz, M. E.; Oshin, K. D.; Pintauer, T.; Oliver, A. G., Crystal structure of {(but-3-en-1-yl)bis-[(pyridin-2-yl)meth-yl]amine-κ(3) N,N′,N″}di-chlorido-copper(II) diethyl ether hemisolvate. *Acta Crystallographica Section E: Crystallographic Communications* **2015,** *71* (Pt 3), 309-311.

8.   Reiser, O., Shining Light on Copper: Unique Opportunities for Visible-Light-Catalyzed Atom Transfer Radical Addition Reactions and Related Processes. *Acc Chem Res* **2016,** *49* (9), 1990-6.

9.   Ribelli, T. G.; Konkolewicz, D.; Bernhard, S.; Matyjaszewski, K., How are Radicals (Re)Generated in Photochemical ATRP? *Journal of the American Chemical Society* **2014,** *136* (38), 13303-13312.

10.   Anastasaki, A.; Nikolaou, V.; McCaul, N. W.; Simula, A.; Godfrey, J.; Waldron, C.; Wilson, P.; Kempe, K.; Haddleton, D. M., Photoinduced Synthesis of α,ω-Telechelic Sequence-Controlled Multiblock Copolymers. *Macromolecules* **2015,** *48* (5), 1404-1411.

11.   Anastasaki, A.; Nikolaou, V.; Pappas, G. S.; Zhang, Q.; Wan, C.; Wilson, P.; Davis, T. P.; Whittaker, M. R.; Haddleton, D. M., Photoinduced sequence-control via one pot living radical polymerization of acrylates. *Chemical Science* **2014,** *5* (9), 3536-3542.

12.   Anastasaki, A.; Nikolaou, V.; Zhang, Q.; Burns, J.; Samanta, S. R.; Waldron, C.; Haddleton, A. J.; McHale, R.; Fox, D.; Percec, V.; Wilson, P.; Haddleton, D. M., Copper(II)/Tertiary Amine Synergy in Photoinduced Living Radical Polymerization: Accelerated Synthesis of ω-Functional and α,ω-Heterofunctional Poly(acrylates). *Journal of the American Chemical Society* **2014,** *136* (3), 1141-1149.

13.   Balili, M. N. C.; Pintauer, T., Photoinitiated ambient temperature copper-catalyzed atom transfer radical addition (ATRA) and cyclization (ATRC) reactions in the presence of free-radical diazo initiator (AIBN). *Dalton Transactions* **2011,** *40* (12), 3060-3066.

14.   Cohen, N. A.; Tillman, E. S.; Thakur, S.; Smith, J. R.; Eckenhoff, W. T.; Pintauer, T., Effect of the Ligand in Atom Transfer Radical Polymerization Reactions Initiated by

Photodimers of 9-Bromoanthracene. *Macromolecular Chemistry and Physics* **2009,** *210* (3-4), 263-268.

15.   Konkolewicz, D.; Schröder, K.; Buback, J.; Bernhard, S.; Matyjaszewski, K., Visible Light and Sunlight Photoinduced ATRP with ppm of Cu Catalyst. *ACS Macro Letters* **2012,** *1* (10), 1219-1223.

16.   Mitani, M. K., Isao; Koyama, Kikuhiko Photoadditions of Alkyl Halides to Olefins Catalyzed by Copper(I) Complexes. *Journal of the American Chemical Society* **1983,** *105* (22), 6719-6721.

17.   Pan, X.; Malhotra, N.; Simakova, A.; Wang, Z.; Konkolewicz, D.; Matyjaszewski, K., Photoinduced Atom Transfer Radical Polymerization with ppm-Level Cu Catalyst by Visible Light in Aqueous Media. *Journal of the American Chemical Society* **2015,** *137* (49), 15430-15433.

18.   Pan, X.; Tasdelen, M. A.; Laun, J.; Junkers, T.; Yagci, Y.; Matyjaszewski, K., Photomediated controlled radical polymerization. *Progress in Polymer Science* **2016,** *62*, 73-125.

19.   Wallentin, C.-J.; Nguyen, J. D.; Finkbeiner, P.; Stephenson, C. R. J., Visible Light-Mediated Atom Transfer Radical Addition via Oxidative and Reductive Quenching of Photocatalysts. *Journal of the American Chemical Society* **2012,** *134* (21), 8875-8884.

20.   Yilmaz, G.; Iskin, B.; Yagci, Y., Photoinduced Copper(I)-Catalyzed Click Chemistry by the Electron Transfer Process Using Polynuclear Aromatic Compounds. *Macromolecular Chemistry and Physics* **2014,** *215* (7), 662-668.

21.   Kolb, H. C.; Finn, M. G.; Sharpless, K. B., Click Chemistry: Diverse Chemical Function from a Few Good Reactions. *Angewandte Chemie International Edition* **2001,** *40* (11), 2004-2021.

22.   Kolb, H. C.; Sharpless, K. B., The growing impact of click chemistry on drug discovery. *Drug Discovery Today* **2003,** *8* (24), 1128-1137.

23.   Tornøe, C. W.; Christensen, C.; Meldal, M., Peptidotriazoles on Solid Phase: [1,2,3]-Triazoles by Regiospecific Copper(I)-Catalyzed 1,3-Dipolar Cycloadditions of Terminal Alkynes to Azides. *The Journal of Organic Chemistry* **2002,** *67* (9), 3057-3064.

24.   de Souza, I. C.; Faro, L. V.; Pinheiro, C. B.; Gonzaga, D. T.; da Silva Fde, C.; Ferreira, V. F.; Miranda Fda, S.; Scarpellini, M.; Lanznaster, M., Investigation of cobalt(iii)-triazole systems as prototypes for hypoxia-activated drug delivery. *Dalton Trans* **2016,** *45* (35), 13671-4.

25.   Evans, V.; Duncanson, P.; Motevalli, M.; Watkinson, M., An investigation into the synthesis of azido-functionalised coumarins for application in 1,3-dipolar "click" cycloaddition reactions. *Dyes and Pigments* **2016,** *135*, 36-40.

26.   Ricardo, C. L.; Pintauer, T., Synthesis of Functionalized Polytriazoles via One-Pot Sequential Copper-Catalyzed Azide-Alkyne [3+2] Cycloaddition and Atom Transfer Radical Addition (ATRA). *Israel Journal of Chemistry* **2012,** *52* (3/4), 320-327.

27.   Shi, Y.; Cao, X.; Gao, H., The use of azide-alkyne click chemistry in recent synthesis and applications of polytriazole-based nanostructure polymers. *Nanoscale* **2016,** *8*, 4864-4881.

28.   Wang, W.; Wei, F.; Ma, Y.; Tung, C.-H.; Xu, Z., Copper(I)-Catalyzed Three-Component Click/Alkynylation: One-Pot Synthesis of 5-Alkynyl-1,2,3-triazoles. *Organic Letters* **2016,** *18* (17), 4158-4161.

29.   Pintauer, T., Recent advances in small molecule synthesis using copper catalyzed atom transfer radical addition (ATRA). *Polymer Preprints* **2011,** *52* (2), 723-724.

30.   Ricardo, C. L.; Pintauer, T., One-Pot Sequential Azide–Alkyne [3+2] Cycloaddition and Atom Transfer Radical Addition (ATRA): Expanding the Scope of In Situ Copper(I)

Regeneration in the Presence of Environmentally Benign Reducing Agent. *European Journal of Inorganic Chemistry* **2011,** *2011* (8), 1292-1301.

31.   Ricardo, C. L. P., Tomislav, Highly Efficient Organicand Macromolecular Synthesis Using Sequential CopperCatalyzed Azide-Alkyne [3+2] Cycloaddition and ATRA/ATRP. *ACS symposium series* **2012,** *1100* (Progress in Controlled Radical), 73-98.

32.   Walsh, J. C. K., Hartmuth C., Application of Click Chemistry in Radiopharmaceutical Development. *Chimia* **2010,** *64*, 29-33.

33.   Mandal, P.; Choudhury, S.; Singha, N. K., Acrylic ABA triblock copolymer bearing pendant reactive bicycloalkenyl functionality via ATRP and tuning its properties using thiol-ene chemistry. *Polymer* **2014,** *55* (22), 5576-5583.

34.   Church, D. C.; Peterson, G. I.; Boydston, A. J., Comparison of Mechanochemical Chain Scission Rates for Linear versus Three-Arm Star Polymers in Strong Acoustic Fields. *ACS Macro Letters* **2014,** *3* (7), 648-651.

35.   Matyjaszewski, K.; Miller, P. J.; Pyun, J.; Kickelbick, G.; Diamanti, S., Synthesis and Characterization of Star Polymers with Varying Arm Number, Length, and Composition from Organic and Hybrid Inorganic/Organic Multifunctional Initiators. *Macromolecules* **1999,** *32* (20), 6526-6535.

36.   Jankova, K.; Bednarek, M.; Hvilsted, S., Star polymers by ATRP of styrene and acrylates employing multifunctional initiators. *Journal of Polymer Science Part A: Polymer Chemistry* **2005,** *43* (17), 3748-3759.

37.   Dufils, P.-E.; Chagneux, N.; Gigmes, D.; Trimaille, T.; Marque, S. R. A.; Bertin, D.; Tordo, P., Intermolecular radical addition of alkoxyamines onto olefins: An easy access to advanced macromolecular architectures precursors. *Polymer* **2007,** *48* (18), 5219-5225.

38.   Tsarevsky, N. V.; Sumerlin, B. S.; Matyjaszewski, K., Step-Growth "Click" Coupling of Telechelic Polymers Prepared by Atom Transfer Radical Polymerization. *Macromolecules* **2005,** *38* (9), 3558-3561.

39.   Urien, M.; Erothu, H.; Cloutet, E.; Hiorns, R. C.; Vignau, L.; Cramail, H., Poly(3-hexylthiophene) Based Block Copolymers Prepared by "Click" Chemistry. *Macromolecules* **2008,** *41* (19), 7033-7040.

40.   Sivakumar, K.; Xie, F.; Cash, B. M.; Long, S.; Barnhill, H. N.; Wang, Q., A Fluorogenic 1,3-Dipolar Cycloaddition Reaction of 3-Azidocoumarins and Acetylenes. *Organic Letters* **2004,** *6* (24), 4603-4606.

3. SYNTHESIS OF AMPHIPHILIC BLOCK COPOLYMERS FOR SMALL MOLECULE ENCAPSULATION

3.1 *Motivation*

The objective of this research was to develop a method in which amphiphilic block copolymers containing di(ethylene glycol)ethyl ether acrylate and lauryl acrylate could be synthesized and employed to encapsulate small molecules. It was envisioned that the end-goal of this material could be utilized in the field of transdermal drug delivery; however, the materials encapsulation properties were evaluated by quantitation of a polar Rhodamine B in a squalane solvent. The initiating structure of the polymer was tailored to multifunctional analogues to determine if a higher Rhodamine B concentration could be quantified. Additionally, with higher-order star-shaped systems, there is a possibility of the aggregation to occur in a unimolecular fashion. This is highly advantageous for drug delivery due to the inability of micellular dissociation upon dilution or environmental changes.

3.2 *Research Objectives*

Specific Aim #1: *Synthesis of poly(di(ethylene glycol)ethyl ether acrylate-co-lauryl acrylate)*

Specific Aim #2: *Characterization using NMR, GPC, and mass spectrometry*

Specific Aim #3: *Encapsulation of Rhodamine B in squalane using amphiphilic block copolymers*

3.3 *Introduction*

The application range of polymeric materials has significantly expanded within the past two decades. The utilitarian nature of these synthetic macromolecules has cemented their foundation in all aspects of opto-electronics, data storage, alternative energy sources, and biomedical technology.[1] In particular, drug delivery and small molecule encapsulation by

synthetic carriers has garnered much interest. Various classes of polymers have since offered the potential to increase bioavailability and therapeutic index of drug molecules, without leaving hazardous byproducts within the body.[2] Although the majority of drugs are delivered orally or through site-injections, drawbacks exist within both.[3-4] Administered drugs are often hydrophobic and exhibit poor aqueous stability. Additionally, they are susceptible to hydrolytic, enzymatic, and oxidative degradation within the body.[4-5] Hypodermic injections are often associated with decreased compliance, pain, and a potential for infection.[6] Moreover, they are patient-friendly and require do not require a medical professional.

Pioneering efforts of drug delivery focused on liposomal assemblies, which can dissociate in vivo, reducing the efficacy of the drug.[3, 7-8] Synthetic polymers can be used as an alternative, which can be easily prepared using commercially-available and inexpensive reagents. Often, they are smaller in size than liposomes, exhibiting the potential for longer circulation.[3-4] However, synthetic polymer micelles are still susceptible to dissociation in vivo under the critical micelle concentration (CMC).[9-13] Furthermore, they are typically not stable upon dilutions and are sensitive to environmental changes such as temperature and pH, which can greatly hamper their application.[14]

Within a polymeric system, various intermolecular interactions dictate amphiphilic polymers to self-assemble into nano- or microstructures. The self-assembly behavior often relies on physical interactions to form micelles with low thermal stability.[13] Traditionally, linear polymers have dominated this area of research; however, with recent advances in polymer chemistry, more complex architectures have become a focal point.[2, 15] In particular, star polymers have been of interest due to their differing hydrodynamic properties, reduced solution viscosity, and compact morphology.[2, 4-5, 13, 16-20]

The synthesis of star polymers began in the 1950's with anionic polymerization; however, efforts have since shifted to other controlled radical polymerization (CRP) techniques. ATRP is a particularly attractive CRP process which allows for the synthesis of well-defined polymers with predetermined molecular weights and narrow dispersities.[17, 21-27] Additionally, the retention of the halogen moiety allows for alternative post-polymerization transformations, especially nucleophilic substitutions.[23-24] Moreover, the "core-first" or "arm-first" method can be enacted using ATRP, making this synthetic strategy an excellent candidate for star polymer formation.

An interesting chemical behavior of star polymers are their ability to exhibit unimolecular behavior. With this, self-assembly does not occur, unlike their linear analogues. Unimolecular micelles are characterized as single-molecule micelles and tend to be highly branched dendritic or star-shaped systems.[14] These three-dimensional structures possess a covalently linked-core-shell, and tend to display increased solution stability, eliminating the dynamic equilibrium between micellular structures and free amphiphiles.[9-10, 13] This behavior jettisons the possibility of dissociations through dilution or other environmental changes.[5]

Herein, the synthesis of amphiphilic block copolymers containing polar di(ethylene glycol)ethyl ether acrylate and nonpolar lauryl acrylate with varying architectures (linear, telechelic, 3-arm star) are presented. These architectures were chosen due to the availability and inexpensive nature of the corresponding initiating structures, as compared to higher-order star-shaped systems. The block copolymers were prepared using a one-pot, photoinduced ATRP methodology from initiators containing 1, 2, and 3 tertiary bromide functionalities at their margin. The micellular properties of the resulting copolymers were characterized by nuclear magnetic resonance (NMR) spectroscopy, single-stage and tandem mass spectrometry (MS and

MS^2), and gel permeation chromatography (GPC). The copolymers ability to encapsulate a small polar molecule, rhodamine B, was measured by UV/vis spectroscopy.

3.4 *Results and Discussion*

3.4.1 *Synthesis of amphiphilic block copolymers*

The amphiphilic polymers explored in this study were prepared from commercially-available linear, telechelic, and 3-arm star-shaped initiators; however, the telechelic and 3-arm star initiators were synthesized in house through a facile esterification reaction using primary alcohols with 2-bromoisobutyryl bromide (Appendix). These initiating structures contained tailored amounts of bromine functionalities depending on the architecture (**1**, **2**, **3**), which was required by the photoinduced atom transfer radical polymerization (photoATRP) technique. The photoATRP methodology was carried out using a [Cu^{II}(Me$_6$TREN)Br][Br] complex with excess ligand and UV radiation. The solvent system was modified from methanol to a methanol/THF mixture to aid in solubility of the second monomer block. This technique can be easily modified with other monomer functionalities and solvents due to the robust nature of photoATRP. Additionally, rapid monomer conversion could be realized with well-defined functionalities without the need for stringent techniques such as freeze-pump-thaw or use of drybox. However, prior to polymerization, the reaction mixture was bubbled with an inert gas for 5 minutes to remove any oxygen within the vessel.

The first monomer block was polymerized from the variable initiating structures with a di(ethylene glycol)ethyl ether acrylate. This dEGEEA block provided a polar core for biocompatibility and solubilization of the amphiphilic dye (rhodamine B). The photoATRP method allowed for a one-pot block copolymer formation, therefore mitigating the need to isolate and purify homopolymer intermediates (Scheme 1). Aliquots of the reaction mixture were taken

to analyze with NMR, GPC, and MS before injection of the second monomer. Lauryl acrylate

was chosen as the second block to provide a nonpolar shell to the amphiphilic polymers which

could aid in solubilization of the media chosen for encapsulation. Additionally, the pendant arms

of the lauryl acrylate block are quite similar in size to the extracellular lipophilic matrix of

human skin, making these materials and ideal candidate for transdermal drug delivery. The

polymerization of the second block occurred through injection of the LA monomer with a fresh

solvent (methanol/THF) in a 1:1 ratio, bubbled with inert gas, and reintroduced to the UV lamp

atop a stir plate. After the monomer was exhausted through confirmatory ^{1}H NMR analysis, the

mixture was dilute with methylene chloride, washed with water (x3), dried over anhydrous

MgSO$_4$, and passed thru a plug of silica to remove any residual catalyst.   This procedure was

repeating with the varying architectures (**1**, **2**, **3**) and targeted MW sizes (**a=7500 Da**, **b=15000**

Da, **c=50000 Da**). This vernacular will be adopted throughout the course of this text to eliminate

any confusion with the nomenclature of the copolymers, with respect to their functionality and

molecular weight range.

Scheme 3.1 One-pot photoATRP for the preparation of amphiphilic block copolymers with

varying architectures.
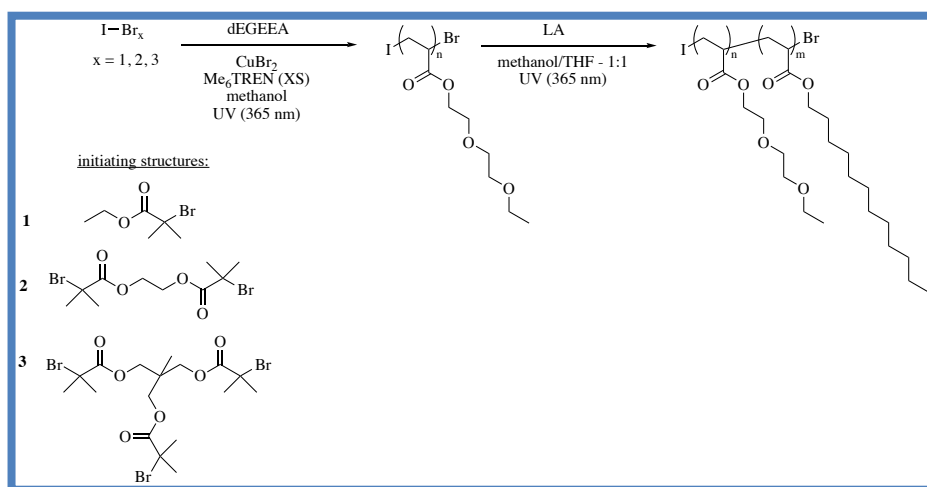
3.4.2 *Characterization using ^1H NMR, GPC, DLS, and single-stage MS*

Throughout the course of the study, ^{1}H NMR spectroscopy was utilized to monitor monomer conversion due to the facile nature of sample preparation and rapid analysis. Additionally, purified block copolymers were analyzed for M_n via end-group analysis on copolymers within the **a** (7500 Da) and **b** (15000 Da) molecular weight ranges. The large amphiphiles were not analyzed for M_n with ^{1}H NMR as the capabilities of are limited to polymers under 20000 Da. However, the block ratios could be obtained for all variants synthesized, ideally trying to achieve a 1:1 relation between the blocks. Differing ratios for the amphiphiles may provide an inability to encapsulate the guest molecule (RB) or solubilize the polymer within the matrix (squalane). Unfortunately, the 3-arm star polymer (**3a**, **3b**, **3c**) block ratios were unable to be accurately obtained via ^{1}H NMR due to overlapping peaks between one of the monomer blocks and initiating structures. The block ratios for those variants were obtained using GPC in that case, which is not ideal due to the GPC instrument being calibrated with poly(styrene) standards. An example is shown below in Figure 1 illustrated with corresponding structure and annotated integration values. All other ^{1}H NMR spectra can be viewed in the Appendix of this chapter.
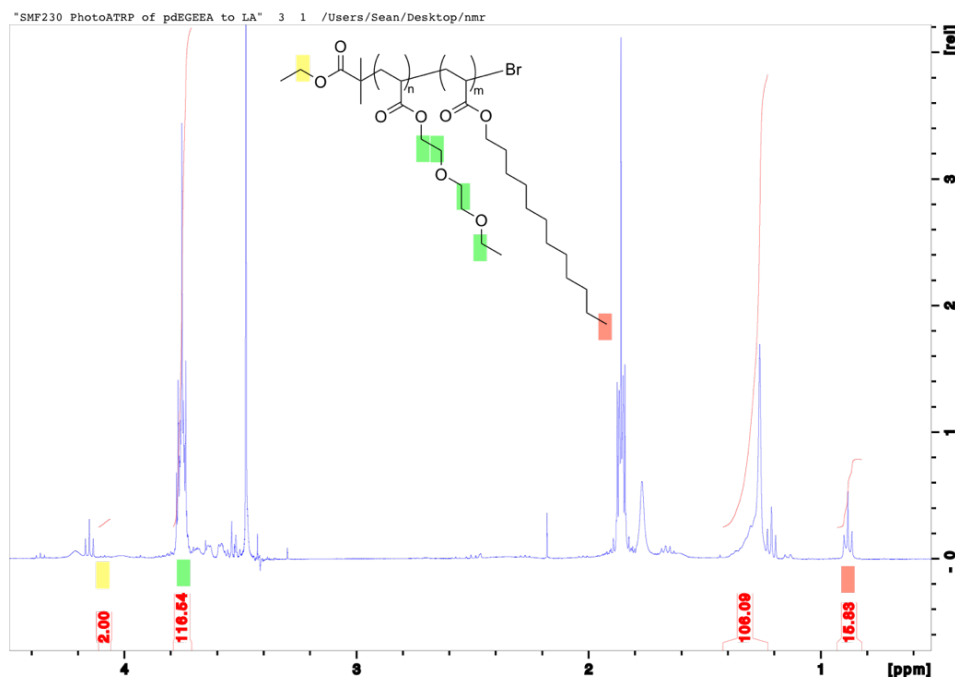
Figure 3.1 ^{1}H NMR spectrum of linear amphiphilic block copolymer for Mn and block ratio determination.

Determining the molecular weight ranges were primarily determined via GPC with a refractive index detector in a THF solvent. Additionally, a shift in the molecular weight distribution could be easily observed with a decreased retention time when analyzing the aliquots from the homopolymer/copolymer samples. This decrease in retention is crucial to visualize an increase in molecular weights when adding a second block, confirming the retention of the halogen moiety, which is essential for the photoATRP process. The molecular weights determined by GPC, as well as the block ratios determined by ^{1}H NMR, are summarized below in Tables 3.1-3.3. In most cases, the targeted molecular weight range was not obtained. Due to the complete monomer conversion for all reactions, it is hypothesized that radical-radical termination reactions consuming initiating chains is the cause. Additionally, disproportionation

reactions create a possibility to terminate the polymer chains, eliminating the ability for

additional monomer additions. All GPC data can be viewed in the Appendix of this chapter.

Table 3.1 Molecular weights (Mn) and block ratios of linear block copolymers.

Copolymer	Target MW (Da)	Copolymer MW (Da) (GPC)	Block Ratio (^{1}H NMR)
1a	7500	3500	1.76
1b	15000	14100	0.82
1c	50000	33000	1.2

Table 3.2 Molecular weights (Mn) and block ratios of telechelic block copolymers.

Copolymer	Target MW (Da)	Copolymer MW (Da) (GPC)	Block Ratio (^{1}H NMR)
2a	7500	5600	0.4
2b	15000	16200	1.1
2c	50000	37700	1.36

Table 3.3 Molecular weights (Mn) and block ratios of 3-arm star block copolymers.

Copolymer	Target MW (Da)	Copolymer MW (Da) (GPC)	Block Ratio (GPC)
3a	7500	2900	1.1
3b	15000	8700	1.4
3c	50000	33700	1.5

Single-stage MS was utilized to analyze the small variants (**1a**, **2a**, **3a**) to visualize the

shift in molecular weight distributions. Higher molecular weight samples were unable to be

analyzed with MS due to the inability of the polymer analytes to retain a charge during the ESI-

TOF analysis. Tandem mass spectrometry was also utilized to characterize the copolymers

through CID experiments; however, those results are highlighted in Chapter 4 of this text. For all

other mass spectra, please view the Appendix for this chapter.
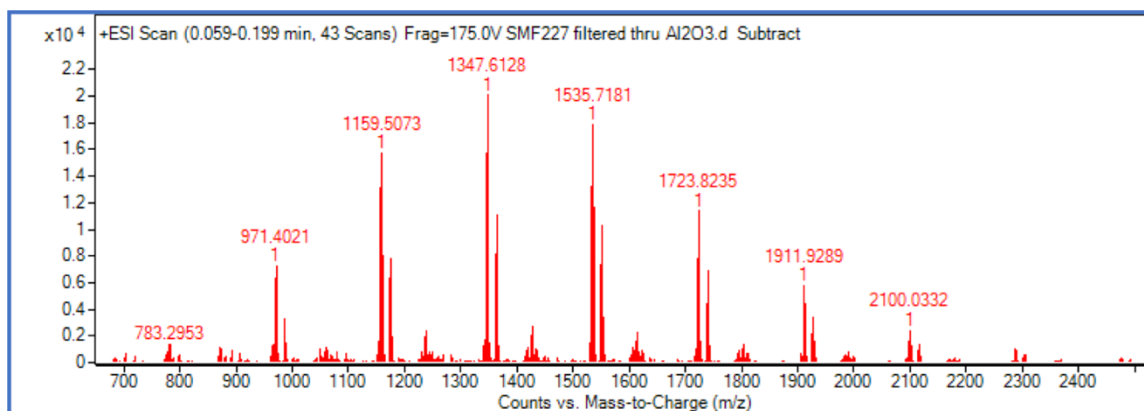
Figure 3.2 Single-stage mass spectrum of linear poly(dEGEEA). All measurements are within 5 ppm error.
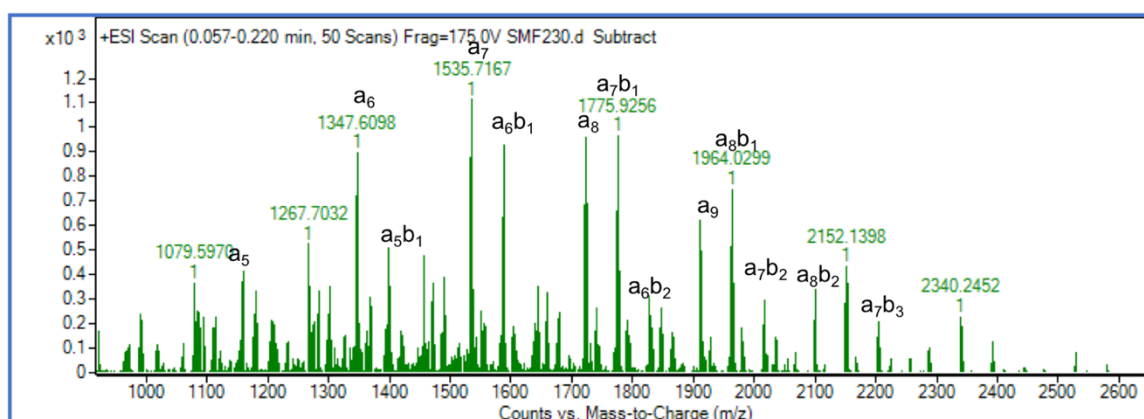
Figure 3.3 Single-stage mass spectrum of poly(dEGEEA)-*co*-LA. Peaks are annotated with a/b, corresponding to the number of monomer units for dEGGEA and LA, respectively. All measurements are within 5 ppm error.

3.4.3 *Encapsulation of Rhodamine B using amphiphilic block copolymers*

The amphiphilic block copolymers were synthesized in a fashion to generate reverse micelles, commonly referred to as water-in-oil micelles. The interior of the amphiphiles consist of dEGEEA, a polar monomer which will aid in encapsulation of a polar, rhodamine B dye. Rhodamine B was chosen as the polar dye to facile measurement via UV/vis absorption in the region of 543 nm. The corona of the amphiphiles consist of LA blocks, creating a hydrophobic

56

exterior which will aid in solubilization within the nonpolar squalane solvent. Squalane was chosen as a matrix due to its cosmetic use and availability.

For a control experiment, a UV/vis spectrum was obtained for rhodamine B-saturated solutions in both squalane and water. This was conducted to ensure that there is no activity in the region which rhodamine B would appear within the squalane solvent, illustrating the lack of solubility. Indeed, the control studies using rhodamine B in squalane showed no UV/vis activity, indicating the polar dye was insoluble within the nonpolar solvent (Figure 3.4, blue). Additionally, a solution of pure copolymer in squalane was prepared and testing using UV/vis in an analogous fashion, to ensure there is no activity in the region in which rhodamine B would appear, suggesting a proper catalyst removal (Figure 3.4, orange). For the water solution, a strong absorption band was seen within the region of 543 nm (Figure 3.5). Control solutions were prepared by adding an excess amount of rhodamine B or copolymer in the respective solvent, stirring at room temperature overnight, and filtering using 0.45 μm PTFE filters to remove any undissolved dye/polymer.
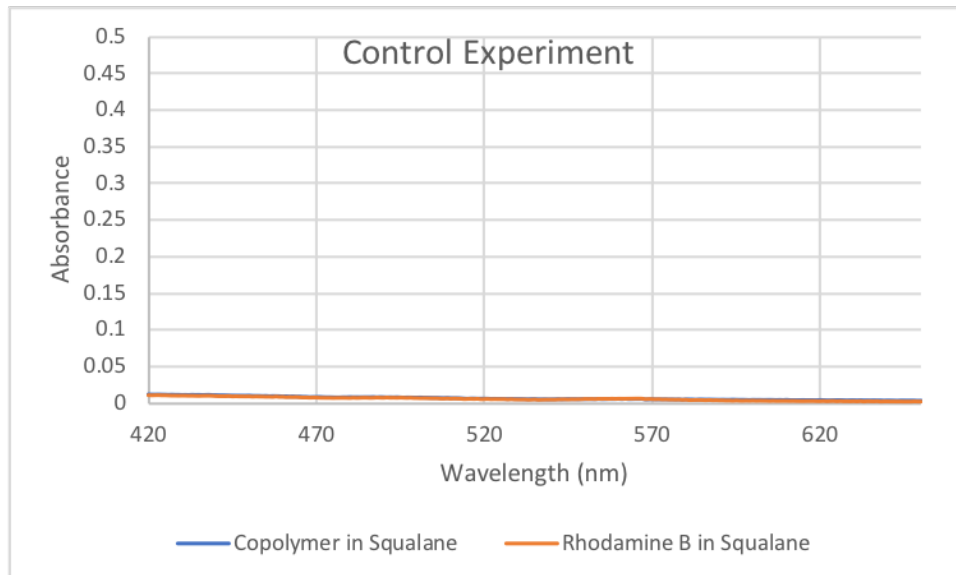
Figure 3.4 UV/vis spectra of the copolymer in squalane (blue) and rhodamine B in squalane (orange) showing no response in the region of 420-650 nm. Measurements were collected in triplicate for statistical analysis.
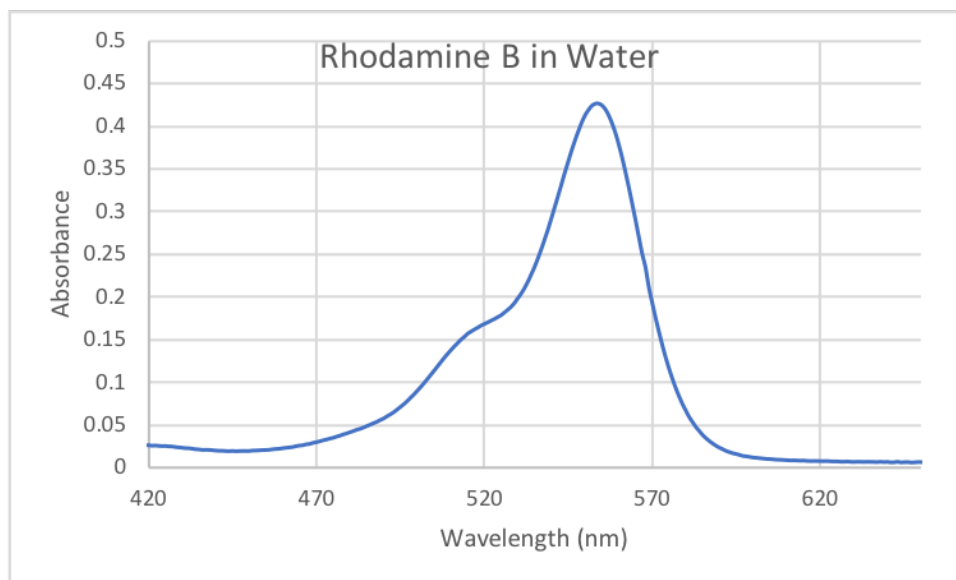

Figure 3.5 UV/vis spectrum of Rhodamine B in water. Absorption band is centered at 543 nm. Measurements were collected in triplicate for statistical analysis.

In a similar manner, solutions containing both rhodamine B and copolymer for linear, telechelic, and 3-arm star analogues were prepared, and their UV/vis activity measured in the

same region as control groups. This verifies that any UV/vis activity seen with rhodamine B/polymer solutions was attributed to the solubilization of the rhodamine B dye which was imparted by the copolymer in solution. In all cases, a bathochromatic shift was visualized from 543 nm to ~566 nm, indicating the dye being solubilized by polar interior of the amphiphiles, which is consistent with dendritic polymers.[28] The UV/vis spectrum of the linear copolymer in squalane can be seen below in Figure 6. It must be noted that the medium (15000 Da) and small (7500 Da) analogues outperform the large (50000 Da) copolymer. This indicates that the large linear analogue is not as thermodynamically favored to form micellular structures as the smaller counterparts, reducing the efficacy of the encapsulation process. It is assumed the higher-order star shaped systems will allow for greater encapsulation with higher molecular weight polymers.
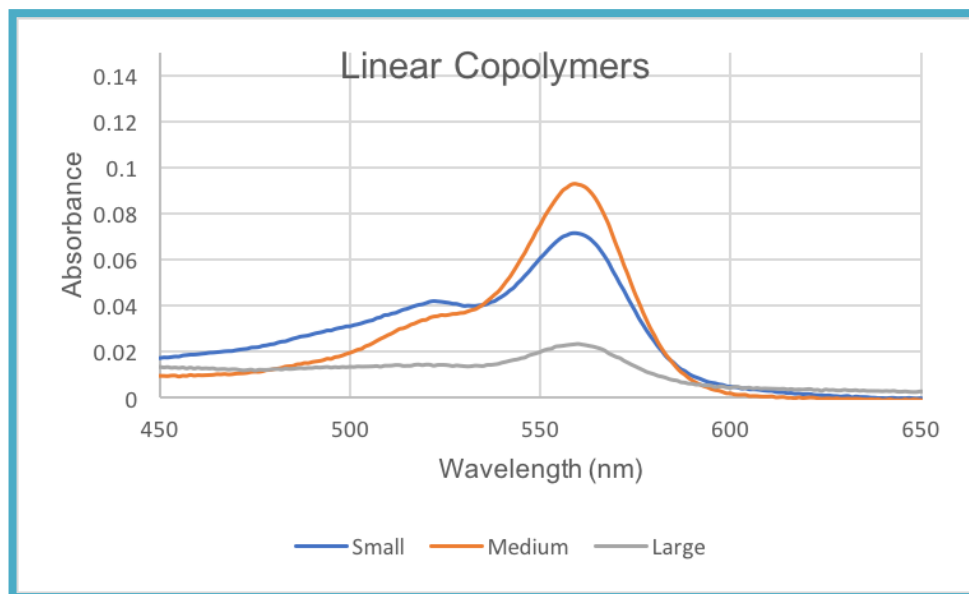
Figure 3.6 UV/vis spectra of various sized linear copolymer in squalane saturated with rhodamine B. All measurements were conducted in triplicate for statistical analysis.

Very similarly, the medium telechelic variant outperformed the small and large-sized copolymers in rhodamine B encapsulation (Figure 7). Moreover, the small analogue in this subset showed very little UV/vis response, indicating minimal RB uptake. This may be attributed

to the poorly controlled block ratio, which was determined to be 0.4 by ^{1}H NMR analysis. However, it must be noted that UV/vis response of the medium copolymer has nearly doubled in comparison with the linear architecture, suggesting a higher encapsulation efficiency at that molecular weight range.
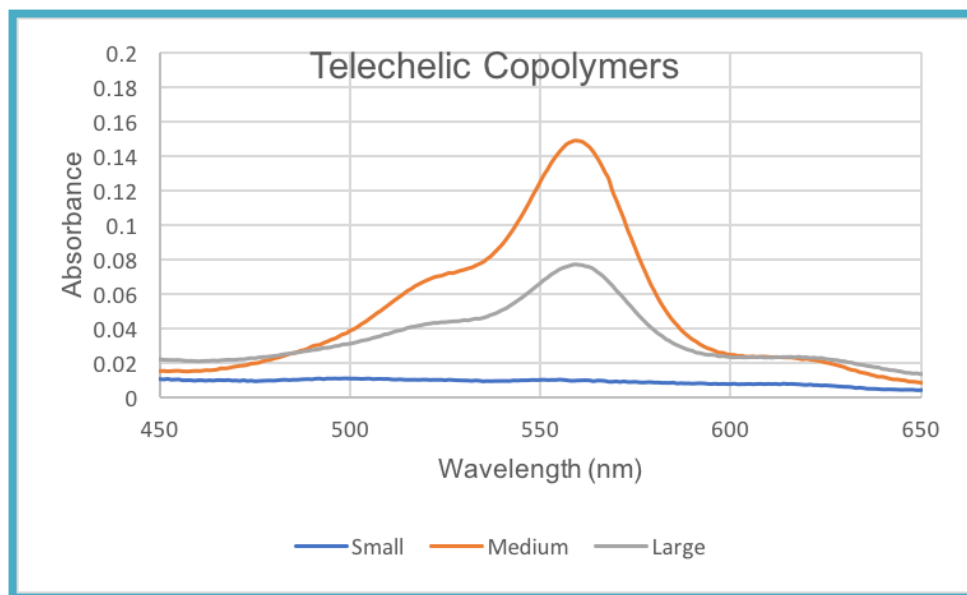

Figure 3.7 UV/vis spectra of various sized telechelic copolymer in squalane saturated with rhodamine B. All measurements were conducted in triplicate for statistical analysis.

Transitioning from a telechelic to star-shaped architecture had a substantial effect on the rhodamine B encapsulation. For the 3-arm star copolymers, the large variant showed a considerable UV/vis response in the rhodamine B region, followed by the medium variant. This could be attributed to the thermodynamic favorability of the star-shaped system to form micelles over the other two architectures. Additionally, greater control over the block ratio was realized during those reactions. This enables efficient RB uptake and consequently a greater ability to be solvated by the nonpolar solvent. Unfortunately, the small variant showed little to no UV/vis activity, indicating no rhodamine B encapsulation. This is attributed to the poorly-controlled photoATRP reaction, only achieving a molecular weight of 2900 Da. With the initiating structure

having a molecular weight of nearly 1000 Da, there could have been insufficient block addition of either the polar EG-based core or LA corona. Additionally, more complex initiating architecutres can lead to more side reactions, hindering monomer availability. The UV/vis spectrum of the 3-arm star variant can be seen below in Figure 8.
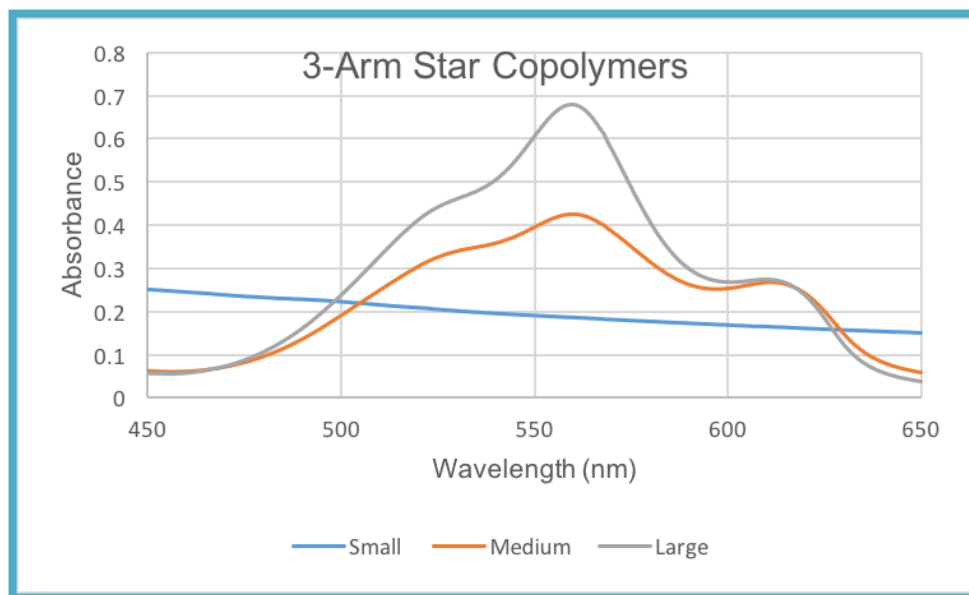
Figure 3.8 UV/vis spectra of various sized 3-arm star copolymer in squalane saturated with rhodamine B. All measurements were conducted in triplicate for statistical analysis.
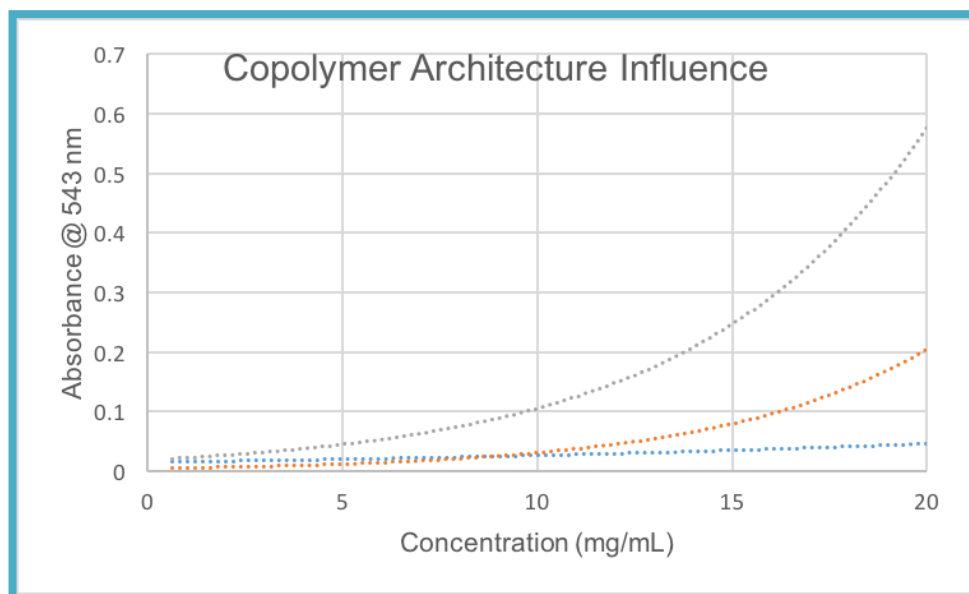
Plotting the UV/vis response at 543 nm of the large variants enables a visualization of the architecture influence, which can be seen below in Figure 9. Clearly, there is a trend indicating the higher-order star shaped systems have a greater encapsulation efficiency in comparison to the other two architectures. The highest performing copolymer is the 3-arm star, followed by the telechelic and then the linear. There is a near 7-fold increase in the UV/vis response at 543 nm when comparing the linear to the 3-arm star analogue. Unfortunately, unimolecular behavior was not observed, which was indicated by the low RB uptake at very low concentrations (>0.1 mg/mL); however, it is envisioned that applying this methodology to 6- and 12-arm star initiating structures would allow for unimolecular behavior.

Figure 3.9 UV/vis response at 543 nm of large variants of all three architectures. Top (**3c**, 3-arm star), middle (**2c**, telechelic), bottom (**1c**, linear).

In addition to the visualized encapsulation by UV/vis, increasing the concentration of polymer in solution led to an increase in the concentration of rhodamine B in solution, again indicating that the copolymers were responsible for solubilization of the dye. This was measured by creating serial dilutions of the polymer sample, starting with 20 mg/mL. Higher concentrations of polymers in squalane were not achievable, as solubility issues were encountered; however, it is believed that extending concentrations greater than 20 mg/mL would enable for a higher dye uptake. A calibration curve of known concentrations of rhodamine B in water was constructed, enabling the quantification of rhodamine B in the copolymer solutions. The calibration curve for rhodamine B in water is shown below in Figure 10.
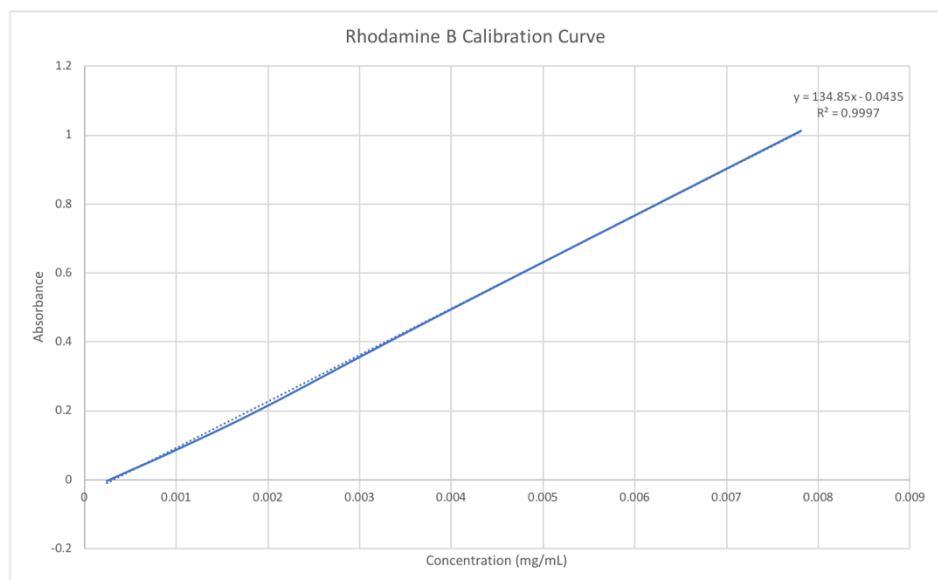
Figure 3.10 Calibration curve of rhodamine B in water. UV/vis spectra was collected at 543 nm.

Using the known concentration values from the calibration curve, rhodamine B was quantified in all three copolymer architectures, which results are summarized in the Appendix of this chapter. The results indicate that the concentration of RB in solution is increased when higher copolymer concentrations are generated. Additionally, the overall trend from the experiments verify that increase the complexity of the architecture, as well as increasing the molecular weights have a positive impact on the amount of RB encapsulated. The statistical analysis conducted ensure a very low standard uncertainty with the measurements, which is attributed to the measurements conducted in triplicate.

3.5 *Conclusion*

The goal of the project was focused on encapsulating polar dyes in a nonpolar solvent with the use of amphiphilic block copolymers. A photoinduced ATRP methodology was developed for the production of poly(dEGEEA)-*co*-(LA) in a one-pot fashion with varying architectures. Three varying molecular weight ranges were targeted to expand the scope of the study by determining a relationship between polymer size and encapsulation efficiency. It was

found that the dye chosen, rhodamine B, was insoluble in squalane, the matrix chosen to test encapsulation properties. This result was highlighted via the lack of UV/vis response in the region of 543 nm. Addition of copolymer to the rhodamine B-saturated solutions led to a response within the UV/vis spectra. The solubilization of the rhodamine B dye was attributed to the copolymers, whos interior block aided in solubilization of the polar dye. The nonpolar corona of the copolymers assisted in solubilization in the squalane solvent. Unfortunately, unimolecular behavior was not detected in any of the copolymers, which would have been highlighted by dye uptake at very low concentrations. However, it was found that more complex architectures, in conjunction with an increase in molecular weight, led to higher dye concentrations in the solutions. It is anticipated that utilizing more complex initiating structures, generating 12- or 24-arm star copolymers, would enable unimolecular behavior. It is envisioned that these materials will be found useful in the growing field of transdermal drug delivery.

3.6 *References*

1.   Lutz, J.-F., Polymerization of oligo(ethylene glycol) (meth)acrylates: Toward new generations of smart biocompatible materials. *Journal of Polymer Science Part A: Polymer Chemistry* **2008,** *46* (11), 3459-3470.

2.   Khanna, K.; Varshney, S.; Kakkar, A., Miktoarm star polymers: advances in synthesis, self-assembly, and applications. *Polymer Chemistry* **2010,** *1* (8), 1171-1185.

3.   Yi, Y.; Lin, G.; Chen, S.; Liu, J.; Zhang, H.; Mi, P., Polyester micelles for drug delivery and cancer theranostics: Current achievements, progresses and future perspectives. *Materials Science and Engineering: C* **2018,** *83*, 218-232.

4.   Poree, D. E.; Giles, M. D.; Lawson, L. B.; He, J.; Grayson, S. M., Synthesis of Amphiphilic Star Block Copolymers and Their Evaluation as Transdermal Carriers. *Biomacromolecules* **2011,** *12* (4), 898-906.

5.   Kreutzer, G.; Ternat, C.; Nguyen, T. Q.; Plummer, C. J. G.; Månson, J.-A. E.; Castelletto, V.; Hamley, I. W.; Sun, F.; Sheiko, S. S.; Herrmann, A.; Ouali, L.; Sommer, H.; Fieber, W.; Velazco, M. I.; Klok, H.-A., Water-Soluble, Unimolecular Containers Based on Amphiphilic Multiarm Star Block Copolymers. *Macromolecules* **2006,** *39* (13), 4507-4516.

6.   Park, J.-H.; Allen, M. G.; Prausnitz, M. R., Biodegradable polymer microneedles: Fabrication, mechanics and transdermal drug delivery. *Journal of Controlled Release* **2005,** *104* (1), 51-66.

7.   Discher, D. E.; Eisenberg, A., Polymer Vesicles. *Science* **2002,** *297* (5583), 967-973.

8.   Torchilin, V. P., Micellar Nanocarriers: Pharmaceutical Perspectives. *Pharmaceutical Research* **2006,** *24* (1), 1.

9.   Oelmann, S.; Meier, M. A. R., Synthesis and unimolecular micellar behavior of amphiphilic star-shaped block copolymers obtained via the Passerini three component reaction. *RSC Advances* **2017,** *7* (71), 45195-45199.

10.   Oelmann, S.; Travanut, A.; Barther, D.; Romero, M.; Howdle, S. M.; Alexander, C.; Meier, M. A. R., Biocompatible Unimolecular Micelles Obtained via the Passerini Reaction as Versatile Nanocarriers for Potential Medical Applications. *Biomacromolecules* **2019,** *20* (1), 90-101.

11.   Adams, M. L.; Lavasanifar, A.; Kwon, G. S., Amphiphilic block copolymers for drug delivery. *Journal of Pharmaceutical Sciences* **2003,** *92* (7), 1343-1355.

12.   Kurniasih, I. N.; Keilitz, J.; Haag, R., Dendritic nanocarriers based on hyperbranched polymers. *Chemical Society Reviews* **2015,** *44* (12), 4145-4164.

13.   Jin, X.; Sun, P.; Tong, G.; Zhu, X., Star polymer-based unimolecular micelles and their application in bio-imaging and diagnosis. *Biomaterials* **2018,** *178*, 738-750.

14.   Wu, Y.-L.; Li, Z., The perspectives of using unimolecular micelles in nanodrug formulation. *Therapeutic Delivery* **2019,** *10* (6), 333-335.

15.   Matyjaszewski, K.; Miller, P. J.; Pyun, J.; Kickelbick, G.; Diamanti, S., Synthesis and Characterization of Star Polymers with Varying Arm Number, Length, and Composition from Organic and Hybrid Inorganic/Organic Multifunctional Initiators. *Macromolecules* **1999,** *32* (20), 6526-6535.

16.   Jankova, K.; Bednarek, M.; Hvilsted, S., Star polymers by ATRP of styrene and acrylates employing multifunctional initiators. *Journal of Polymer Science Part A: Polymer Chemistry* **2005,** *43* (17), 3748-3759.

17.   Gao, H.; Matyjaszewski, K., Synthesis of Miktoarm Star Polymers via ATRP Using the "In−Out" Method: Determination of Initiation Efficiency of Star Macroinitiators. *Macromolecules* **2006,** *39* (21), 7216-7223.

18.   Aryal, S.; Prabaharan, M.; Pilla, S.; Gong, S., Biodegradable and biocompatible multi-arm star amphiphilic block copolymer as a carrier for hydrophobic drug delivery. *Int J Biol Macromol* **2009,** *44* (4), 346-352.

19.   Das, S.; Ghosh, R.; Chatterjee, D. P.; Nandi, A. K., Water Soluble Dual Responsive Star Copolymer for Encapsulation of Hydrophobic Dye Molecules. *Macromolecular Symposia* **2016,** *369* (1), 74-80.

20.   Li, Y.; Guo, H.; Zheng, J.; Gan, J.; Zhang, Y.; Guan, X.; Wu, K.; Lu, M., Synthesis and encapsulation of an amphiphilic thermoresponsive star polymer with [small beta]-cyclodextrin and hyperbranched poly(oligo(ethylene glycol)methacrylate) as building blocks. *RSC Advances* **2014,** *4* (97), 54268-54281.

21.   Matyjaszewski, K., From Atom Transfer Radical Addition to Atom Transfer Radical Polymerization. *Current Organic Chemistry* **2002,** *6*, 67-82.

22.   Matyjaszewski, K., Atom Transfer Radical Polymerization (ATRP): Current Status and Future Perspectives. *Macromolecules* **2012,** *45* (10), 4015-4039.

23.   Gao, H.; Matyjaszewski, K., Synthesis of functional polymers with controlled architecture by CRP of monomers in the presence of cross-linkers: From stars to gels. *Progress in Polymer Science* **2009,** *34* (4), 317-350.

24.   Gao, H.; Matyjaszewski, K., Synthesis of Star Polymers by a Combination of ATRP and the "Click" Coupling Method. *Macromolecules* **2006,** *39* (15), 4960-4965.

25.   Matyjaszewski, K., Architecturally Complex Polymers with Controlled Heterogeneity. *Science* **2011,** *333* (6046), 1104-1105.

26.   Matyjaszewski, K.; Jakubowski, W.; Min, K.; Tang, W.; Huang, J.; Braunecker, W. A.; Tsarevsky, N. V., Diminishing catalyst concentration in atom transfer radical polymerization with reducing agents. *Proceedings of the National Academy of Sciences* **2006,** *103* (42), 15309.

27.   Matyjaszewski, K.; Tsarevsky, N. V., Nanostructured functional materials prepared by atom transfer radical polymerization. *Nat Chem* **2009,** *1* (4), 276-288.

28.   Vutukuri, D. R.; Basu, S.; Thayumanavan, S., Dendrimers with Both Polar and Apolar Nanocontainer Characteristics. *Journal of the American Chemical Society* **2004,** *126* (48), 15636-15637.

4. ANALYSIS OF SYNTHETIC POLYMERS USING TANDEM MASS SPECTROMETRY

4.1 *Motivation*

Analyzing synthetic polymers present unique challenges due to the intrinsic complexity of their chemical makeup. This work is focused on characterizing acrylate- and methacrylate-based polymers using tandem mass spectrometry (MS/MS) to contribute to the growing field known as polymeromics. Much like proteomics, the structural details of synthetic polymers can be realized through collision-induced dissociation (CID) experiments. However, unlike proteomics, there is not a wide array of software tools yet available for product fragment identification. Therefore, manual spectral interpretation must be conducted to elucidate polymer structure, sequence, or architecture.

4.2 *Research Objectives*

<u>*Specific Aim 1:*</u> Single-stage mass spectrometry of homo- and copolymers

<u>*Specific Aim 2:*</u> Acrylate-based homopolymer fragmentation pathways

<u>*Specific Aim 3:*</u> Acrylate-based copolymer fragmentation pathways

4.3 *Introduction*

Polymer science and engineering applications have substantially increased since the introduction of soft-ionization methods such as matrix-assisted laser-desorption ionization (MALDI) and electrospray ionization (ESI).[1-3] These ionization sources enable coupling with a mass analyzer, which reveals a great number of advantages. The pioneering efforts of synthetic polymer characterization focused on utilizing MALDI as an ionization source; however, ESI has recently become more prevalent due to the availability of instrumentation.[4] One limitation of this methodology is typically governed by the solubility of the polymer sample within a solvent, as the solution needs to be electro-sprayed for ionization to occur. Unfortunately, some larger

polymer samples may be unable to support a charge, therefore rendering them undetectable by the mass spectrometer. Encouragingly, ESI can be easily interfaced with additional separation techniques such as reversed-phase, normal-phase, and the more popular size-exclusion/gel-permeation, simplifying the analysis.

Pairing these ion formation processes with quadrupole-time-of-flight (Q-TOF) mass analyzer provides well-resolved and detailed dispersity information which is key to macromolecular characterization.[5-8] This process allows access to molecular weight distributions, expressed in their dispersity (Đ), as well as mass-to-charge ratios.[9] However, single-stage mass spectrometry alone is unable to provide detailed structural information.[7, 10] Tandem mass spectrometry involves the isolation of a polymer ion within a mass spectrometer and fragmentation using a neutral gas molecule. This is often referred to as collision-induced dissociation, which provides a fragment ion spectrum containing diagnostic ions. These fragment ions can elucidate copolymer sequences/architectures, differentiate isobaric/isomeric species, or even characterize end-groups.[11-14] This is crucial for the predictive design and fabrication of polymeric materials.[15] This methodology was initially employed for sequencing peptides in the field of proteomics; however, much less research has been focused on synthetic polymers.

The pioneering efforts of synthetic polymer characterization was conducted by Jackson *et al*,[16-17] where MALDI-MS/MS was used to obtain structural information from poly(alkyl methacrylates) and poly(styrene). This seminal research laid the groundwork for what was to become a powerful, yet under-utilized, characterization technique for synthetic polymers. It was discovered that ATRP-produced poly(methyl methacrylate) (PMMA) using brominated- and chlorinated initiators provided intense fragment signals formed during the CID experiments. The

primary fragment was identified as a lactone moiety on the end-group of the polymer ion (Figure 4.1, bottom). Additionally, parent ion fragments were still detectable during the experiment.
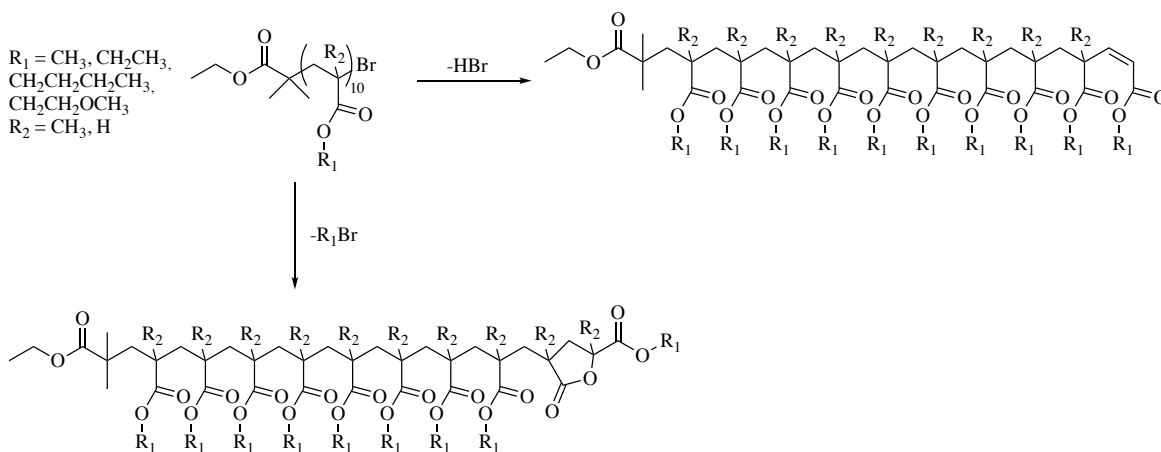
Figure 4.1 Possible end-group rearrangements of poly(alkyl acrylates) and poly(methacrylates) during CID experiments.

In 2000, Jackson's research was expanded to analyzing copolymers containing MMA and butyl acrylate (BA) blocks using MALDI-MS/MS.[18] It was found that a successful sequencing could be realized using similar methodologies. Later in 2004, Jackson *et al.* transitioned to using ESI-MS/MS to sequence poly(alkyl methacrylates).[18] The research had shown that by using ESI, end-group information as well as backbone structure could be identified. Promisingly, multiply charged species were able to be identified by the ESI source. Moreover, the researchers claimed that the high signal-to-noise ratio of polymer ions larger than 4,000 Da indicated that this technique could be used to characterize larger molecular weight polymers.

In 2013, Altuntas *et al.* compared various ionization methods (MALDI, APCI, ESI) for MS/MS comparison of poly(alkyl acrylates). It was discovered that APCI and ESI are more well-suited for analyzing the end-group fragmentation patterns of polymers produced using a controlled radical polymerization (e.g. ATRP, RAFT, etc.). MALDI, however, if far superior when determining molar mass characteristics and dispersity of the polymer sample. Additionally,

MALDI outperformed ESI when handling samples above 5,000 Da, as using ESI or APCI would require multiply charged species selection, further convoluting the fragment spectrum. Therefore, ESI is better suited when conducting routine MS/MS analysis of lower MW polymers.

Herein, low MW acrylate- and methacrylate-based homopolymers and copolymers were analyzed by mass spectrometry. Single-stage MS was utilized to analyze the molar mass distributions of various homopolymers, which provided insight on the end-groups, as well as the charged species of various polymer analytes. Using this information, the homopolymers were fragmented using CID to understand the end-group fragmentation pathways of the polymers. Block copolymers consisting of methyl acrylate and methyl methacrylate were synthesized in a specific fashion and additionally analyzed with MS/MS to determine any irregularities with the end-group fragmentation patterns. Additionally, linear block copolymers consisting of di(ethylene glycol)ethyl ether acrylate (dEGEEA) and lauryl acrylate (LA) were analyzed by MS/MS, using the end-group fragmentation patterns to structurally confirm the block placement. It is envisioned that this work will contribute to the growing field becoming known as polymeromics.

4.4 *Results and Discussion*

4.4.1 *Single-stage mass spectrometry of polymers*

Acrylate-based homopolymers were synthesized using a photoinduced ATRP method previously reported in the literature,[19] including methyl-, ethyl-, butyl-, and ethylene glycol methyl ether acrylate. Methyl methacrylate was incorporated in the study for comparison purposes regarding the isomeric copolymer study (S.A. #3). Methyl acrylate was the first homopolymer analyzed by single-stage MS, with the corresponding spectrum shown in Figure

4.2. Typically, acrylate-based analytes are charged with sodium due to the ester functionalities; however, protonated and potassium-charged species can be found in low abundances. The polymer ions within the distribution range from m/z 563.1296 to m/z 1423.4991, with the most abundant peak corresponding to m/z 907.2779, which is an 8mer (DP=8).
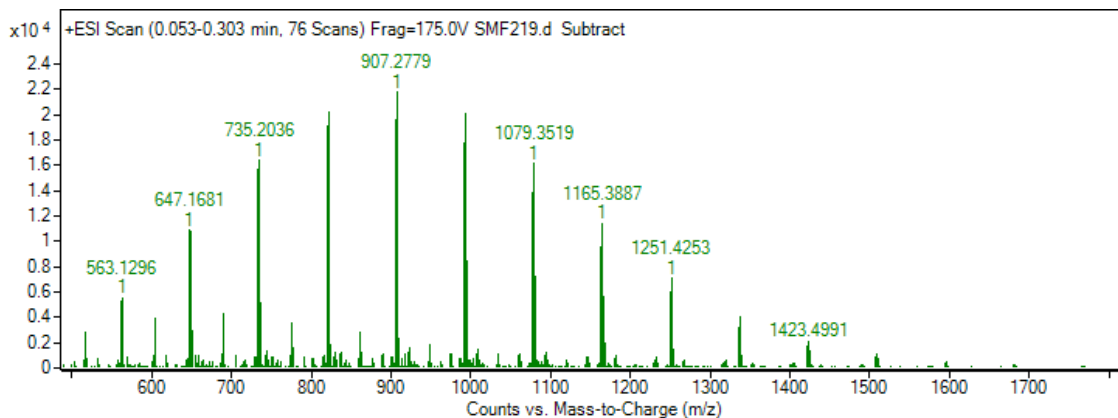
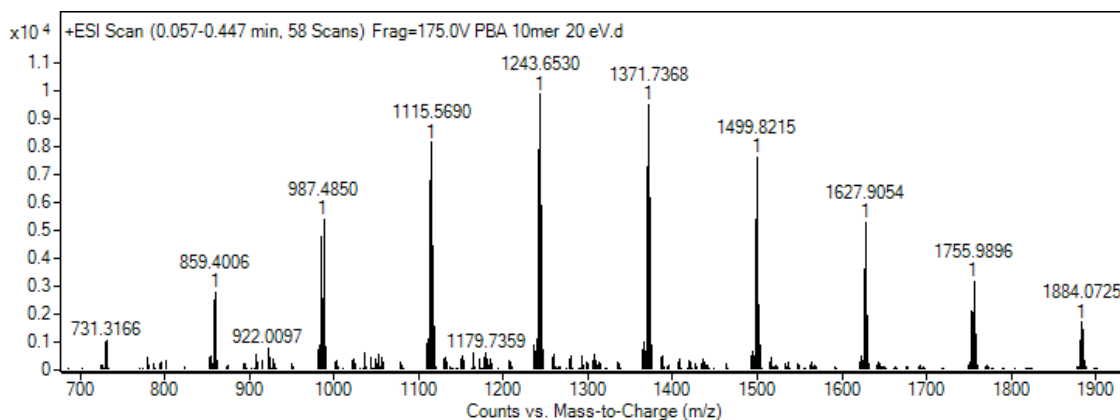**Figure 4.2** Single-stage mass spectrum of poly(MA).

Very similarly, the polymer analytes detected within the poly(ethyl acrylate) sample contained protonated and potassiated species; however, sodium was the most prevalent. The annotated peaks within the sample range from m/z 619.1916 to m/z 1419.6148 (Figure 4.3). Additionally, a non-brominated distribution is present, which is attributed to a coupling product from radical-radical terminations. The most prevalent peak within the spectrum belongs to m/z 1019.4030.
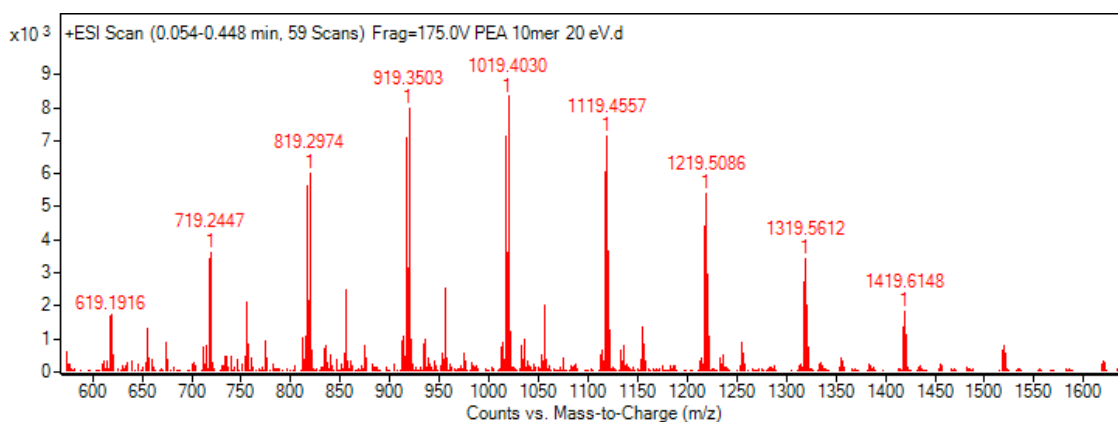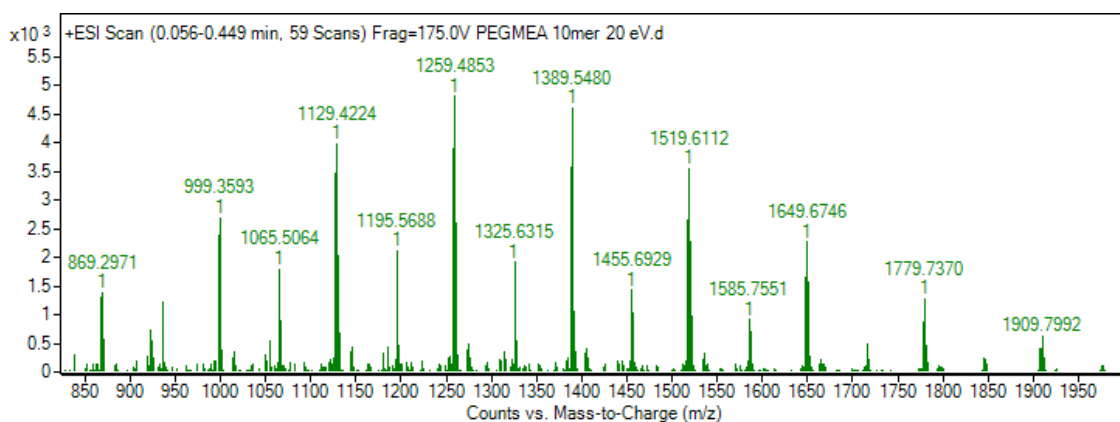

Figure 4.3 Single-stage mass spectrum of poly(EA).

73

Analyzing poly(butyl acrylate) revealed less abundant distributions containing $[M+H]^+$ and $[M+K]^+$ analytes in comparison with $[M+Na]^+$. The sodiated distribution ranges from m/z 731.3166 to m/z 1884.0725 (Figure 4.4), with no distribution present which indicates radical-radical coupling. The most abundant peak in the sample belongs to m/z 1243.6530 (DP=8).
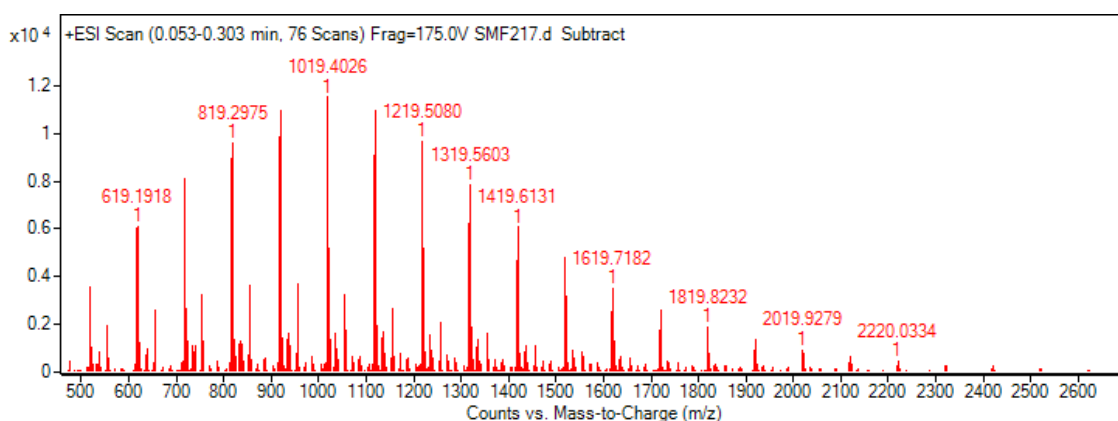

Figure 4.4 Single-stage mass spectrum of poly(BA).

Polymerizing ethylene glycol methyl ether acrylate provided a sample whose spectrum is similar to the other acrylate-based homopolymers. Protonated, sodiated, and potassiated species were all present, with the sodiated being the most predominant. The distribution is annotated below in Figure 4.5, and ranges from m/z 869.2971 to m/z 1909.7992. An additional non-brominated distribution can be seen at m/z 1065.5064 to m/z 1585.7551.

Figure 4.5 Single-stage mass spectrum of poly(EGMEA).

For comparison purposes in S.A. #3, MMA was polymerized in a similar fashion and analyzed by single-stage MS. Shown below in Figure 4.6 is the mass spectrum, with sodiated analytes ranging from m/z 619.1918 to m/z 2220.03345. Protonated and potassiated species were all found, but with a decreased intensity. Similar to PEA, a non-brominated distribution is present, indicating radical-radical coupling reactions. These terminations were attributed to an increased reactivity of the tertiary radical produced during the ATRP with PMMA, as there is methyl group on the backbone which is not present for other alky(acrylates).


Figure 4.6 Single-stage mass spectrum of poly(MMA).

4.4.2 *Tandem mass spectrometry of acrylate- and methacrylate-based homopolymers*

Shown below in Figure 4.7 are the generic fragment ion possibilities of poly(alkyl acrylates). Figure 4.8 outlines the fragment ion possibilities for poly(MMA), with a slightly more complex pathway.
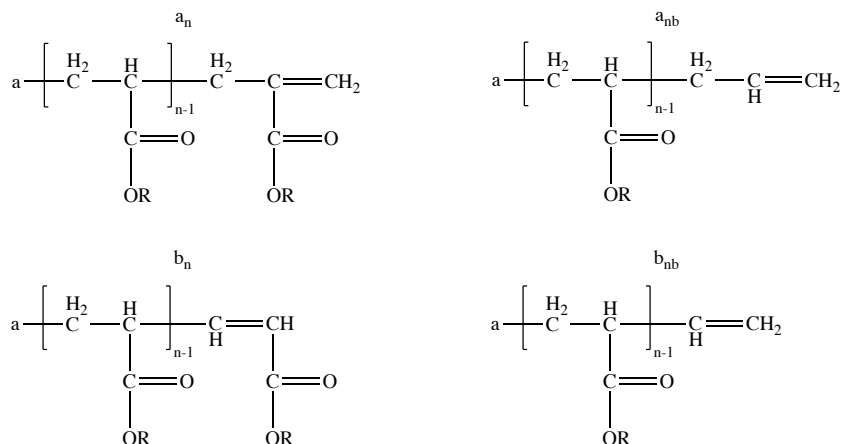
Figure 4.7 Possible fragmentation pathway for poly(alkyl acrylates).
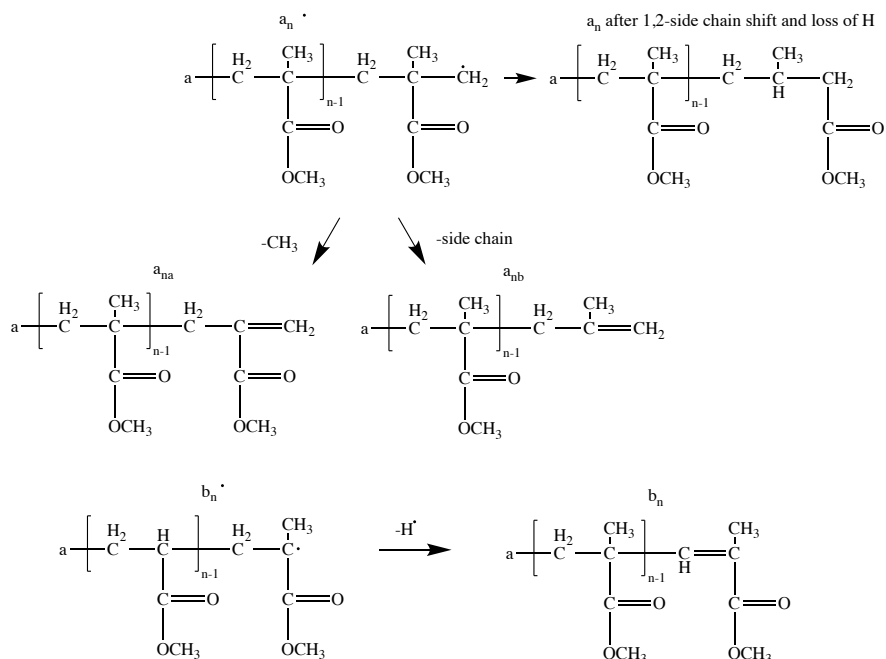
**Figure 4.8** Possible fragmentation pathway for poly(methyl methacrylate).

The PMA 10mer (DP=10) peak was selected at m/z 1079.3536 for CID experiments

ranging from 20-80 eV collisional energy. The calculated value for the corresponding peak was

found to be m/z 1079.3505, indicating under 3 ppm error for the measurement. As the collisional

energy is ramped upwards, a stark decrease in the parent ion signal is seen, with 80 eV providing

nearly quantitative fragmentation and a convoluted low-mass spectrum. As stated above,

poly(acrylates) exhibit an end-group lactonization when subjected to CID. This can be seen in

Figure 4.9, where 60 eV C.E. reduced the parent ion peak by 75%, and two primary high-mass

fragments are visible. The most abundant fragment ion peak at m/z 983.4089 corresponds to the

lactonization product, where the smaller peak at m/z 997.4244 indicates a bromine end-group

removal through elimination.
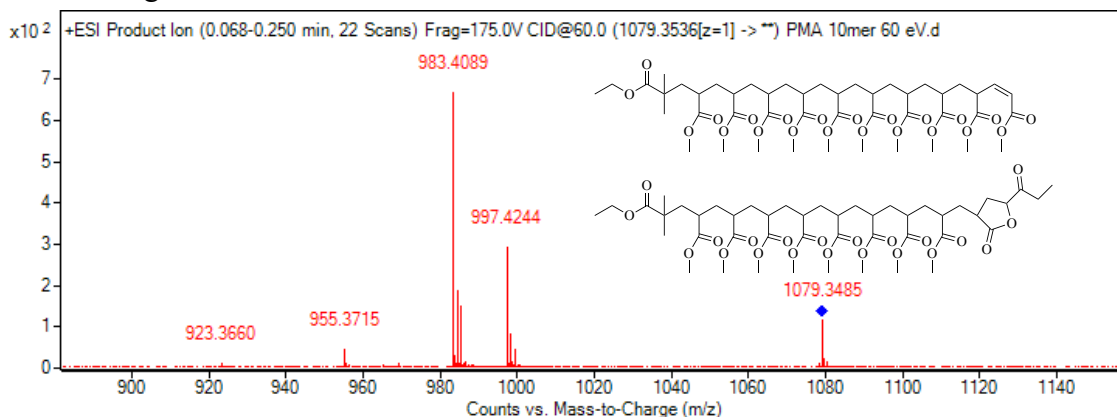
Figure 4.9 High-mass fragments from poly(MA) 10mer at 60 eV collisional energy.

Two other low-abundant peaks can be seen in the MS/MS spectrum at m/z 955.3715 and

m/z 923.3660. The peak at m/z 955.3715 corresponds to the removal of the ethyl group from the

initiating-end of the polymer ion, creating a carboxylic acid. The peak at m/z 923.3660 indicates

the ester functionality of the end-group on the lactone rearranges to an aldehyde-terminated

moiety. The polymer ion structures can be seen annotated below in the MS/MS spectrum (Figure

4.10)
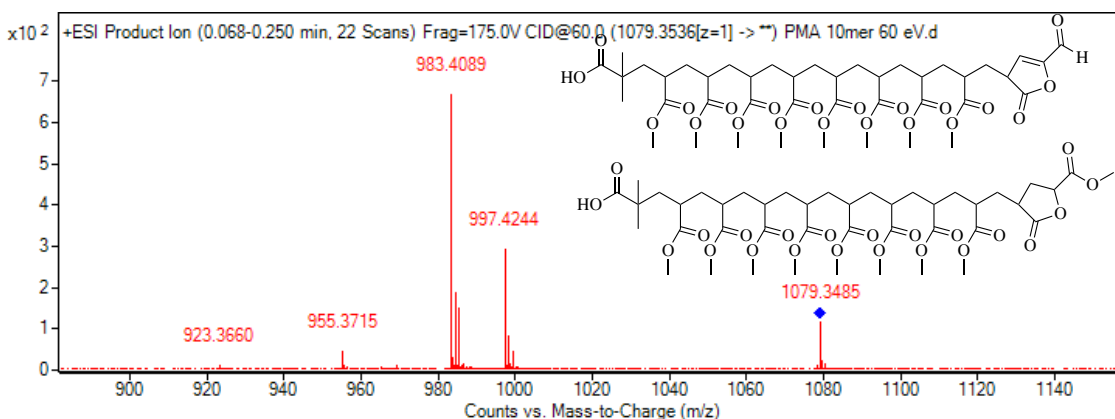
Figure 4.10 High-mass fragments from poly(MA) 10mer at 60 eV collisional energy.

The mid-mass region of the MS/MS spectrum contained many diagnostic ions previously outlined in Figure 4.7. The primary ions found were associated with the a_n series; however, additional fragments containing the α-end group are present. Moreover, the most abundant peak at m/z 281.1001 corresponds to 3 monomers linked together whilst being charged with a sodium atom, which is common for acrylate-based polymers to exhibit during CID. The peak at m/z 171.0656 and m/z 233.0744 were unable to be identified.
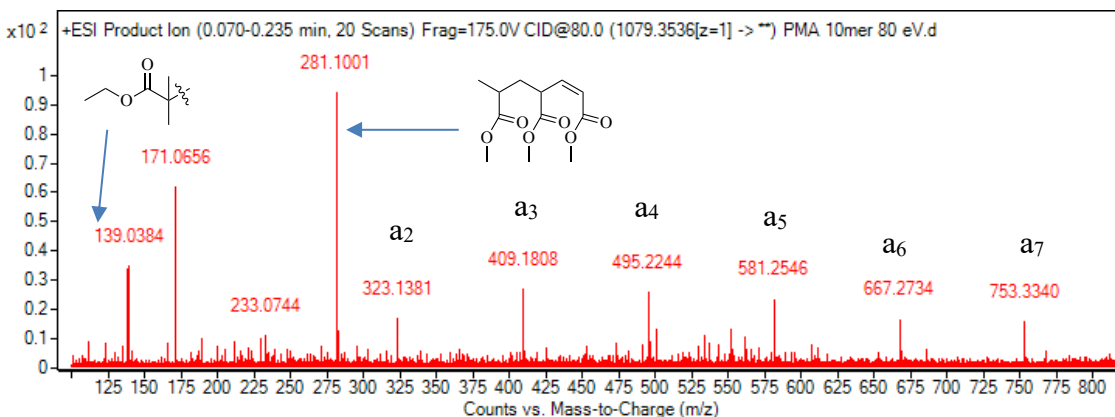
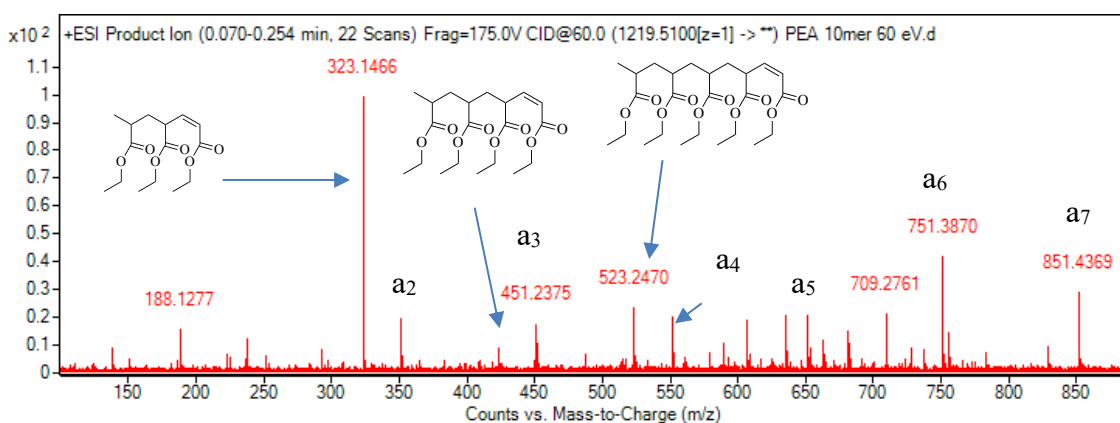**Figure 4.11** Mid-mass fragments from poly(MA) 10mer at 80 eV collisional energy.

Ethyl acrylate was polymerized in an identical fashion to methyl acrylate using the photoinduced ATRP. The 10mer at m/z 1219.5088 was selected and fragmented using 20-80 eV collisional energy. The calculated value for the parent ion peak was found to be m/z 1219.5100, indicating very low error with the measurement. Similar results were obtained regarding the

high-mass fragments within the MS/MS spectrum. First, the loss of HBr is observed, leading to a fragment ion with m/z 1137.5834. Followed by that is the more-abundant lactonization product at m/z 1109.5514, both of which are under 1 ppm experimental error. Additionally, the product ion at m/z 1081.5064 was found to be from the removal of the ethyl group on the initiating-end of the polymer ion. The fragment ion spectrum with corresponding structures can be viewed below in Figure 4.12.
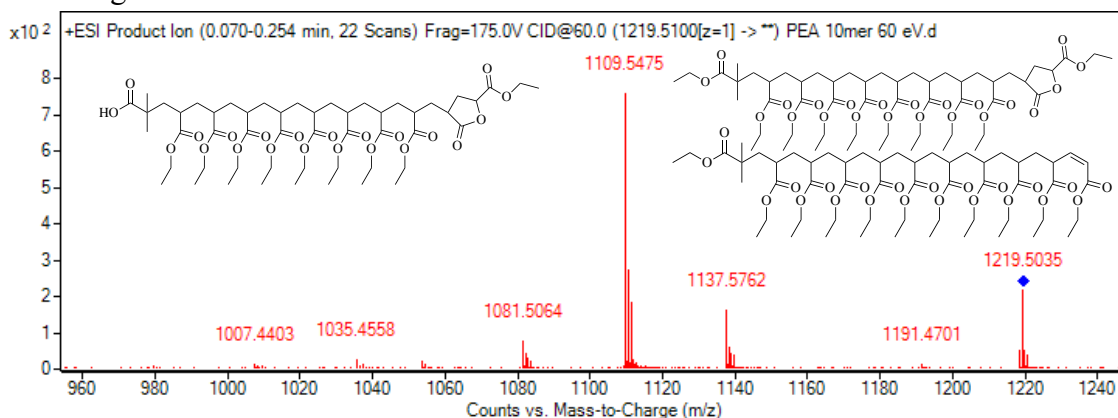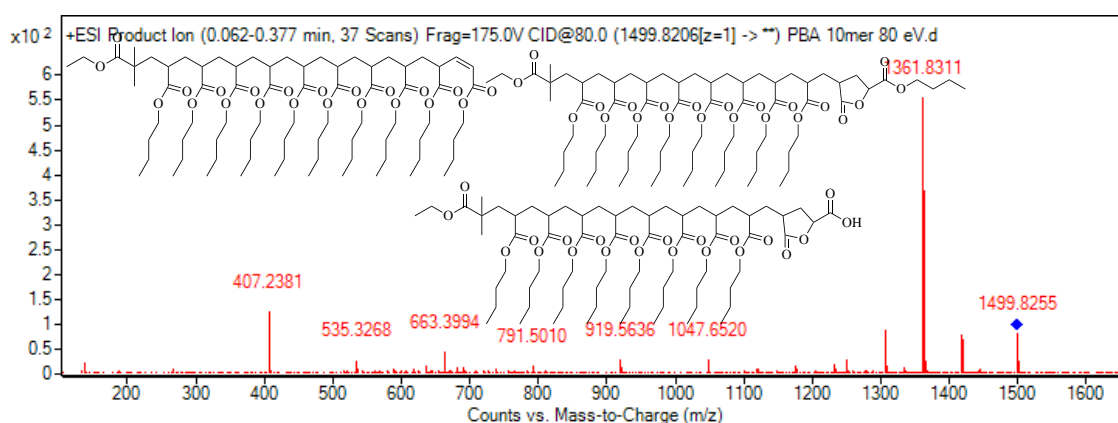

Figure 4.12 High-mass fragments from poly(EA) 10mer at 60 eV collisional energy.

Evaluating the low- and mid-mass spectrum reveals similar results when compared to the poly(MA) 10mer. The a_n series can be seen from m/z 351.1146 to m/z 851.4369, all with measurements under 5 ppm error. Additionally, a series of monomers charged with a sodium atom can be viewed from m/z 323.1466 to m/z 523.2470. Moving past 5 monomers, no additional ions can be detected, indicating a greater stability than the poly(MA) analogues.

Figure 4.13 Low- and mid-mass fragment ion spectrum of PEA 10mer.

Poly(BA) was synthesized and analyzed using tandem MS from 20-80 eV. The 10mer was

calculated to be m/z 1499.8206 and was found at m/z 1499.8189, indicating a very low error

with the measurement. It is notable that as the molecular weight of the monomer is increased as

with PBA, the parent ion is not as reduced as PMA/PEA with the same fragmentation energy.

Using 60 eV collisional energy for PBA reduces the parent ion signal by a small amount (~20%),

compared to PMA (~75%). This indicates that higher energy is required to reduce the parent ion

signal to the same degree.

Figure 4.14 Mid-mass fragments from PBA 10mer.

The first fragment observed in the high-mass spectrum is associated with the loss of HBr

at m/z 1417.8969. Followed by that is the lactonization product at m/z 1361.8322 and removal of

Bu group on the lactone at m/z 1305.7594 (Figure 4.14). There were less polymer fragment ions

within the low- and mid-mass spectrum, indicating a higher degree of instability or lessened

ability to accept a charge. Unfortunately, there were no measured a_n series fragments as there

were for PMA and PEA. However, there were fragments with a larger abundance which

correspond to monomers linked together charged with a sodium atom from m/z 407.2381 (3

monomer units) to 1047.6520 (8 monomer units). This trend suggests that the longer the alkyl

chain within the monomer, the more able the analyte is to accept a charge and subsequently be detected.

Poly(EGMEA) 10mer was analyzed next, with a calculated m/z value of 1519.6158. The experimental value was found to be m/z 1519.6108, indicating an extremely low error with the measurement (under 1 ppm). Unlike the other alkyl acrylates, the first fragment ion in the high-mass spectrum is correlated to the loss of one of the alkyl chains within the parent ion at m/z 1461.5880. It is assumed that the penultimate pendant is lost, as that must occur for the lactonization process. Followed by that are two fragment ions at m/z 1437.6822 and m/z 1379.6362, which are identified as the loss of HBr and lactone product, respectively (Figure 4.15).
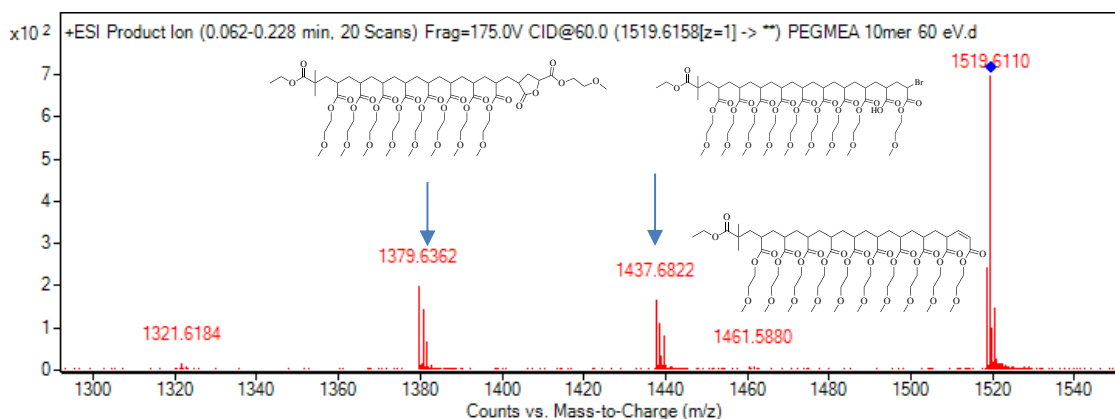
Figure 4.15 High-mass fragments from PEGMEA 10mer with 60 eV collisional energy.

When subjected to CID, PEGMEA behaved fairly similarly when compared to PBA regarding the low- and mid-mass fragment ions. However, unlike PBA, PEGMEA did offer some fragments belonging to the a_n series from m/z 541.2673 to m/z 1321.6184 (Figure 4.16). Additionally, monomer units sequenced together can be viewed at m/z 153.0540 (1mer), m/z 413.1762 (3mer), and m/z 673.3122 (5mer), all charged with a sodium atom.
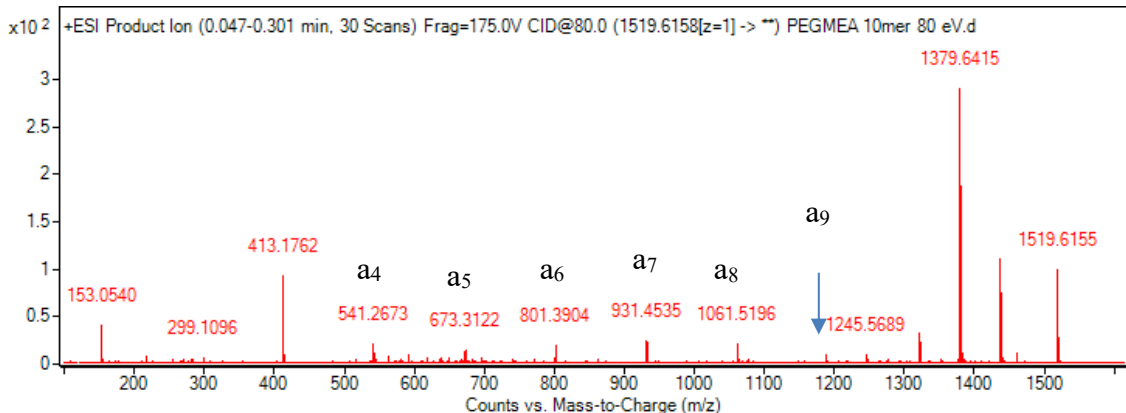
Figure 4.16 Low- and mid-mass fragments from PEGMEA at 80 eV collisional energy.

The last homopolymer analyzed by MS/MS was poly(MMA), and was performed in an analogous fashion to the other alkyl acrylates. This study was conducted to elucidate any new information which would be helpful whilst analyzing copolymers containing blocks of MMA. Much like the other homopolymers, the 10mer of PMMA was selected at m/z 1219.5096, having a calculated value of m/z 1219.5072, indicating a very low measurement error. The CID experiments were performed using 20-80 eV collisional energy.

The first noticeable different with PMMA is the loss of HBr is very low or even undetectable using 60 eV (Figure 4.17). This is likely due to the availability of Hydrogen during the elimination for alkyl acrylates, but not methacrylates. With PMMA, however, the primary fragment identified is only that of the lactone product through the loss of CH_3Br. As stated above, this is consistent with literature findings dating back to the late 90's. This can be used as a helpful tool when identifying fragments or monomer blocks with polymers which contain MMA. Doubling the collision energy to 80 eV does provide a loss of HBr, but the relative abundance is severely reduced in comparison with the other alkyl acrylate homopolymers (Figure 4.18).
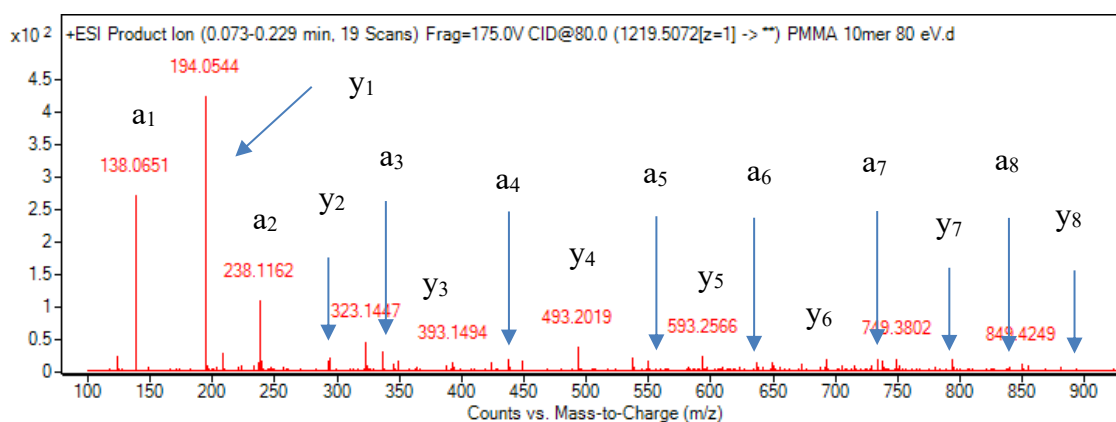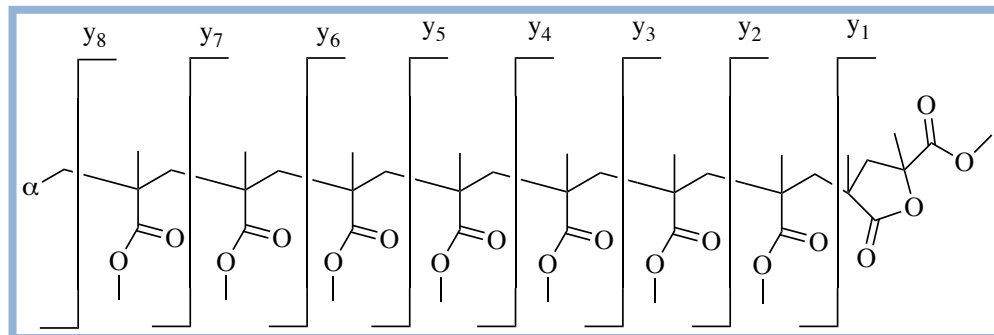
82
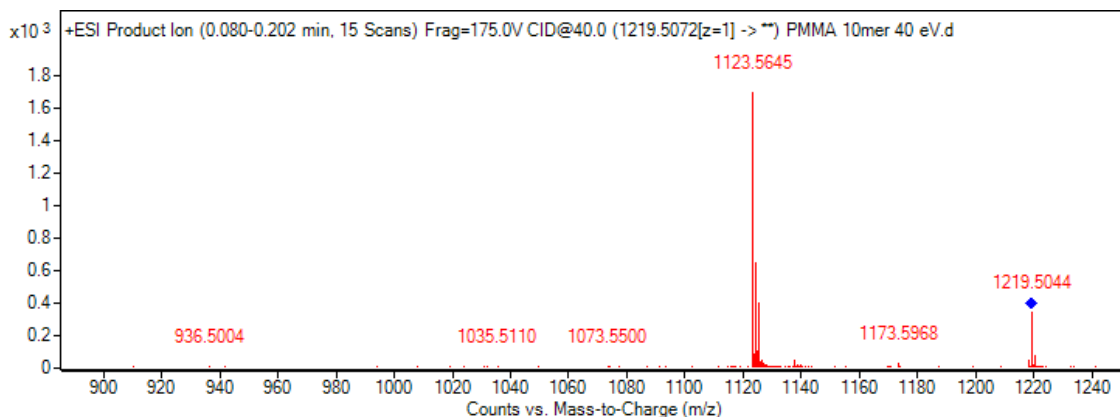
Figure 4.17 High-mass fragments from PMMA 10mer using 40 eV collisional energy.
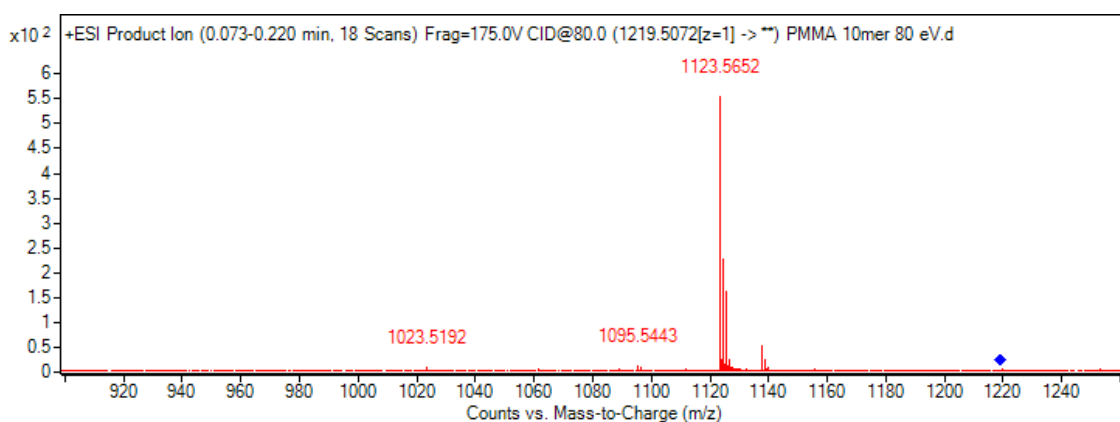
Figure 4.18 High-mass fragments from PMMA 10mer using 80 eV collisional energy.

Additionally, unlike the alky acrylates, the PMMA spectrum contained fragments detectable from the y_n series. This series is terminated with the lactone end-group, and ranges from m/z 194.0544 to m/z 894.6574, spanning the entire mid-mass region. A fragmentation Scheme, as well as the corresponding fragment ion spectrum can be seen below in Scheme 4.1 and Figure 4.16, respectively.

**Scheme 4.1** Fragmentation pathway of y_n series of ions from PMMA.

**Figure 4.19** Mid-mass fragments from PMMA 10mer using 80 eV collisional energy.

4.4.3 *Tandem mass spectrometry of acrylate- and methacrylate-based copolymers*

Copolymers containing blocks of MA and MMA were synthesized in an alternating fashion. The first sample consisted of poly(MA)-*co*-(MMA) and the second poly(MMA)-*co*-(MA). In the first sample, MA was polymerized and flash column chromatography was utilized to isolate the 3mer (DP=3). That 3mer was subjected to polymerization with MMA to generate the second block. Similarly, the second sample had the PMMA 6mer isolated and was further subjected to polymerization with MA as a macroinitiator, generating the second block. In both instances, the chemical composition is identical, as these copolymers are constitutional isomers, generating sodiated analytes of m/z 1077. Shown below in Figure 4.17 is a zoomed image of poly(MA)$_3$-*co*-(MMA)$_6$. Figure 4.18 displays the analyte at m/z 1077 consisting of poly(MMA)$_6$-

co-(MA)$_3$. The isomer analytes m/z values are 1077.4022 and 1077.3992, respectively. Low

error between the two samples at 2.78 ppm was measured, indicating the analytes are of known

origin. With this information, we can fragment the analytes with CID experiments with

confidence on their structural makeup.
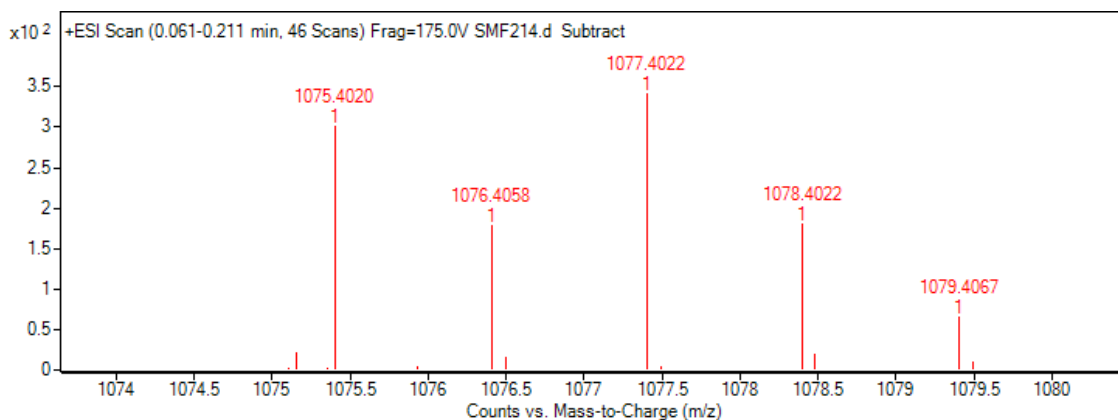
Figure 4.20 Zoomed-in mass spectrum of poly(MA)$_3$-*co*-(MMA)$_6$.
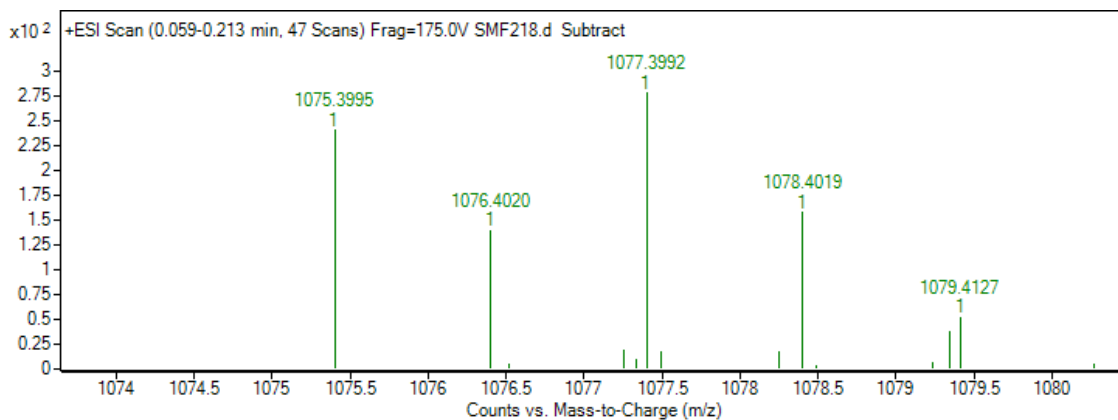
Figure 4.21 Zoomed-in mass spectrum of poly(MMA)$_6$-*co*-(MA)$_3$.

Collisional energy of 40 eV was employed to fragment the peaks at m/z 1077 to elucidate any

structural information. Shown below in Figure 4.19 is the MS/MS spectrum for poly(MA)$_3$-*co*-

(MMA)$_6$, which two primary fragments can be seen. The highest fragment ion belongs to the

end-group lactonization product, much like the homopolymers that were previously analyzed at

m/z 981.4589. However, there is a severely reduced ion peak related to the loss of HBr, a step which occurs before lactonization in acrylate-based homopolymers. Through this information, it is assumed that the loss of HBr and the formation of a stable peak at m/z 995.4661 is hindered due to the lack of Hydrogen availability on the polymer end-group. As this polymer is capped with MMA. Analyzing the MA-capped counterpart with identical MS/MS conditions should reveal a peak at m/z 995 with much larger intensity.
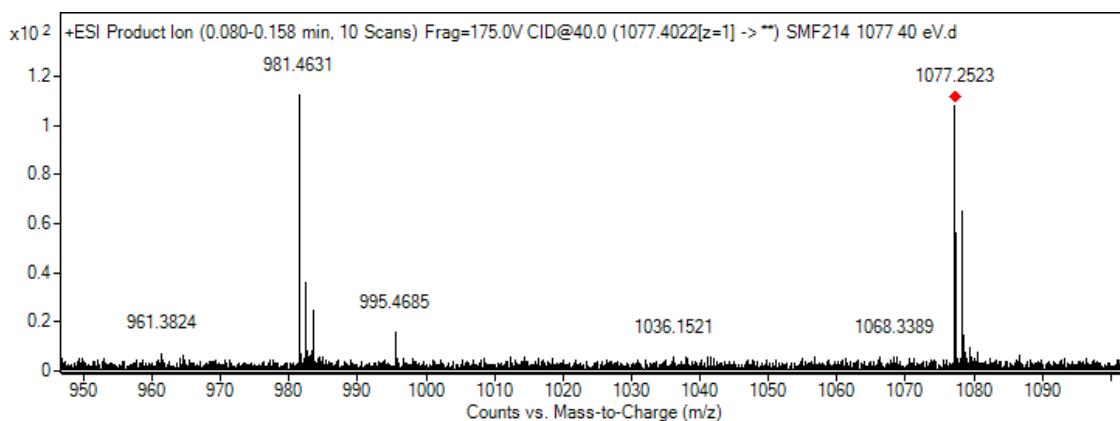

Figure 4.22 High-mass fragments from poly(MA)$_3$-*co*-(MMA)$_6$ using 40 eV collisional energy.

Shown below in Figure 4.20 is the MS/MS spectrum of poly(MMA)$_6$-*co*-(MA)$_3$ using 40 eV collisional energy. The first assessment indicates a greater ion stability, as the same C.E. only reduces the parent ion peak by a small amount, in comparison with the previous example. Additionally, we have a much larger peak at m/z 995, relative to the ion peak at m/z 981. This indicates a greater stability with the rearrangement in which HBr is first loss, as the availability of Hydrogen on the polymer backbone this species is capped with MA.
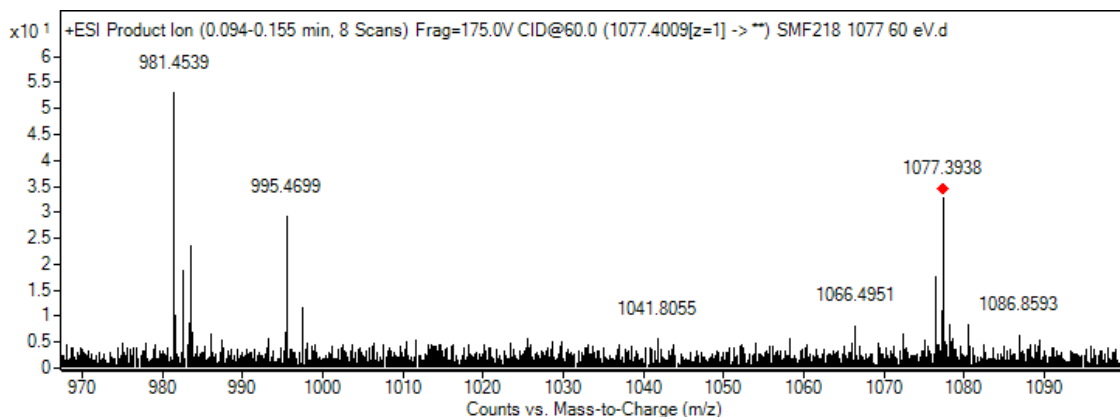
Figure 4.23 High-mass fragments from poly(MMA)$_6$-*co*-(MA)$_3$ using 40 eV collisional energy.

Utilizing the linear copolymers in Chapter 3 of this text, MS/MS analysis was conducted via the end-group lactonization to determine correct monomer sequences within the polymer analytes. The polymers were synthesized such the di(ethylene glycol)ethyl ether acrylate was the first monomer, followed by lauryl acrylate. First, a single-stage mass spectrum was collected to determine the appropriate ion peak, which can be seen below in Figure 4.21. The arrow with highlighted boxes indicate the parent ion peaks which will be fragmented during the CID experiments.
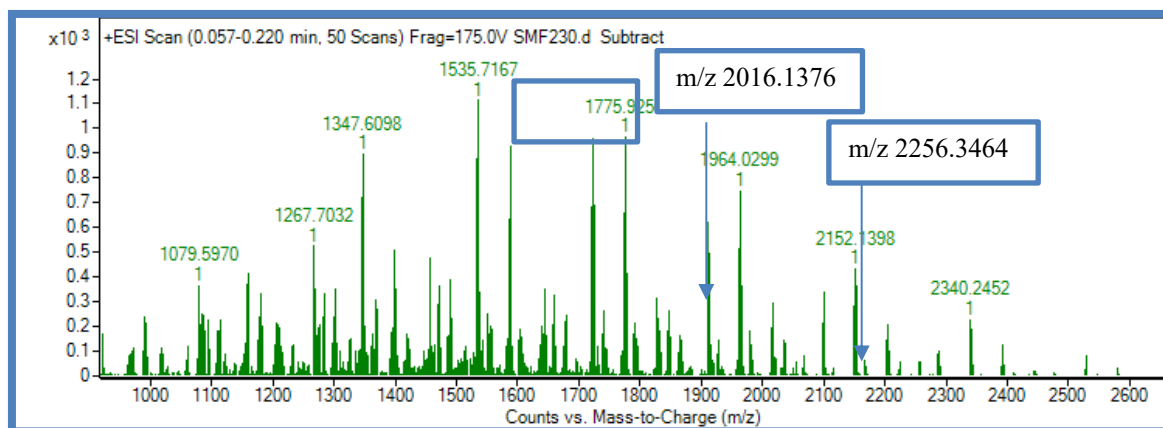

Figure 4.24 Single-stage MS of poly(dEGEEA)-*co*(LA).

The tandem MS experiment would first start with the fragmentation of poly(dEGEEA)$_7$-co-(LA)$_3$, and them systematically reduce the amount of LA on the second block. This will show a loss of a pendant arm functionality alongside Bromine, which combined mass will elucidate the penultimate monomer unit within the species. The first CID experiment is highlighted below in Figure 4.22, with corresponding structure annotations. It must be noted that 10 eV collisional energy, although quite high, reduces the parent ion peak by only 30%. The first loss is associated with HBr, much like the acrylate-based homopolymers outline previously in this chapter. Followed by that is the end-group lactonization product at m/z 2007.2268. The loss of 249.1158 indicates a pendant arm of LA in conjunction with Bromine, is lost during the rearrangement.
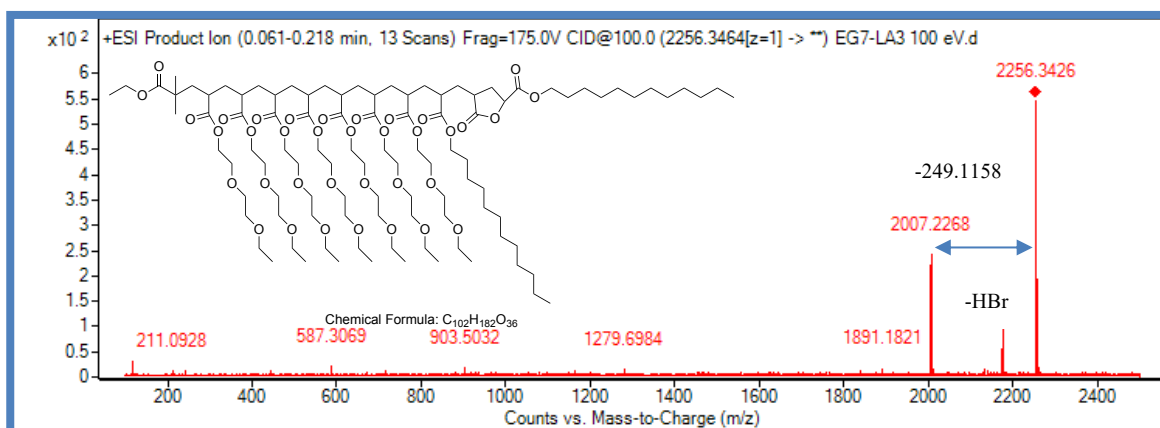
Figure 4.25 MS/MS spectrum of poly(dEGEEA)$_7$-co-(LA)$_3$ at 100 eV collisional energy.

Fragmenting the next parent ion peak at m/z 2016.1378 revealed similar results, as the penultimate monomer unit still belongs to that of LA. Shown below in Figure 4.23 is the correspond MS/MS spectrum. Again, we see the loss of HBr followed by a rearrangement with loss of the LA pendant arm with Bromine.
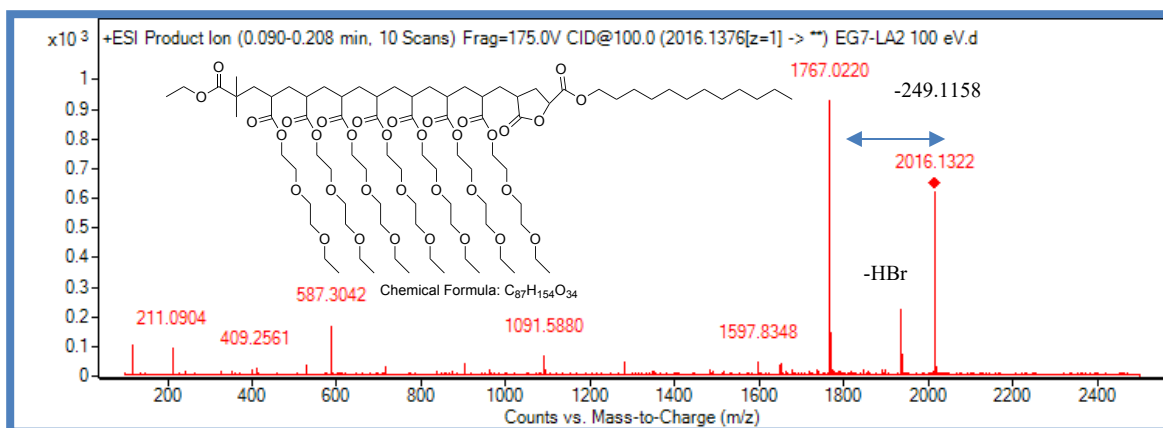
Figure 4.26 MS/MS spectrum of poly(dEGEEA)$_7$-*co*-(LA)$_2$ at 100 eV collisional energy.

Fragmenting the next ion peak in the series at m/z 1775.9286 revealed a loss of HBr, as it occurs

with all acrylate-based polymers outline within this text. However, the penultimate unit of this

polymer chain now belongs to that of dEGEEA, therefore a loss of the pendant arm functionality

of that monomer should be seen. Indeed, the fragment ion peak at m/z 1577.9172 indicates the

loss of 198.0038, which is the combined mass of the pendant arm of dEGEEA and Bromine.

This suggests that the linear copolymer synthesized was in true block fashion. Additional mid-

mass fragments were able to be identified, such as m/z 587.3042 which is 3 dEGEEA units

linked together charged with a sodium atom.

4.5 *Conclusion*

  Tandem mass spectrometry is a powerful technique which can be used to structurally

characterize synthetic polymers. Acrylate- and methacrylate-based homopolymers were

synthesized according to a photoinduced ATRP methodology and subsequently characterized

with single-stage mass spectrometry to reveal molar miss distribution profiles. Polymer ion

peaks corresponding to the 10mers (DP=10) were selected for CID experiments using a variety

of collisional energy. Regarding end-group fragmentation, acrylate-based homopolymers first

experience a loss of HBr, indicated by a fragment ion peak 82 Da less than the parent ion. The

next primary high mass fragment is correlated to the formation of a lactone ring on the end-group of the polymer. This fragment can be recognized with the loss of the penultimate monomer pendant arm alongside Bromine. For methacrylate-based polymers, a reduced signal of the HBr loss is exhibited, and the primary high mass fragment is associated with the lactone moiety-bearing polymer ion.

This information was utilized to characterize synthetic polymer samples containing alternating blocks of methyl acrylate and methyl methacrylate. Poly(MA)$_3$-*co*-(MMA)$_6$ and poly(MMA)$_6$-*co*-(MA)$_3$ were fragmented with identical energies to reveal similar results when compared to the homopolymers. Copolymers containing di(ethylene glycol)ethyl ether acrylate and lauryl acrylate were synthesized in a block fashion (CH3), and fragmented with CID in an analogous procedure. The copolymers were sequentially characterized by reducing the number of LA monomers on the polymer ion in increments of one and using the loss of the pendant arm functionality to determine the location of the blocks based on the location of the penultimate monomer unit.

In conclusion, tandem mass spectrometry is a formidable, yet under-utilized technique for polymer characterization. One drawback that currently exists lies within the inability of ESI to properly ionize larger molecular weight polymers, therefore is primarily used for lower molar mass polymer samples. In future endeavors, higher molecular weight polymers will be targeted using MALDI ionization to develop a connection between polymer sizes and their behavior in a tandem environment.

References

1.   Wesdemiotis, C., Multidimensional Mass Spectrometry of Synthetic Polymers and Advanced Materials. *Angewandte Chemie International Edition* **2017,** *56* (6), 1452-1464.

2.   Wesdemiotis, C.; Pingitore, F.; Polce, M. J.; Russell, V. M.; Kim, Y.; Kausch, C. M.; Connors, T. H.; Medsker, R. E.; Thomas, R. R., Characterization of a Poly(fluorooxetane) and Poly(fluorooxetane-co-THF) by MALDI Mass Spectrometry, Size Exclusion Chromatography, and NMR Spectroscopy. *Macromolecules* **2006,** *39* (24), 8369-8378.

3.   Wesdemiotis, C.; Solak, N.; Polce, M. J.; Dabney, D. E.; Chaicharoen, K.; Katzenmeyer, B. C., Fragmentation pathways of polymer ions. *Mass Spectrometry Reviews* **2011,** *30* (4), 523-559.

4.   Crecelius Anna, C.; Baumgaertel, A.; Schubert Ulrich, S., Tandem mass spectrometry of synthetic polymers. *Journal of Mass Spectrometry* **2009,** *44* (9), 1277-1286.

5.   Altuntaş, E.; Kempe, K.; Crecelius-Vitz, A.; Richard, H.; Schubert, U., *ESI-MS & MS/MS Analysis of Poly (2-oxazoline) s with Different Side Groups*. 2010.

6.   Altuntaş, E.; Knop, K.; Tauhardt, L.; Kempe, K.; Crecelius, A. C.; Jäger, M.; Hager, M. D.; Schubert, U. S., Tandem mass spectrometry of poly(ethylene imine)s by electrospray ionization (ESI) and matrix-assisted laser desorption/ionization (MALDI). *Journal of Mass Spectrometry* **2012,** *47* (1), 105-114.

7.   Altuntaş, E.; Krieg, A.; Baumgaertel, A.; Crecelius, A. C.; Schubert, U. S., ESI, APCI, and MALDI tandem mass spectrometry of poly(methyl acrylate)s: A comparison study for the structural characterization of polymers synthesized via CRP techniques and the software

application to analyze MS/MS data. *Journal of Polymer Science Part A: Polymer Chemistry* **2013,** *51* (7), 1595-1605.

8.   Altuntaş, E.; Schubert, U. S., "Polymeromics": Mass spectrometry based strategies in polymer science toward complete sequencing approaches: A review. *Analytica Chimica Acta* **2014,** *808*, 56-69.

9.   Chaicharoen, K.; Polce, M. J.; Singh, A.; Pugh, C.; Wesdemiotis, C., Characterization of linear and branched polyacrylates by tandem mass spectrometry. *Analytical and Bioanalytical Chemistry* **2008,** *392* (4), 595-607.

10.   Crotty, S.; Gerişlioğlu, S.; Endres, K. J.; Wesdemiotis, C.; Schubert, U. S., Polymer architectures via mass spectrometry and hyphenated techniques: A review. *Analytica Chimica Acta* **2016,** *932*, 1-21.

11.   Yol, A. M.; Dabney, D. E.; Wang, S.-F.; Laurent, B. A.; Foster, M. D.; Quirk, R. P.; Grayson, S. M.; Wesdemiotis, C., Differentiation of Linear and Cyclic Polymer Architectures by MALDI Tandem Mass Spectrometry (MALDI-MS2). *Journal of The American Society for Mass Spectrometry* **2013,** *24* (1), 74-82.

12.   Yol, A. M.; Janoski, J.; Quirk, R. P.; Wesdemiotis, C., Sequence Analysis of Styrenic Copolymers by Tandem Mass Spectrometry. *Analytical Chemistry* **2014,** *86* (19), 9576-9582.

13.   Yol, A. M.; Wesdemiotis, C., Multidimensional mass spectrometry methods for the structural characterization of cyclic polymers. *Reactive and Functional Polymers* **2014,** *80*, 95-108.

14.   Bates, F. S.; Hillmyer, M. A.; Lodge, T. P.; Bates, C. M.; Delaney, K. T.; Fredrickson, G. H., Multiblock Polymers: Panacea or Pandora's Box? *Science* **2012,** *336* (6080), 434-440.

15.   Porel, M.; Alabi, C. A., Sequence-Defined Polymers via Orthogonal Allyl Acrylamide Building Blocks. *Journal of the American Chemical Society* **2014,** *136* (38), 13162-13165.

16.   Jackson, A. T.; Yates, H. T.; Scrivens, J. H.; Green, M. R.; Bateman, R. H., Utilizing matrix-assisted laser desorption/ionization-collision induced dissociation for the generation of structural information from poly(alkyl methacrylate)s. *Journal of the American Society for Mass Spectrometry* **1997,** *8* (12), 1206-1213.

17.   Jackson, A. T.; Yates, H. T.; Scrivens, J. H.; Green, M. R.; Bateman, R. H., Matrix-assisted laser desorption/ionization-collision induced dissociation of poly(styrene). *Journal of the American Society for Mass Spectrometry* **1998,** *9* (4), 269-274.

18.   Jackson, A. T.; Slade, S. E.; Scrivens, J. H., Characterisation of poly(alkyl methacrylate)s by means of electrospray ionisation–tandem mass spectrometry (ESI–MS/MS). *International Journal of Mass Spectrometry* **2004,** *238* (3), 265-277.

19.   Anastasaki, A.; Nikolaou, V.; Pappas, G. S.; Zhang, Q.; Wan, C.; Wilson, P.; Davis, T. P.; Whittaker, M. R.; Haddleton, D. M., Photoinduced sequence-control via one pot living radical polymerization of acrylates. *Chemical Science* **2014,** *5* (9), 3536-3542.

5. CONCLUSION

This work focused on utilizing atom transfer radical processes to prepare functionalized materials with subsequent characterization and application testing. The greater impact of each research project is summarized in the corresponding sections below.

In Chapter 2, the objective involved synthesizing small functionalized molecules using a photoinduced atom transfer radical addition in conjunction with a copper-catalyzed azide-alkyne cycloaddition. Through optimization, the ATRA reactions afforded satisfying yields, which were increased from 30% of 70% product selectivity. These atom transfer products contained an alkyne or azide end group, making them suitable for conducting CuAAC with a functionalized Coumarin dye. This transformation afforded near-quantitative yields due to the robust nature of the CuAAC reaction. The reaction mixture prior to CuAAC exhibited no fluorescent activity; however, upon formation of the triazole linkage, the solution displayed sharp fluorescence. The broader impact of this research implicates ATRA as a suitable candidate when selecting a complementary reaction to CuAAC, as it generates adducts with rapid conversion, good product selectivity, and functional group tolerance. Additionally, this reaction can be completed with sub-ppm amounts of copper catalyst and is accepting to altered reaction conditions.

The goal of Chapter 3 was focused on encapsulating polar dyes in a nonpolar solvent with the use of amphiphilic block copolymers. A photoinduced ATRP methodology was developed for the production of poly(dEGEEA)-*co*-(LA) in a one-pot fashion with varying architectures. Three molecular weight ranges were targeted to expand the scope of the study by determining a relationship between polymer size and encapsulation efficiency. It was found that the dye chosen for the study, rhodamine B, was insoluble in squalane, the matrix chosen to test encapsulation properties. The solubilization of the rhodamine B dye was attributed to the

copolymers, whose interior block aided in solubilization of the polar dye. The nonpolar corona of the copolymers assisted in solubilization in the squalane solvent. Additionally, the exterior block of the copolymer mimics the lipophilic hydrocarbon chains within human skin, making these materials excellent applicants for potential transdermal drug delivery.

In Chapter 4, tandem mass spectrometry was used to structurally characterize synthetic polymers. Acrylate- and methacrylate-based homopolymers were characterized with single-stage mass spectrometry to reveal molar miss distribution profiles. Polymer ion peaks corresponding to the 10mers (DP=10) were selected for CID experiments using a variety of collisional energy. Using that information, tandem MS was utilized to characterize synthetic polymer samples containing alternating blocks of methyl acrylate and methyl methacrylate: poly(MA)$_3$-*co*-(MMA)$_6$ and poly(MMA)$_6$-*co*-(MA)$_3$. Additionally, samples of poly(dEGEEA)-*co*-(LA) were synthesized in a block fashion and fragmented with CID in an analogous procedure. The copolymers were sequentially characterized by reducing the number of LA monomers on the polymer ion in increments of one and using the loss of the pendant arm functionality to determine the location of the blocks based on the penultimate monomer unit. The broader impact of this work focuses of illustrating how tandem mass spectrometry is a formidable, yet under-utilized technique for polymer characterization. It is anticipated that performing more complex MS/MS analyses of synthetic copolymer samples will assist in growing the field of polymeromics, so that one-day, software assistance can be used as an aid, much like proteomics.

Chapter 2 Appendix

General Procedures.

All chemicals were purchased from commercial sources and used as received unless otherwise noted. Inhibitors were removed from all commercial acrylates by utilizing silica gel flash column chromatography.

Instrumentation and Equipment.

Bruker Avance 400 MHz NMR for ^{1}H and ^{13}C NMR spectroscopy characterization. MestReNova version 8.0.1-10878 was used to generate images of NMR spectra. MelodySusie VIOLET II 365 nm UV lamp was used for photo-initiated ATRA reactions (available on Amazon). Agilent Technologies 6530B AccurateMass QTOF was utilized for adduct characterization (source: Agilent Jet Stream Electrospray Ionization Source, flow rate = 0.5 mL/min).

Copper-catalyzed photoATRA kinetic study.

The alkyl halide BBiBE, CuBr$_2$, Me$_6$TREN, 1,4-dimethoxybenzene, and DMSO were added to a scintillation vial with a magnetic stir bar. The vial was capped with a septum and sealed tightly with copper wire. The solution was placed on a magnetic stir plate where the copper species could complex with the ligand (Me$_6$TREN). When the catalyst solution was fully complexed, the solution vial was purged with nitrogen on a Schlenk line for 10 minutes. While the initiator/complex solution was purging, a small vial with methyl acrylate was sparged with nitrogen for 10 minutes. After the methyl acrylate was sufficiently degassed, a nitrogen-purged micro syringe was used to transfer an aliquot to the degassed initiator/complex solution. After injection, the reaction vessel was placed under a UV light source while stirring to begin the reduction of the Cu^{II}L-X complex, and the time was recorded. ^{1}H NMR integrations (relative to

internal standard) were utilized to measure consumption of methyl acrylate starting material at various time intervals and calculate final yield.

Copper-catalyzed photoATRA catalyst loading studies.

A stock solution of initiator (1.25 mmol), alkene (2.5 mmol), internal standard (10 mol% relative to initiator), and solvent (~200 μL) was prepared a 20 mL scintillation vial and thoroughly mixed. 6 NMR tubes were prepared and labeled time 0, catalyst loading (1-4), and blank. 50 μL of the stock solution was placed in the "time 0" NMR tube and placed in the fridge. The remaining stock solution was evenly distributed between the other NMR tubes. The appropriate amount of catalyst solution (0.1-0.2 M) was added to the respective tubes. Solvent was added to each tube to maintain the desired alkene concentration, each tube was individually sparged with nitrogen for 30 seconds, and quickly capped and taped with electrical tape to ensure inert conditions. The tubes were placed under the UV lamp to react until completion. Once the reaction was complete, tubes were removed and most the contents discarded. Each tube was diluted with $CDCl_3$ and analyzed via Bruker Avance 400 MHz NMR.

General procedure for nucleophilic substitution of bromine for azide.

Once flash column chromatography has been conducted to separate the desired adduct, it was placed in a scintillation vial with a magnetic stir bar. DMF was added to the vial, keeping the brominated adduct 0.1 M in solution, and the solution is allowed for mix for 10 minutes. Sodium azide is added, and the solution was stirred overnight at room temperature. Once complete, the reaction vessel is placed in an ice bath, while stirring, and diluted with distilled water to quench the reaction for 3 to 4 hours. The product was extracted with diethyl ether, dried with $MgSO_4$, and the solvent was removed under reduced pressure. Products were characterized with Bruker Avance 400 MHz NMR.

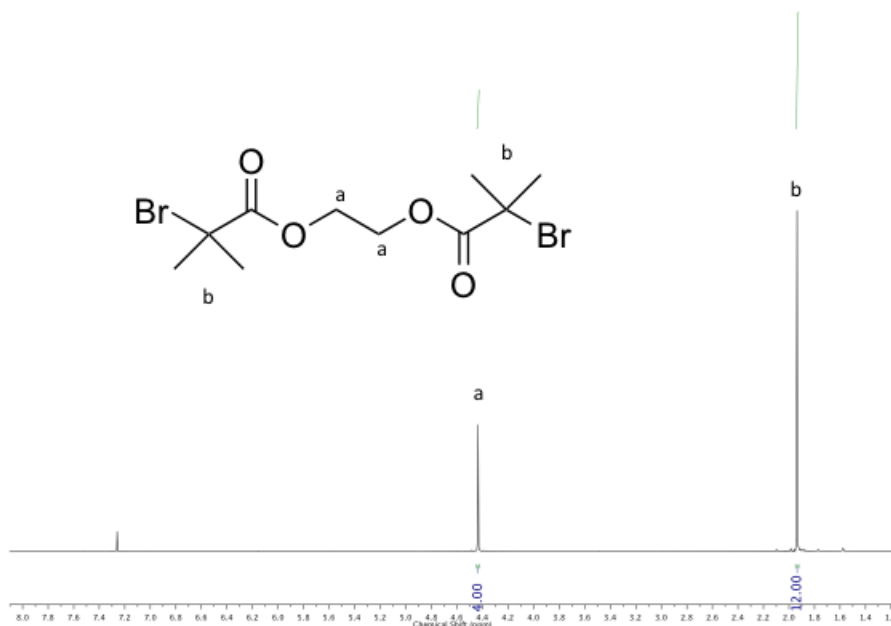**General procedure for copper-catalyzed azide-alkyne [3+2] cycloaddition.**

The isolated azide adduct was placed in a 4 mL glass vial, alongside a mini magnetic stir bar. The *t*-buOH/H_2O (1:1) mixture was added to the vial to keep $[azide]_0 = 0.1$ M. The solution was placed on a stir plate to mix thoroughly. A stoichiometric amount of alkyne was added to the vial. Copper sulfate pentahydrate was added to the vial, and the glass vial was tightly capped with a septum. The solution was bubbled with nitrogen briefly (5 mins) and placed in an oil bath on a magnetic stir plate (60 °C). A sodium ascorbate solution was prepared in H_2O (1.0 M) and injected into the vial. The mixture can react overnight. Upon completion, the vial was removed from the oil bath and placed on a magnetic stir plate. The solution was diluted with a small amount of distilled water (~1 mL), which induced the product to crash out of solution in the form of an oil. The oil was extracted with diethyl ether (3x5 mL), dried with $MgSO_4$, and the solvent removed under reduced pressure. The product was analyzed via Bruker Avance 400 MHz NMR and HRMS.

Synthesis of 1,2-bis(bromoisobutyryloxy)ethane (BBiBE)

The bifunctional initiator, BBiBE, was synthesized through an esterification reaction between ethylene glycol and 2-bromoisobutyryl bromide in the presence of triethyl amine. In a 250 mL round bottom flask, the following reagents were sequentially added: ethylene glycol (3.35 g, 5.40×10^{-2} mol), triethyl amine (15.2 mL, 1.09×10^{-1} mol), and 80 mL of dry dichloromethane. The solution was put in an ice bath and stirred for 15 minutes, to which 2-bromoisobutyryl bromide (13.5 mL, 1.09×10^{-1} mol) was added drop wise. The mixture was kept on ice for one hour, and afterward allowed to warm to room temperature, where it continued to mix overnight. The mixture was washed several times with water (3×25 mL). The aqueous portion was washed with dichloromethane (25 mL) to extract any remaining product. The

organic fractions were combined and washed with a saturated sodium bicarbonate and brine

solution (35 mL) and dried over $MgSO_4$. The final solution was filtered and concentrated under

reduced pressure at 50 °C, which yielded white/yellow crystalline solid. The initiator was

recrystallized with methanol, which resulted in colorless needle-like crystals. Yield: 11.4 g

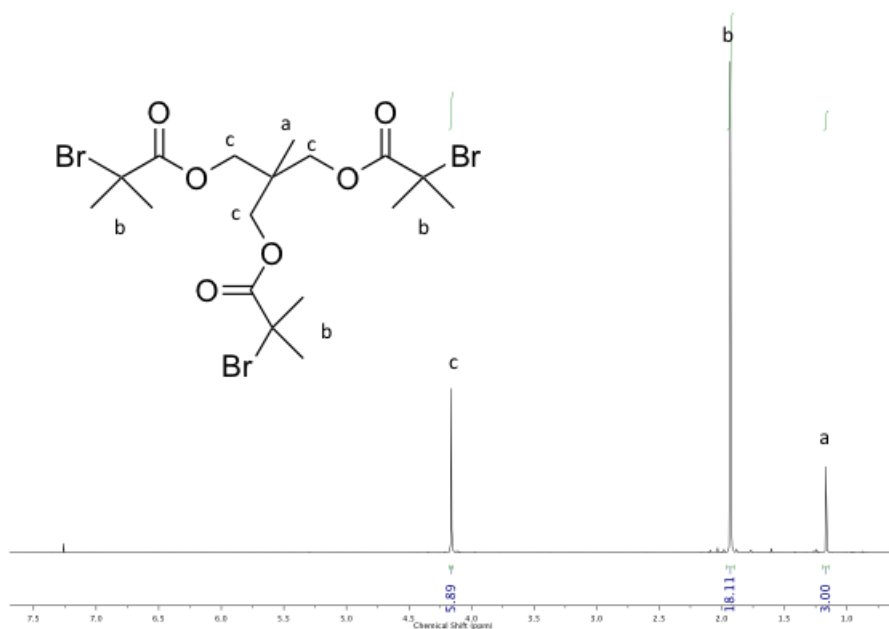(75%). ^{1}H NMR (400 MHz, $CDCl_3$): δ = 4.4 ppm (s, 4H) and 1.9 ppm (s, 12H).

Figure A2.1 ^{1}H NMR (400 MHz, $CDCl_3$, 298 K) spectrum of 1,2-

bis(bromoisobutyryloxy)ethane (**1**).

Synthesis of 1,1,1-tris(2-bromoisobutyryloxymethyl)ethane (TBiBE)

An analogous procedure was followed for the synthesis of TBiBE, but instead the primary

alcohol used was 1,1,1,-tris(hydroxymethyl)ethane (2.67 g, 2.22×10^{-2} mol) with a stoichiometric

amount of triethylamine (9.29 mL, 6.67×10^{-2} mol) and 2-bromoisobutyryl bromide (8.25 mL,

6.67×10^{-2} mol) in THF (100 mL). Flash column chromatography was utilized for purification

after aqueous workup. Product was recrystallized in hexanes. Yield: 5.5 g (44%) ^{1}H NMR (400 MHz, CDCl$_3$): δ = 4.16 ppm (s, 6H), 1.93 ppm (s, 18H), 1.17 ppm (s, 3H).

Figure A2.2 ^{1}H NMR (400 MHz, CDCl$_3$, 298 K) spectrum of 1,1,1-tris(2-bromoisobutyryloxymethyl)ethane (**2**).

Synthesis of propargyl-2-bromoisobutyrate (PBiB)

An analogous procedure was followed for the synthesis of PBiB, but instead the primary alcohol used was propargyl alcohol (1.99 g, 3.50×10^{-2} mol) with a stoichiometric amount of triethylamine (4.94 mL, 3.50×10^{-2} mol) and 2-bromoisobutyryl bromide (4.38 mL, 3.50×10^{-2} mol) in DCM (100 mL). Flash column chromatography was utilized for purification after aqueous workup. Yield: 5.49 g (76%) ^{1}H NMR (400 MHz, CDCl$_3$): δ = 4.75 ppm (s, 2H), 2.5 ppm (d, 1H), 1.9 ppm (s, 6H).
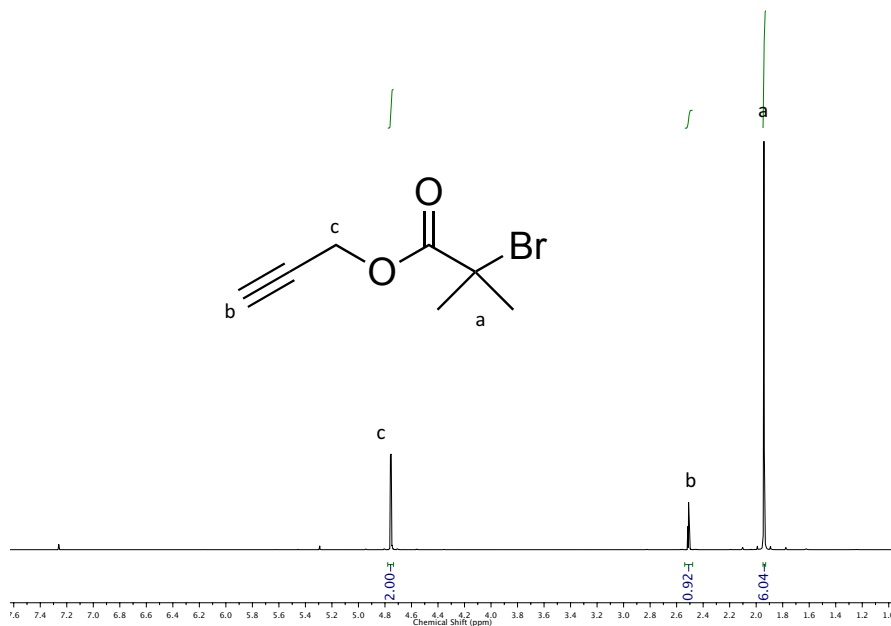
Figure A2.3 ^{1}H NMR (400 MHz, CDCl$_3$, 298 K) spectrum of propargyl-2-bromoisobutyrate (**9**).

Synthesis of 2-bromo-2-methyl-propanoic acid-3-azidopropylester (BMPAP)

The following reagents were added sequentially to a 150 mL RBF: 3-bromo-1-propanol (1.26 mL, 1.44×10^{-2} mol), sodium azide (1.63 g, 2.50×10^{-2} mol), and acetone/H$_2$O mixture of 6:1 (40 mL). A stir bar was added and the reaction was refluxed at 70 °C for 12 hours. After the reaction was complete, the acetone was removed under reduced pressure and the product was extracted with diethyl ether (3x15 mL). The product was dried over MgSO$_4$ and concentrated under reduced pressure to yield 3-azido-1-propanol as a viscous clear liquid. Yield: 1.24 g (85%). An analogous procedure was followed for the esterification reaction to yield BMPAP, but instead the primary alcohol used was 3-azido-1-propanol (1.24 g, 1.23×10^{-2} mol) with a stoichiometric amount of triethylamine (1.71 mL, 1.23×10^{-2} mol) and 2-bromoisobutyryl bromide (1.52 mL, 1.23×10^{-2} mol) in DCM (100 mL). After the reaction was complete, an aqueous workup was

performed following purification through flash column chromatography. The product BMPAP was recovered as a clear oil. Yield: 2.81 g (91%)
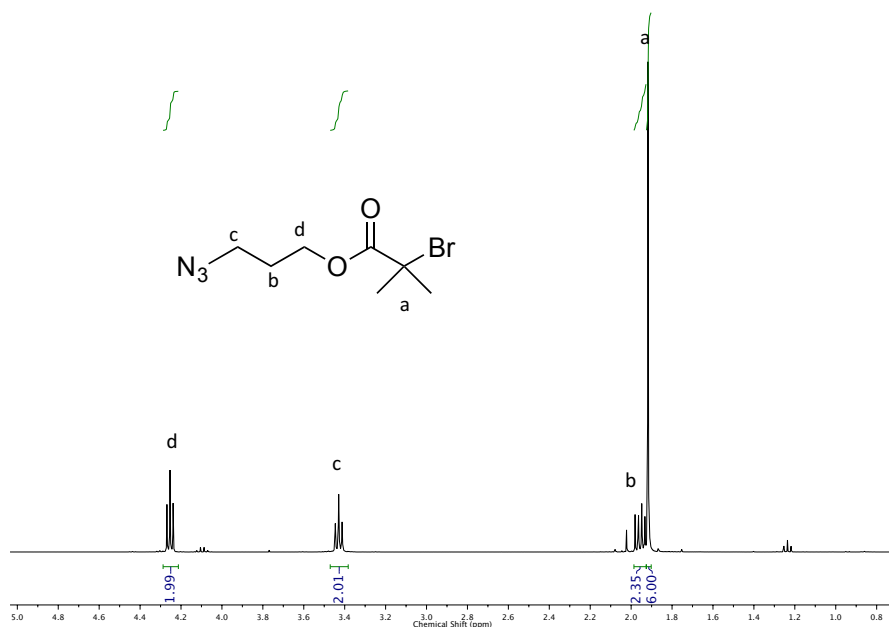
Figure A2.4 ^{1}H NMR (400 MHz, CDCl$_3$, 298 K) spectrum of 2-bromo-2-methyl-propanoic acid-3-azidopropylester (**10**).

Synthesis of ethylene glycol diacrylate (EGDA)

Ethylene glycol diacrylate (EGDA) was prepared through an esterification reaction between ethylene glycol and acryloyl chloride. Ethylene glycol (1.06 g, 1.71×10^{-2} mol) was added to a 150 mL round bottom flask containing a magnetic stir bar. DCM (35 mL) and triethylamine (4.78 mL, 3.42×10^{-2} mol) were added and the flask capped and placed in an ice bath, where it stirred for 15 minutes. Acryloyl chloride was separately purged with nitrogen. Once sufficiently degassed, acryloyl chloride (2.78 mL, 3.42×10^{-2} mol) was injected drop wise into the stirring solution. The mixture was kept on ice for one hour, and afterward allowed to warm to room temperature, where it continued to mix overnight. The mixture was washed

several times with water (3×25 mL). The aqueous portion was washed with dichloromethane (25

mL) to extract any remaining product. The organic fractions were combined and washed with a

saturated sodium bicarbonate and brine solution (35 mL) and dried over MgSO$_4$. The solvent

was removed under reduced pressure, and the product was purified through flash column

chromatography. Yield: 2.13 g (73%) ^{1}H NMR (400 MHz, CDCl$_3$).
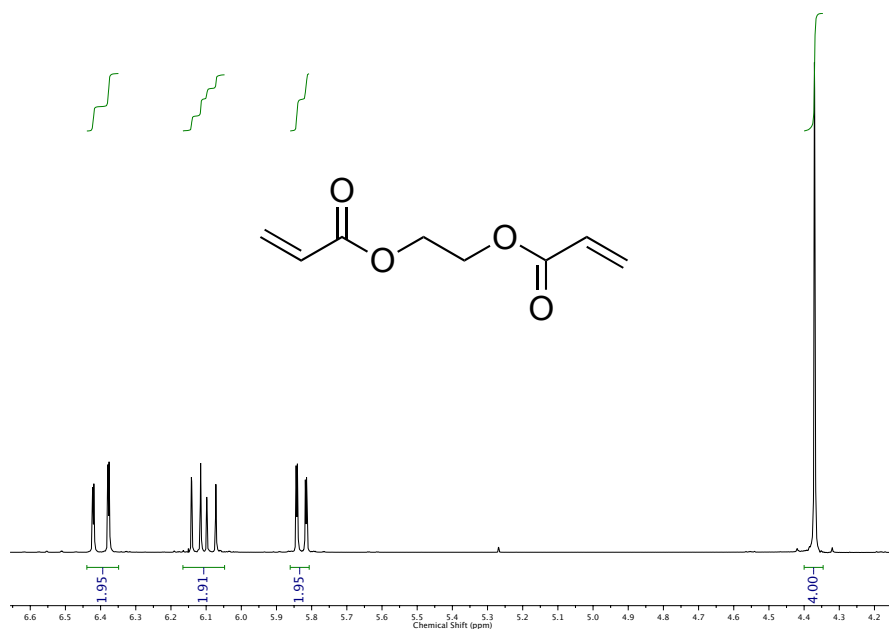
Figure A2.5 ^{1}H NMR (400 MHz, CDCl$_3$, 298 K) spectrum of ethylene glycol diacrylate (**5**).

Isolated adducts and corresponding azide species
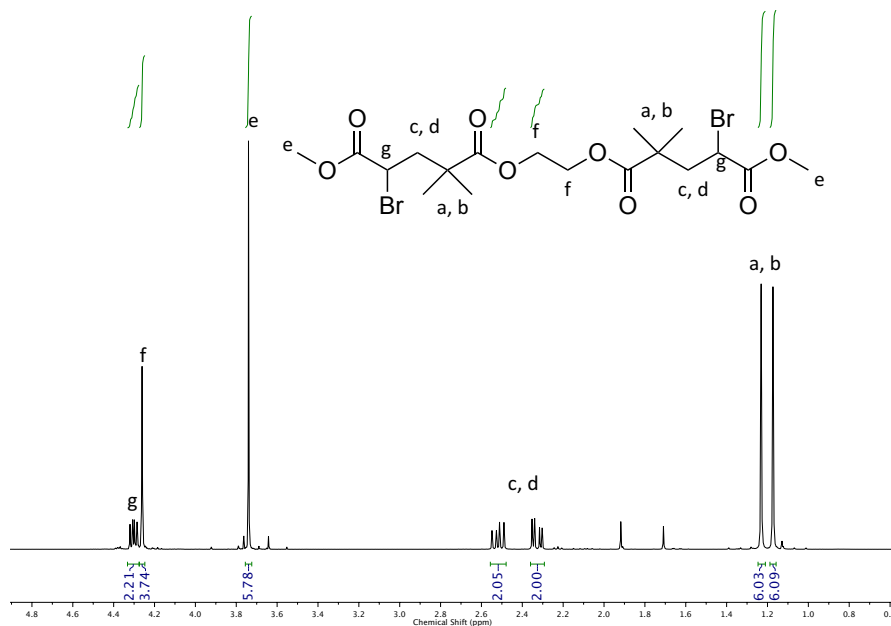
Figure A2.6 ^{1}H NMR (400 MHz, CDCl$_3$, 298 K) spectrum of isolated BBiBE-MA adduct. ^{1}H NMR (CDCl$_3$): δ = 4.33 ppm (dd, 4H, J = 4.0 Hz, 8.0 Hz), 2.38 ppm (s, 4H), 3.67 ppm (s, 6H), 2.54 ppm (dd, 2H, J = 8.0 Hz, 16.0 Hz), 2.35 (dd, 2H, J = 4.0 Hz, 16.0 Hz), 1.25 ppm (s, 6H), 1.19 ppm (s, 6H).
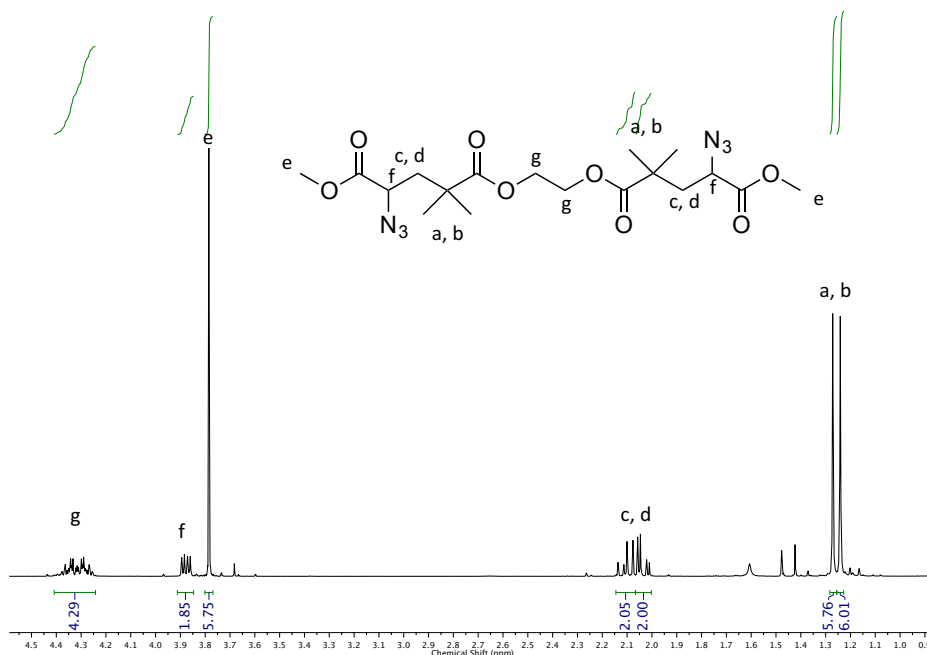
Figure A2.7 ^{1}H NMR (400 MHz, CDCl$_3$, 298 K) spectrum of BBiBE-MA after azide conversion.
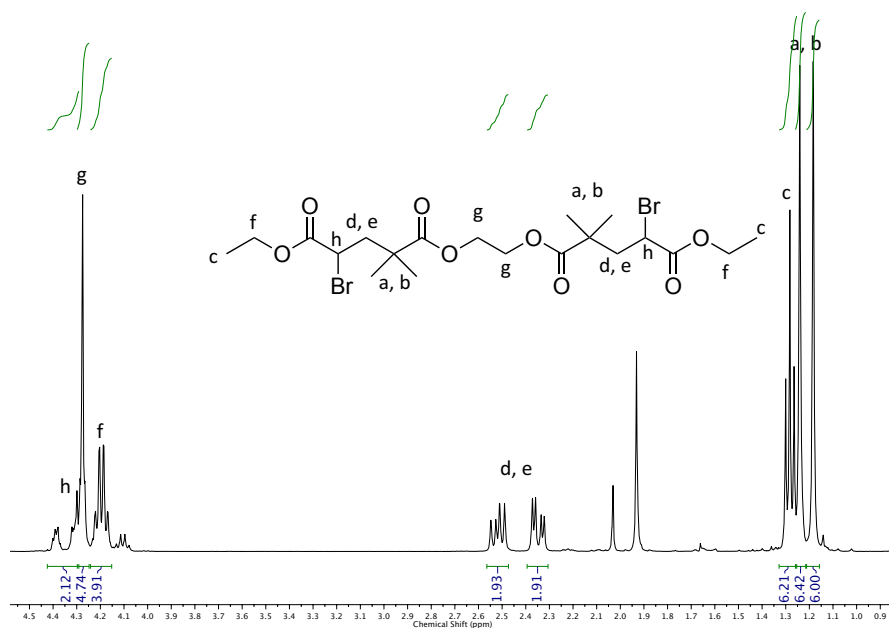
Figure A2.8 ^{1}H NMR (400 MHz, CDCl$_3$, 298 K) spectrum of BBiBE-EA adduct. ^{1}H NMR (CDCl$_3$): δ = 4.29 ppm (dd, 2H, J = 4.0 Hz, 8.0 Hz), 4.28 ppm (s, 4H), 4.20 ppm (qd, 4H, J = 7 Hz, 1 Hz), 2.5 ppm (dd, 2H, J = 8.0 Hz, 16.0 Hz), 2.35 ppm (dd, 2H, J = 4.0 Hz, 16.0 Hz), 1.30 ppm (t, 4h, J = 8.0 Hz), 1.25 ppm (s, 6H), 1.20 ppm (s, 6H).
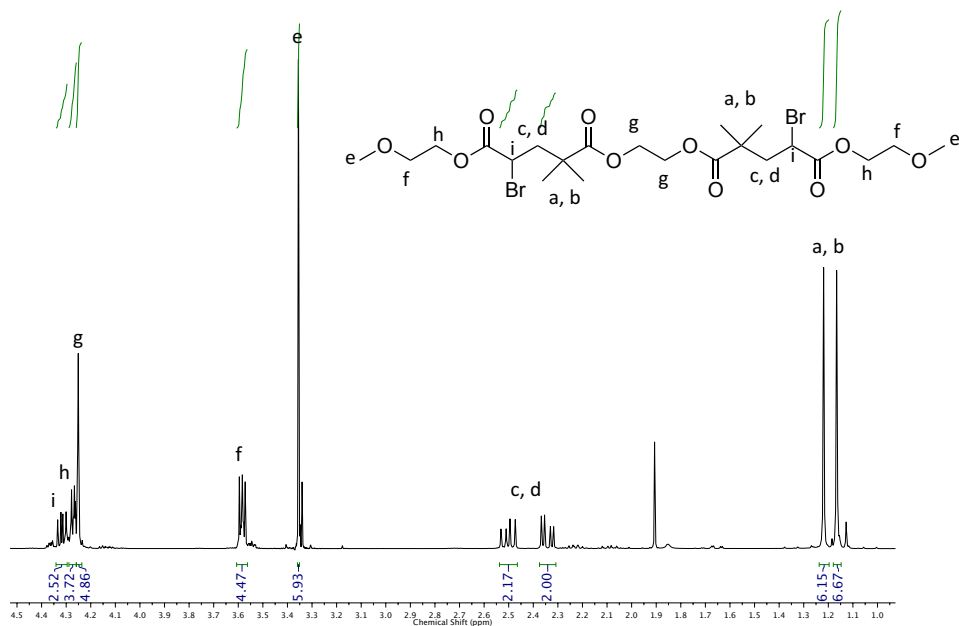
Figure A2.9 ^{1}H NMR (400 MHz, CDCl$_3$, 298 K) spectrum of BBiBE-EGMEA adduct. ^{1}H NMR (CDCl$_3$): δ = 4.32 ppm (dd, 2H, J = 4.0 Hz, 8.0 Hz), 4.275 ppm (t, 2H, J = 3.0 Hz), 4.26 ppm (s, 4H), 3.59 ppm (t, 4H, 10.0 Hz), 3.60 ppm (s, 6H), 2.52 ppm (dd, 2H, J = 8.0 Hz, 16.0 Hz), 2.35 ppm (dd, 2H, J = 6.0 Hz, 15.0 Hz), 1.23 ppm (s, 6H), 1.18 ppm (s, 6H).
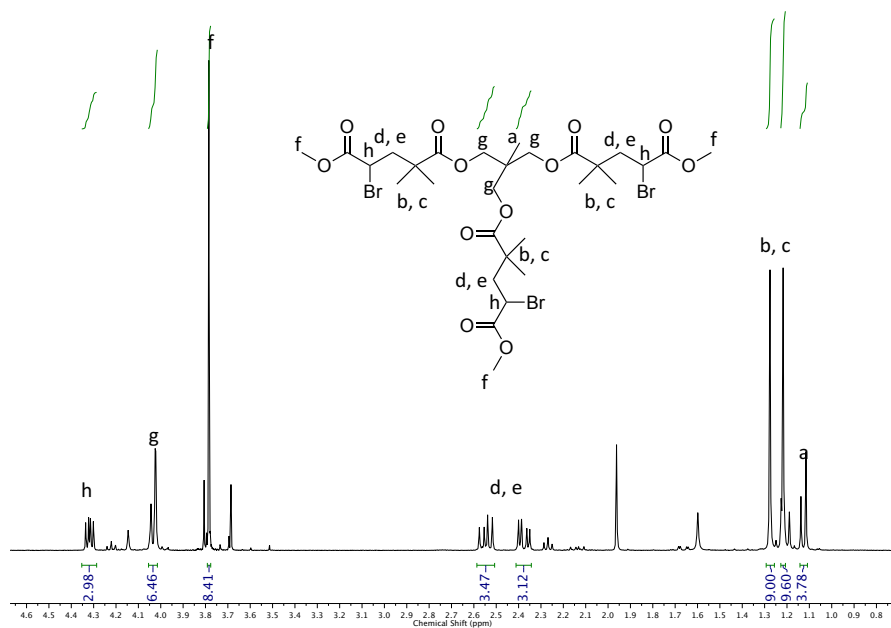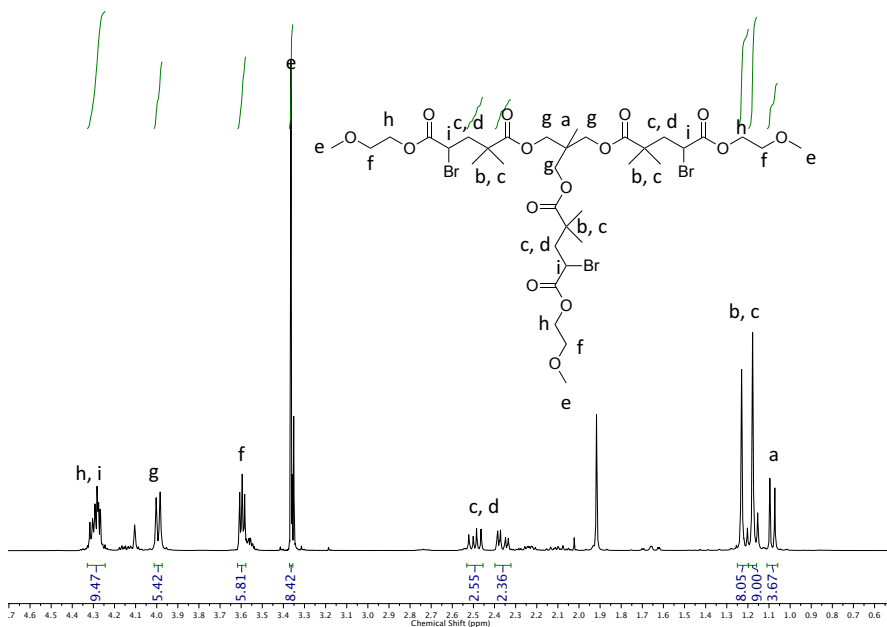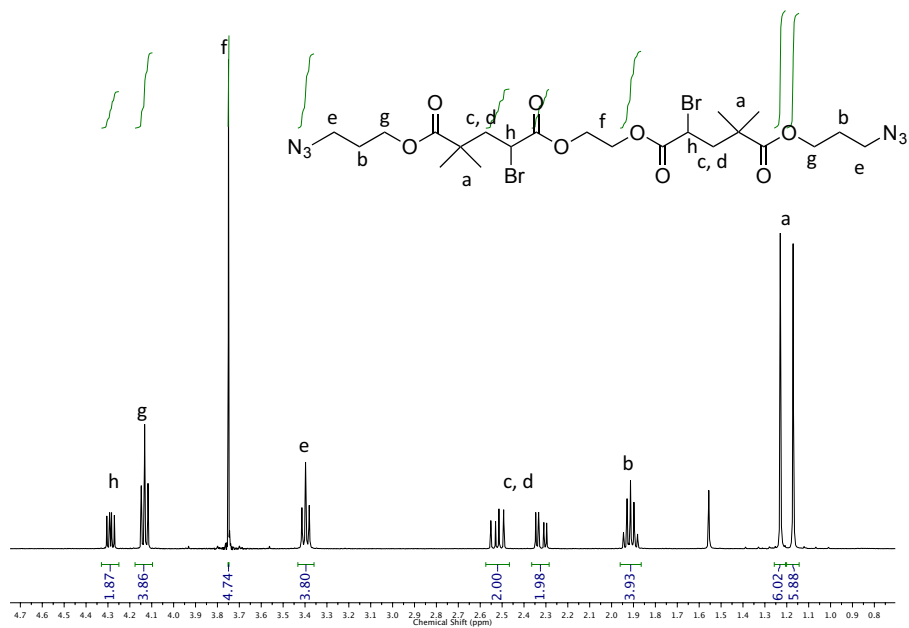
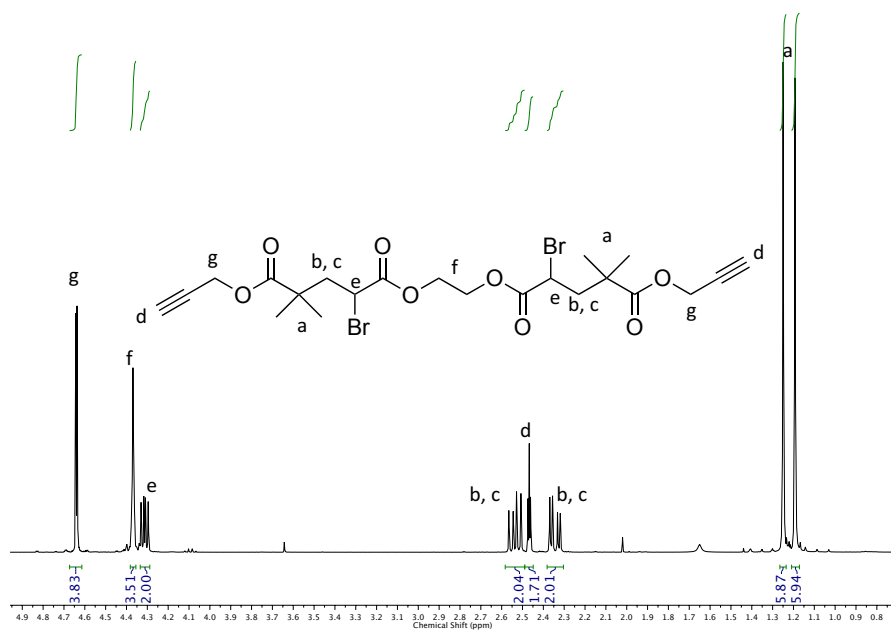**Figure A2.10** ^{1}H NMR (400 MHz, CDCl$_3$, 298 K) spectrum of TBiBE-MA adduct.
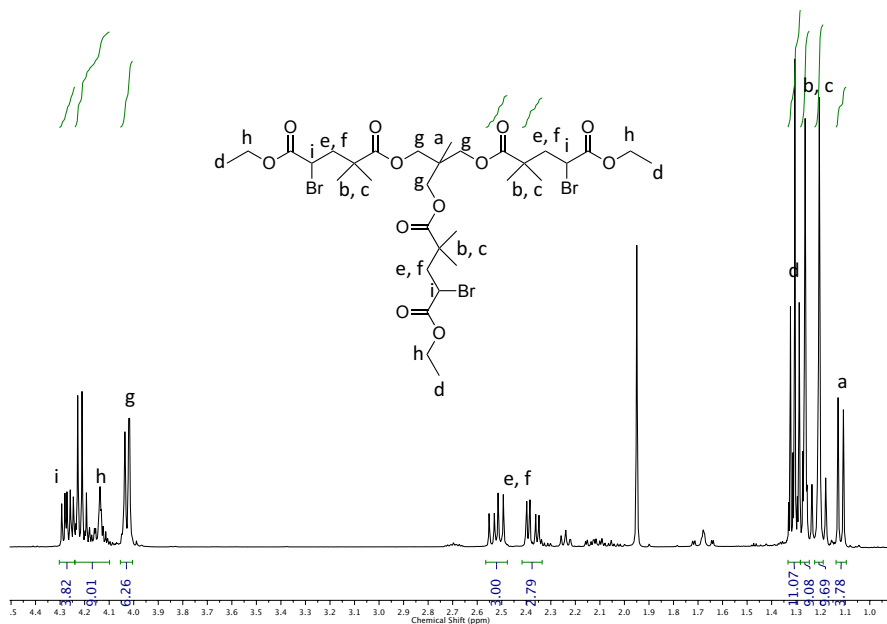
Figure A2.11 ^{1}H NMR (400 MHz, CDCl$_3$, 298 K) spectrum of TBiBE-EA adduct.

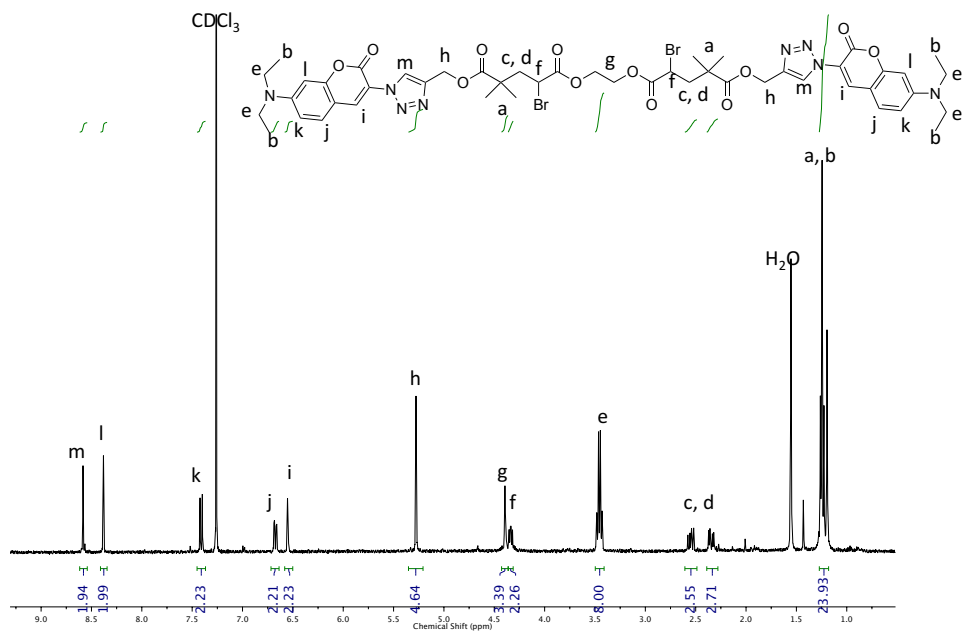**Figure A2.12** ^{1}H NMR (400 MHz, CDCl$_3$, 298 K) spectrum of TBiBE-EGMEA adduct.

Figure A2.13 ^{1}H NMR (400 MHz, CDCl$_3$, 298 K) spectrum of BMPAP-EGDA adduct.

Figure A2.14 ^{1}H NMR (400 MHz, CDCl$_3$, 298 K) spectrum of PBiB-EGDA adduct.

Figure A.2.15 ^{1}H NMR (400 MHz, CDCl$_3$, 298 K) spectrum of coumarin-functionalized PBiB-EGDA.

Chapter 3 Appendix

General Procedures.

All chemicals were purchased from commercial sources and used as received unless otherwise noted. Inhibitors were removed from all commercial acrylates by utilizing silica gel flash column chromatography.

Instrumentation and Equipment.

Bruker Avance 400 MHz NMR for ^{1}H and ^{13}C NMR spectroscopy characterization. MestReNova version 8.0.1-10878 was used to generate images of NMR spectra. MelodySusie VIOLET II 365 nm UV lamp was used for photo-initiated ATRP reactions (available on Amazon). Agilent Technologies 6530B AccurateMass QTOF was utilized for adduct characterization (source: Agilent Jet Stream Electrospray Ionization Source, flow rate = 0.5 mL/min). Waters 1525 binary pump equipped with Waters 2414 RI detector was used for GPC analysis.

Copper-catalyzed photoATRP.

The alkyl halide initiator, monomer, $CuBr_2$, Me_6TREN (XS), 1,4-dimethoxybenzene (internal standard), and solvent were added to a scintillation vial with a magnetic stir bar. The vial was capped with a septum and sealed tightly with copper wire. The solution was placed on a magnetic stir plate where the copper species could complex with the ligand (Me_6TREN). When the catalyst solution was fully complexed, the solution vial was purged with nitrogen on a Schlenk line for 10 minutes. After a thorough degassing, the reaction vessel was placed under a UV light source while stirring to begin the reduction of the Cu^{II}L-X complex, and the time was recorded. ^{1}H NMR integrations (relative to internal standard) were utilized to measure consumption of monomer.

After the monomer was exhausted, the reaction mixture was diluted with methylene chloride and stirred to homogenize the mixture. The solution was poured into a separation funnel and washed with water (3x) to remove any catalyst, indicated by a change in color of the wster phase from clear to blue. The water layer was discarded into halogenated waste, and the organic phase was dried over anhydrous $MgSO_4$. The solution was then gravity filtered to remove $MGSO_4$, before passing thru a plug of alumina or silica to remove any residual catalyst which may remain.

The solvent was removed under reduced vacuum, leaving a viscous, clear oil. To purify to copolymers, they were precipitated into an excess of methanol (3x) and stirred vigorously to remove any impurities such as residual monomer. After 3 cycles of precipitation, the solvent was removed under vacuum to reveal pure copolymer in the form of a very viscous, clear, gelatinous oil. The copolymers were stored in scintillation vials with an inert gas in the headspace at room temperature.

Preparation of ^{1}H NMR samples

For crude solution analysis, 0.050 mL of reaction mixture was diluted with 0.750 mL of $CDCl_3$ and placed into a glass NMR tube before being capped. NMR tube was placed in instrument for analysis.
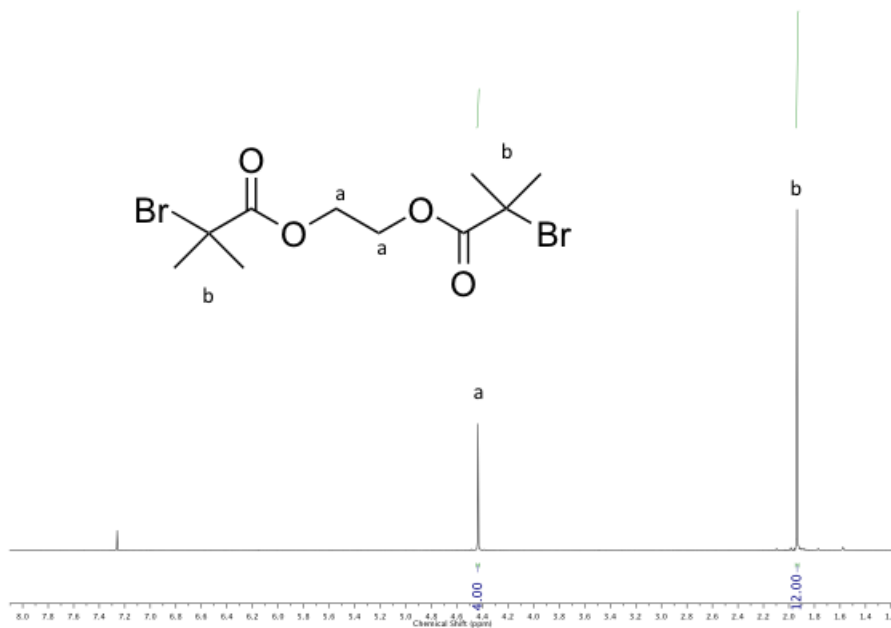
Preparation of MS samples

After the copolymers were purified, 0.1 mg of material was placed into a 1-dram vial and diluted with 1.0 mL of HPLC-grade methanol. The solution was stirred to homogeneity, and then 0.035 mL of the solution was placed into another vial. That solution was further diluted with 0.750 mL of HPLC-grade methanol before being filtered with a 0.2 μm nylon disc filter into an MS vial. The vial was placed into the automated HPLC and analyzed with LC-MS.

Preparation of GPC samples

After the copolymers were purified, 1 mg of material was placed into a 1-dram vial and diluted with 1 mL of Optima-grade THF. The solution was placed on a benchtop and let sit overnight to allow the copolymers to adequately swell. After the time had elapsed, the solution was passed thru a 0.2 μm nylon disc filter into a GPC vial
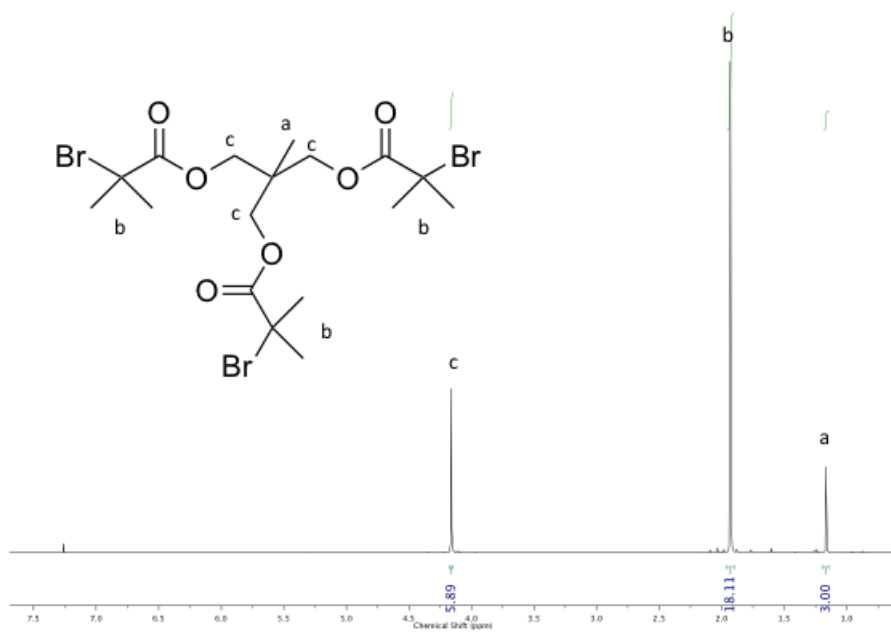
Synthesis of 1,2-bis(bromoisobutyryloxy)ethane (BBiBE)

The bifunctional initiator, BBiBE, was synthesized through an esterification reaction between ethylene glycol and 2-bromoisobutyryl bromide in the presence of triethyl amine. In a 250 mL round bottom flask, the following reagents were sequentially added: ethylene glycol (3.35 g, 5.40×10^{-2} mol), triethyl amine (15.2 mL, 1.09×10^{-1} mol), and 80 mL of dry dichloromethane. The solution was put in an ice bath and stirred for 15 minutes, to which 2-bromoisobutyryl bromide (13.5 mL, 1.09×10^{-1} mol) was added drop wise. The mixture was kept on ice for one hour, and afterward allowed to warm to room temperature, where it continued to mix overnight. The mixture was washed several times with water (3×25 mL). The aqueous portion was washed with dichloromethane (25 mL) to extract any remaining product. The organic fractions were combined and washed with a saturated sodium bicarbonate and brine solution (35 mL) and dried over $MgSO_4$. The final solution was filtered and concentrated under reduced pressure at 50 °C, which yielded white/yellow crystalline solid. The initiator was recrystallized with methanol, which resulted in colorless needle-like crystals. Yield: 11.4 g (75%). ^{1}H NMR (400 MHz, $CDCl_3$): δ = 4.4 ppm (s, 4H) and 1.9 ppm (s, 12H).
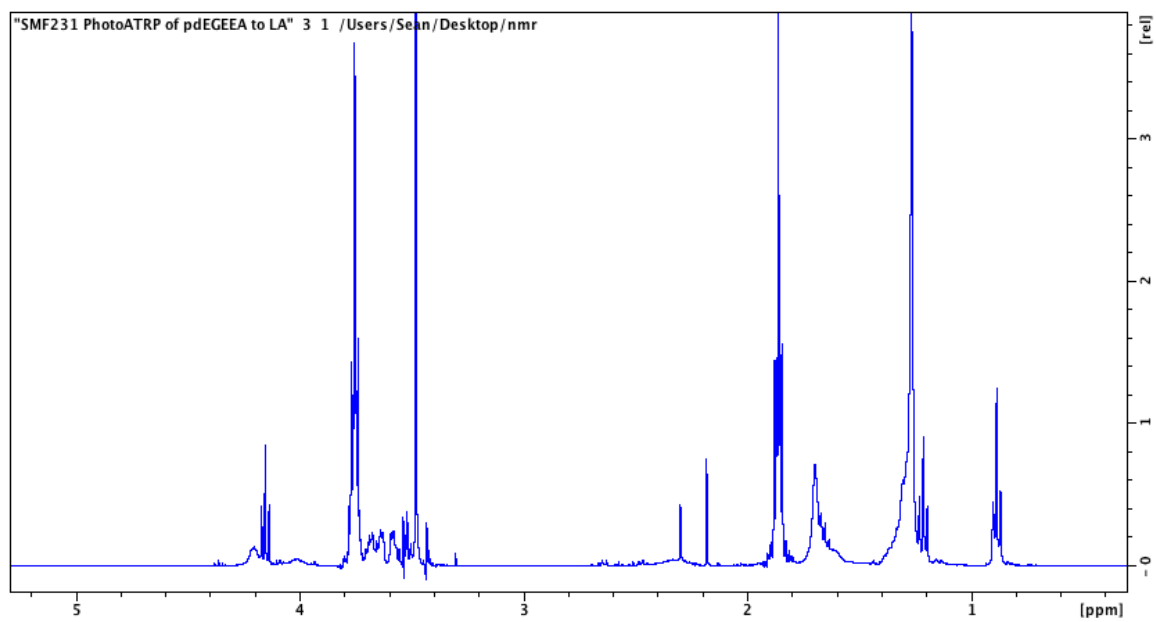
Figure A.3.1. ^{1}H NMR (400 MHz, CDCl$_3$, 298 K) spectrum of 1,2-bis(bromoisobutyryloxy)ethane (**1**).

Synthesis of 1,1,1-tris(2-bromoisobutyryloxymethyl)ethane (TBiBE)

An analogous procedure was followed for the synthesis of TBiBE, but instead the primary alcohol used was 1,1,1,-tris(hydroxymethyl)ethane (2.67 g, 2.22×10^{-2} mol) with a stoichiometric amount of triethylamine (9.29 mL, 6.67×10^{-2} mol) and 2-bromoisobutyryl bromide (8.25 mL, 6.67×10^{-2} mol) in THF (100 mL). Flash column chromatography was utilized for purification after aqueous workup. Product was recrystallized in hexanes. Yield: 5.5 g (44%) ^{1}H NMR (400 MHz, CDCl$_3$): δ = 4.16 ppm (s, 6H), 1.93 ppm (s, 18H), 1.17 ppm (s, 3H).
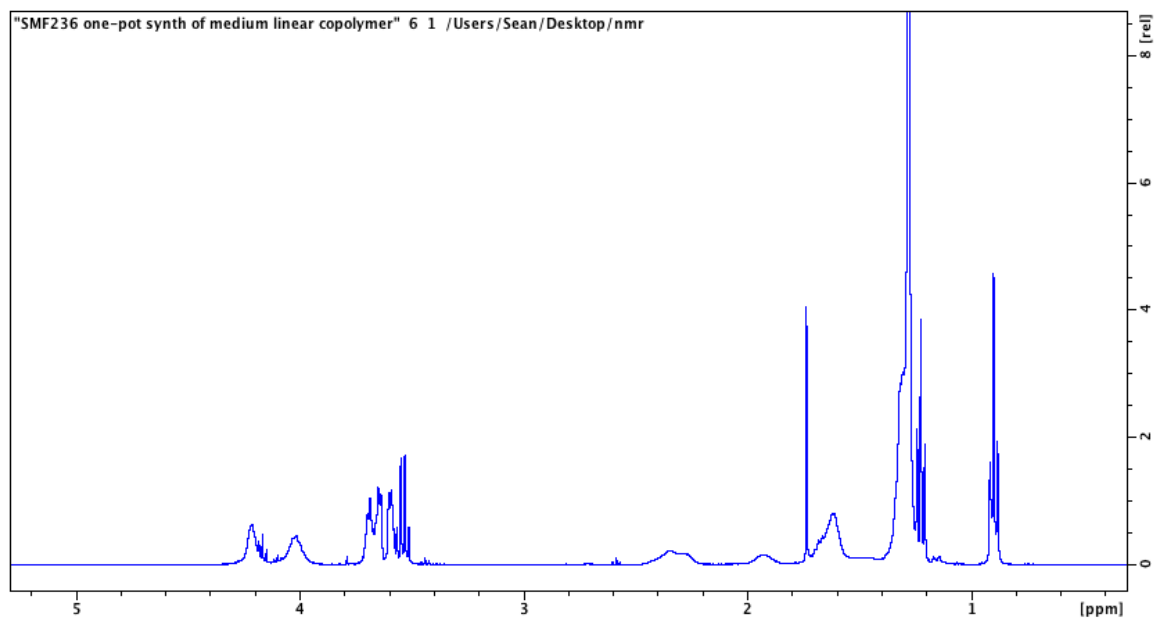
Figure A.3.2. ^{1}H NMR (400 MHz, CDCl$_3$, 298 K) spectrum of 1,1,1-tris(2-bromoisobutyryloxymethyl)ethane (**2**).
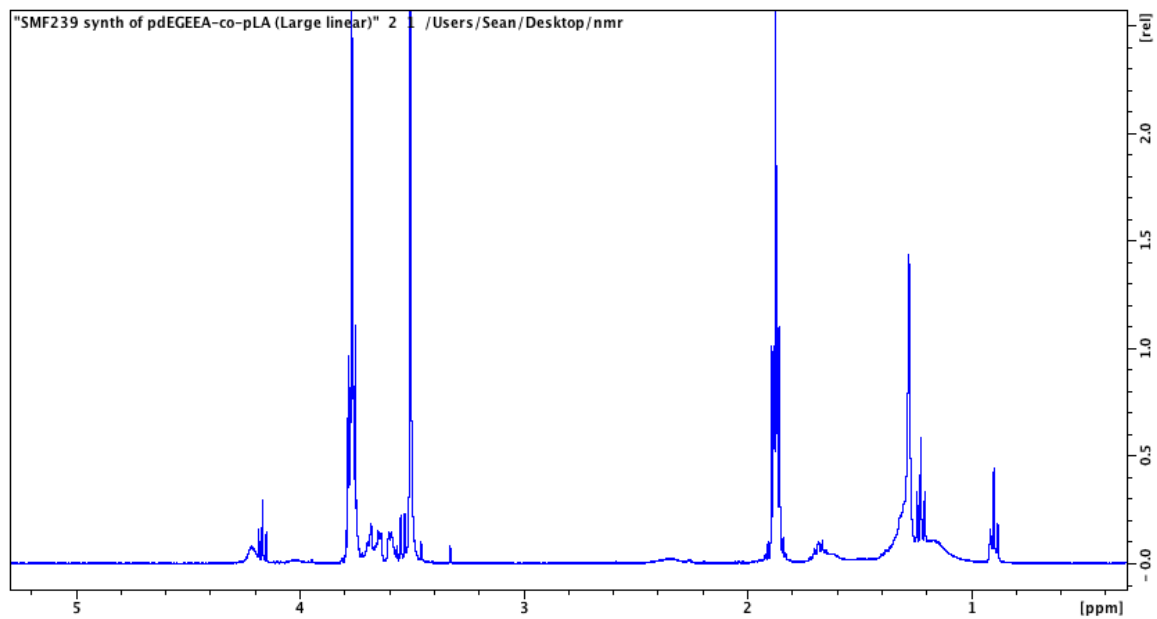

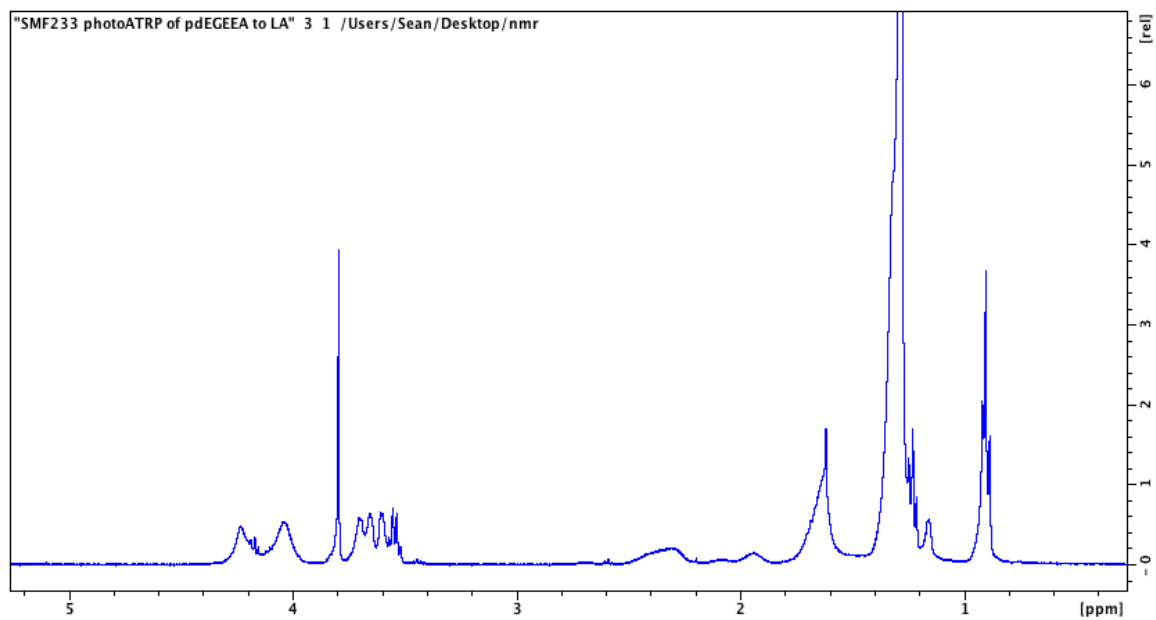**Figure A.3.3.** ^{1}H NMR (400 MHz, CDCl$_3$, 298 K) spectrum of small linear copolymer (**1a**).
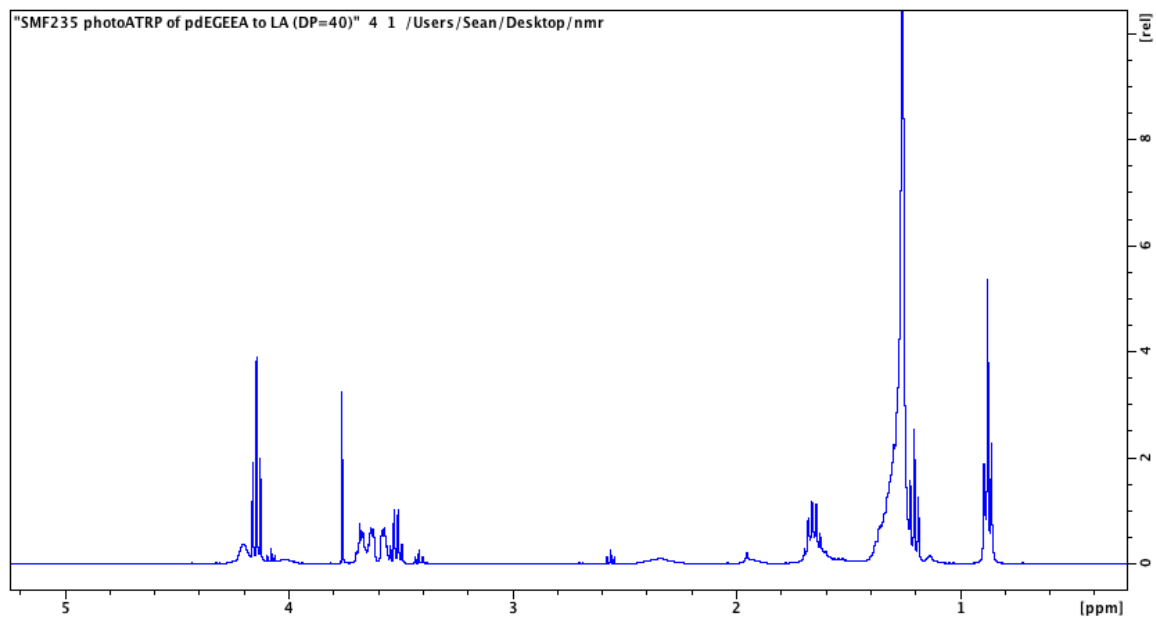
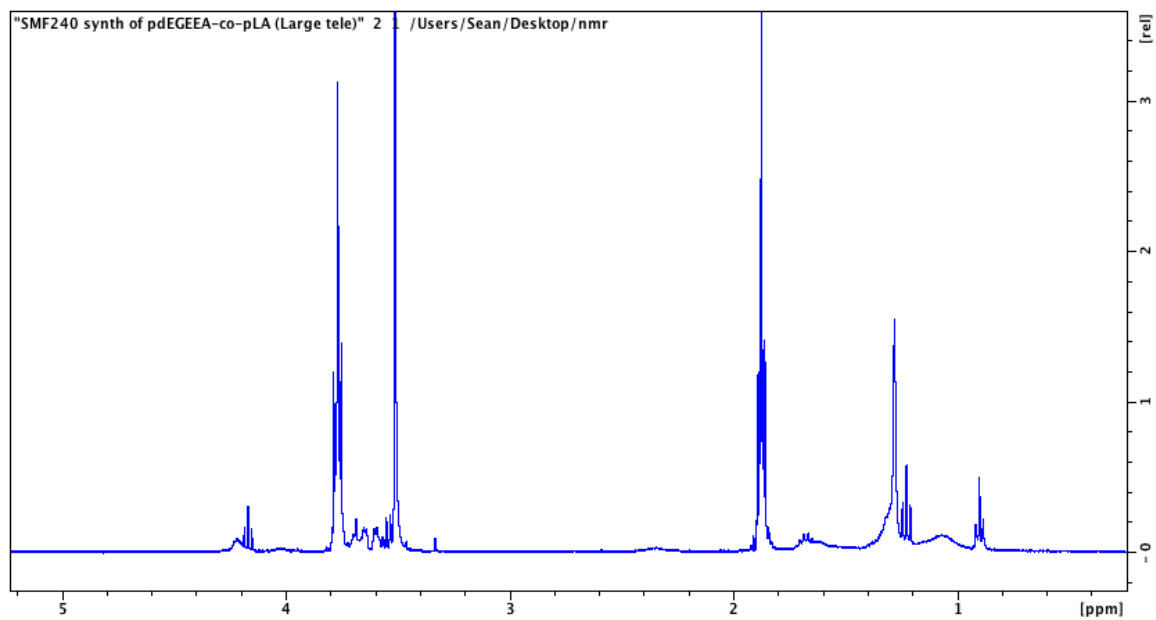**Figure A.3.4** ^{1}H NMR (400 MHz, CDCl$_3$, 298 K) spectrum of medium linear copolymer (**1b**).

Figure A.3.5 ^{1}H NMR (400 MHz, CDCl$_3$, 298 K) spectrum of large linear copolymer (**1c**).

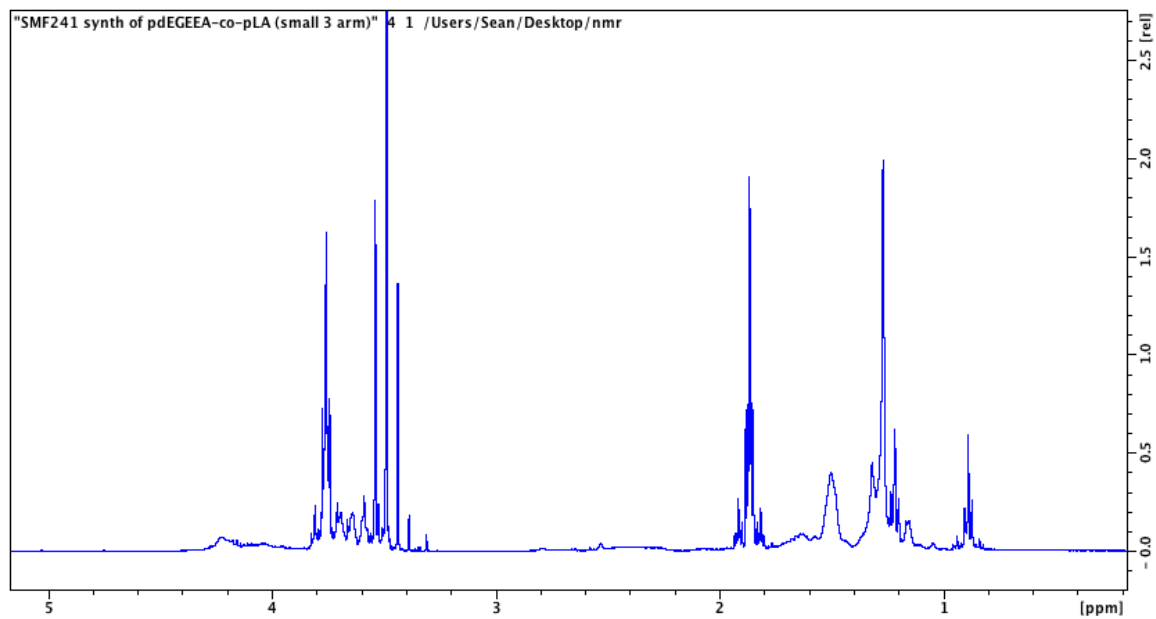**Figure A.3.6.** ^{1}H NMR (400 MHz, CDCl$_3$, 298 K) spectrum of small telechelic copolymer (**2a**).
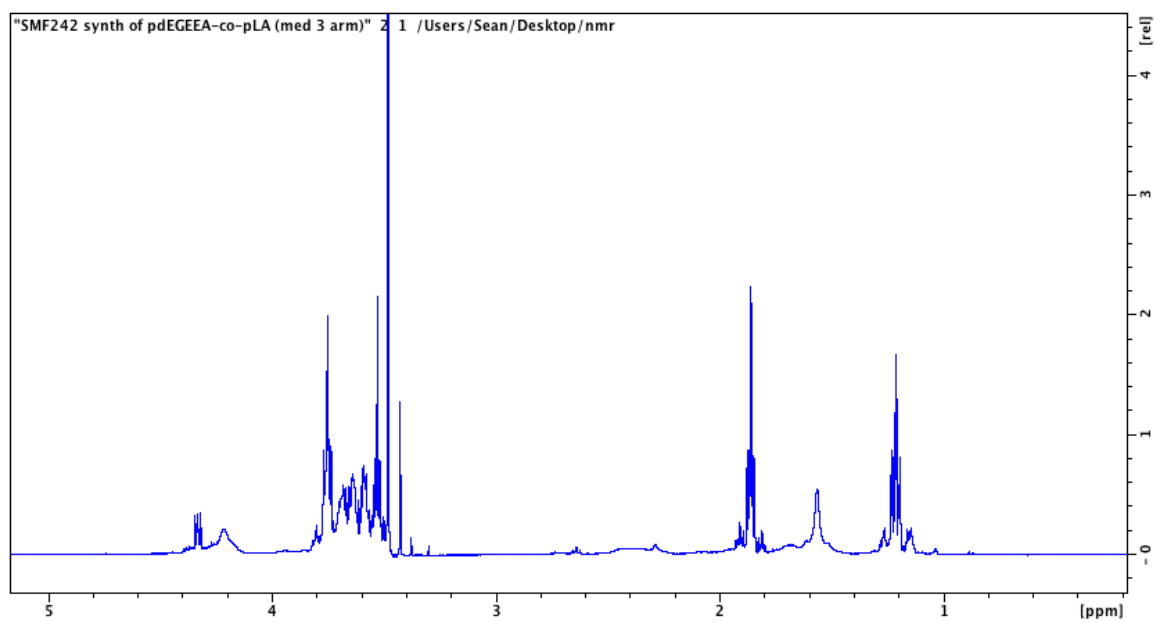

Figure A3.7 ^{1}H NMR (400 MHz, CDCl$_3$, 298 K) spectrum of medium telechelic copolymer (**2b**).

Figure A3.8 ^{1}H NMR (400 MHz, CDCl$_3$, 298 K) spectrum of large telechelic copolymer (**2c**).

Figure A3.9 ^{1}H NMR (400 MHz, CDCl$_3$, 298 K) spectrum of small 3-arm star copolymer (**3a**).

Figure A3.10 ^{1}H NMR (400 MHz, CDCl$_3$, 298 K) spectrum of medium 3-arm star copolymer (**3b**).
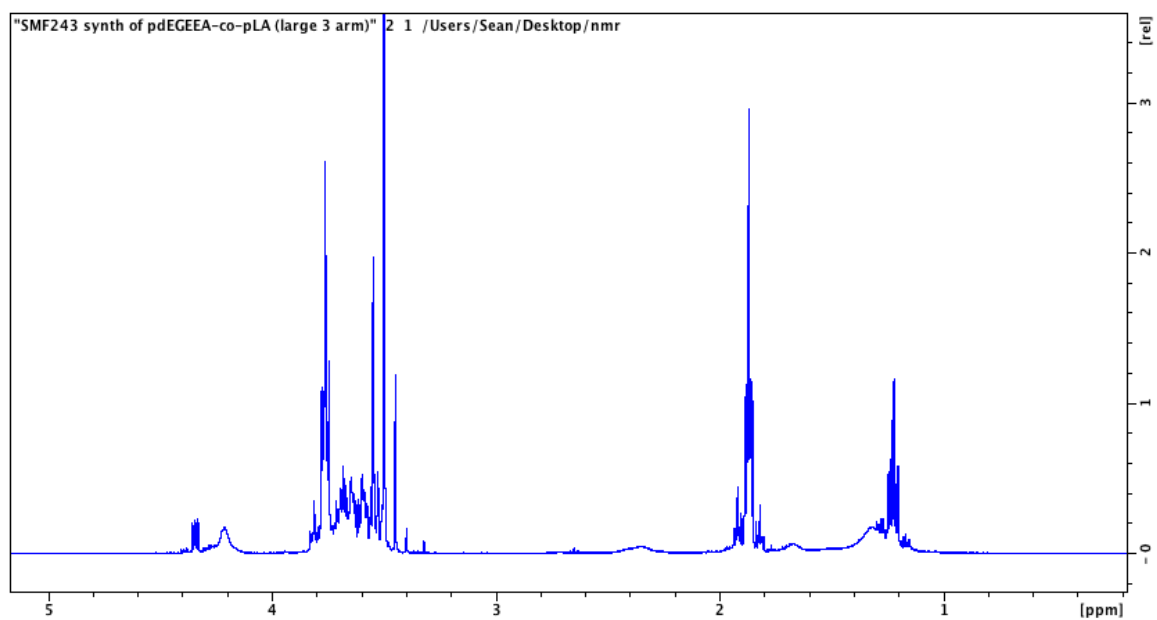
Figure A3.11 ^{1}H NMR (400 MHz, CDCl$_3$, 298 K) spectrum of large 3-arm star copolymer (**3c**).
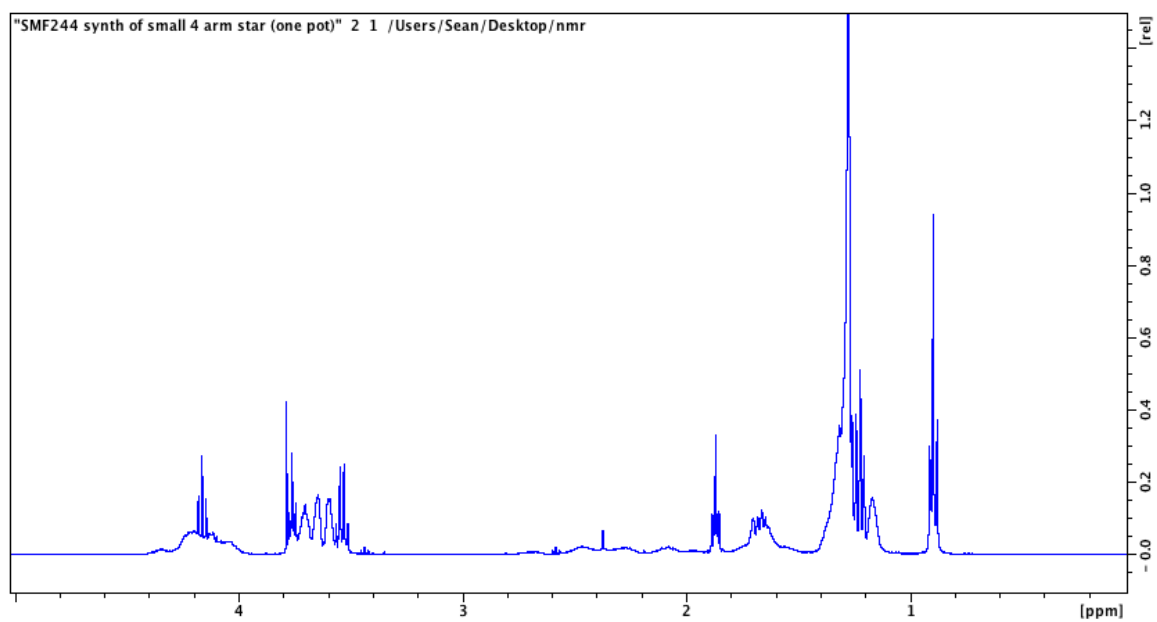
Figure A3.12 ^{1}H NMR (400 MHz, CDCl$_3$, 298 K) spectrum of small 4-arm star copolymer (**4a**).
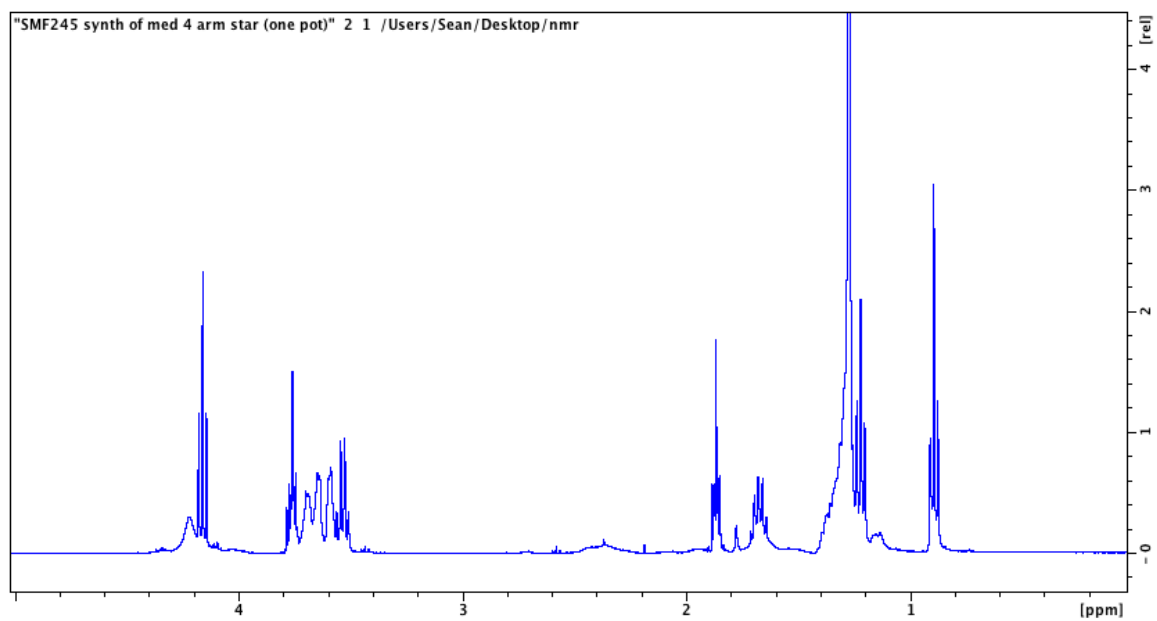
Figure A3.13 ^{1}H NMR (400 MHz, CDCl$_3$, 298 K) spectrum of medium 4-arm star copolymer (**4b**).
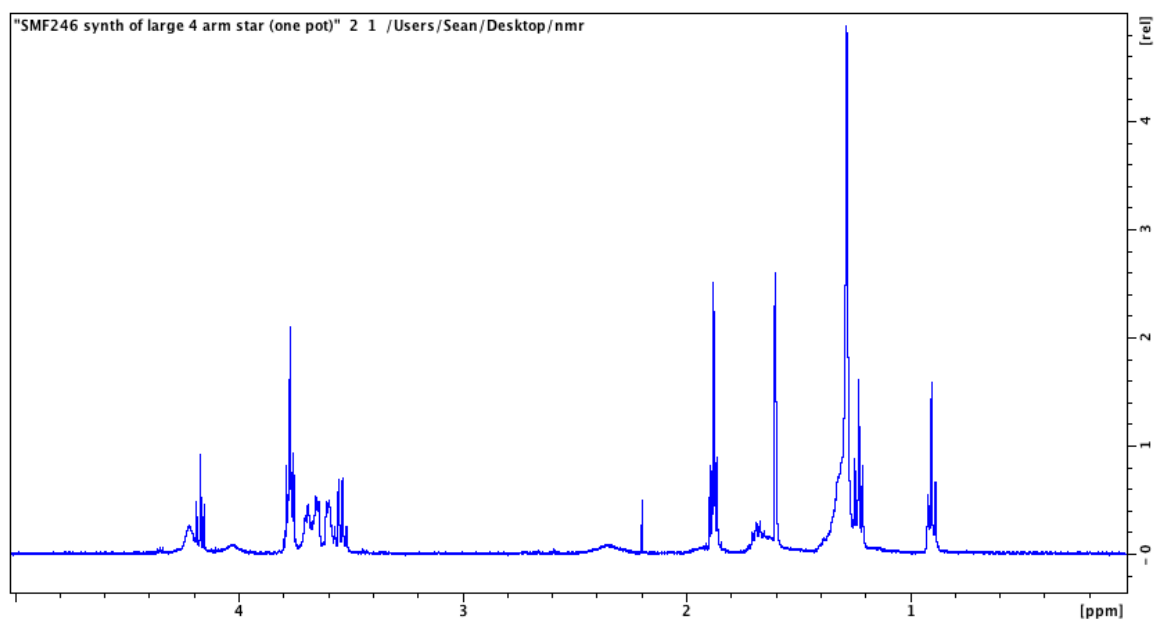
Figure A3.14 ^{1}H NMR (400 MHz, CDCl$_3$, 298 K) spectrum of large 4-arm star copolymer (**4c**).

Table A.3.1 Retention times and corresponding molecular weights determined by GPC with refractive index detector. Instrument was calibrated with PS standards ranging between 162 and 61k Da.

Copolymer Sample	Retention Time (min)	Molecular Weight (Mn)
1a	25.062	3,440
1b	23.072	14,100
1c	21.024	32,960
2a	24.862	5,600
2b	22.889	16,200
2c	20.723	37,750
3a	26.940	2,884
3b	24.251	8,709
3c	20.967	33,700

Table A.3.2 Quantification of rhodamine B in linear copolymer solutions, with corresponding absorbance values. All measurements were conducted in triplicate to determine the standard uncertainty of RB in copolymer solution.

	Copolymer Concentration (mg/mL)	Abs	RB in copolymer sol'n (mg/mL)
1a	0.625	0.0019	3.37E-04 ± 4.51E-05
	1.25	0.0095	3.93E-04 ± 4.49E-05
	2.5	0.0186	4.61E-04 ± 4.47E-05
	5	0.0193	4.66E-04 ± 4.46E-05
	10	0.0596	7.65E-04 ± 4.37E-05
	20	0.0612	7.76E-04 ± 4.37E-05
1b	0.625	0.0045	3.56E-04 ± 4.50E-05
	1.25	0.0153	4.36E-04 ± 4.48E-05
	2.5	0.0238	4.99E-04 ± 4.55E-05
	5	0.0283	5.32E-04 ± 4.44E-05
	10	0.0393	6.14E-04 ± 4.41E-05
	20	0.068	8.29E-04 ± 4.36E-05
1c	0.625	0.0089	3.89E-04 ± 4.49E-05
	1.25	0.0112	4.06E-04 ± 4.49E-05
	2.5	0.0259	5.15E-04 ± 4.43E-05
	5	0.0315	5.56E-04 ± 4.45E-05
	10	0.0406	6.23E-04 ± 4.42E-05
	20	0.033	5.67E-04 ± 4.43E-05

Table A.3.3 Quantification of rhodamine B in telechelic copolymer solutions, with corresponding absorbance values. All measurements were conducted in triplicate to determine the standard uncertainty of RB in copolymer solution.

	Copolymer Concentration (mg/mL)	Abs	RB in copolymer sol'n (mg/mL)
2a	0.625	0.001	3.30E-04 ± 4.50E-05
	1.25	0.005	3.59E-04 ± 4.50E-05
	2.5	0.0031	3.45E-04 ± 4.50E-05
	5	0.0053	3.61E-04 ± 4.50E-05
	10	0.0106	4.01E-04 ± 4.48E-05
	20	0.0123	4.13E-04 ± 4.48E-05
2b	0.625	0.0013	3.32E-04 ± 4.50E-05
	1.25	0.0055	3.63E-04 ± 4.49E-05
	2.5	0.0103	3.98E-04 ± 4.47E-05
	5	0.0153	4.36E-04 ± 4.14E-05
	10	0.2213	1.96E-04 ± 4.34E-05
	20	0.0731	8.64E-04 ± 4.49E-05
2c	0.625	0.0074	3.77E-04 ± 4.49E-05
	1.25	0.0051	3.60E-04 ± 4.50E-05
	2.5	0.0101	3.97E-04 ± 4.48E-05
	5	0.0149	4.33E-04 ± 4.47E-05
	10	0.0269	5.22E-04 ± 4.44E-05
	20	0.0555	7.31E-04 ± 4.38E-05

Table A.3.4 Quantification of rhodamine B in 3-arm star copolymer solutions, with corresponding absorbance values. All measurements were conducted in triplicate to determine the standard uncertainty of RB in copolymer solution.

	Copolymer Concentration (mg/mL)	Abs	RB in copolymer sol'n (mg/mL)
3a	0.625	0	0
	1.25	0	0
	2.5	0	0
	5	0	0
	10	0	0
	20	0	0
3b	0.625	0.0686	$8.31E\text{-}04 \pm 4.35E\text{-}05$
	1.25	0.5034	$4.06E\text{-}03 \pm 4.29E\text{-}05$
	2.5	0.3374	$2.82E\text{-}03 \pm 4.11E\text{-}05$
	5	0.2084	$1.87E\text{-}03 \pm 4.15E\text{-}05$
	10	0.4382	$3.57E\text{-}03 \pm 4.19E\text{-}05$
	20	0.3734	$3.09E\text{-}03 \pm 4.29E\text{-}05$
3c	0.625	0.0194	$4.66E\text{-}04 \pm 4.12E\text{-}05$
	1.25	0.0115	$4.07E\text{-}04 \pm 4.13E\text{-}05$
	2.5	0.0618	$7.80E\text{-}04 \pm 4.48E\text{-}05$
	5	0.0513	$7.03E\text{-}04 \pm 4.39E\text{-}05$
	10	0.1108	$1.14E\text{-}03 \pm 4.27E\text{-}05$
	20	0.5231	$4.20E\text{-}03 \pm 4.32E\text{-}05$